ITTC2024
30TH INTERNATIONAL TOWING TANK CONFERENCE
22–27 SEPTEMBER 2024 | HOBART TASMANIA AUSTRALIA

Report of the Resistance & Propulsion Committee

RESISTANCE & PROPULSION COMMITTEE

1. INTRODUCTION

1.1 Membership and Meetings

The members of the Resistance and Propulsion Committee of the 30th ITTC were:

- Nicholas Dawson (Chair)
  QinetiQ,
  UK
- Bryson Metcalf (Secretary)
  NSWC Carderock Division,
  USA
- Tokihiro Katsui
  Kobe University,
  JAPAN
- Yasuhiko Inukai
  Japan Maritime United Corporation,
  JAPAN
- Kwang-Soo Kim
  KRISO,
  SOUTH KOREA
- Byoung-Guk Kim
  Hanwha Ocean Company,
  SOUTH KOREA
- Matteo Diez
  CNR-INM,
  ITALY
- Stefano Gaggero
  University di Genova,
  ITALY
- Weichao Shi
  Newcastle University,
  UK
- Renchuan Zhu,
  Shanghai Jao-Tong University,
  CHINA
- Nikolaj Larsen (Former Chair, departed committee 2023)
  FORCE Technology,
  DENMARK

Three in-person committee meetings were held during the work period:

- The first meeting was held at FORCE Technology, in Copenhagen, Denmark, on the 9th – 10th November 2022.
- The second meeting was held at Kobe University in Kobe, Japan, on the 8th – 9th June 2023.
- The third meeting was held at CRN-INM in Rome, Italy between 31st January – 1st February 2024.

Additional video meetings were conducted to enable the participation of those who were unable to attend the in-person meetings and to try to maintain progress between meetings.

1.2 Tasks

The recommendations for the work of the Resistance and Propulsion Committee as given by the 29th ITTC were as follows:

1. Update the state-of-the-art for predicting the performance of different ship concepts emphasizing developments since the 2021 ITTC Full Conference. The committee report should include sections on:

A) The potential impact of new technological developments on the ITTC, including, for example new types of hull and propeller coatings, propulsors, rudders.
B) New experimental techniques and extrapolation methods.
C) New benchmark data.
D) Practical applications of computational methods to performance predictions and scaling.
E) The need for R&D for improving methods of model experiments, numerical modelling and full-scale measurements.

2. Review ITTC Recommended Procedures relevant to resistance and propulsion, and

A) Identify any requirements for changes in the light of current practice, and, if approved by the Advisory Council, update them,
B) Identify the need for new procedures and outline the purpose and contents of these.

3. Rewrite procedure 7.5-02-03-01.2, Uncertainty Analysis, Example for Propulsion Test (old procedure deleted 2021), complying with current ITTC guidelines for uncertainty analysis. Include a worked example complying with current ITTC procedures for propulsion tests. Cooperate closely with the Quality Systems Group
4. Rewrite procedure 7.5-02-03-02.2, Uncertainty Analysis, Example for Open Water Test (old procedure deleted 2021), complying with current ITTC guidelines for uncertainty analysis. Include a worked example complying with current ITTC procedures for open water tests. Cooperate closely with the Quality Systems Group.
   Update procedure 7.5-02-05-03.3, Uncertainty Analysis, Example for Water Jet Propulsion Test, complying with current ITTC guidelines for uncertainty analysis. Include a worked example complying with current ITTC procedures for water jet propulsion tests. Cooperate closely with the Quality Systems Group.
5. Conduct a benchmark study focusing on the effect of Re at model scale and scaling methods for full scale prediction. CFD calculations would be run at a range of Re at model scale and full scale, along with openwater model tests at a range of Re. The study could use two propellers that were provided for the previous benchmark study run by the 28th ITTC.
6. Investigation of the issue of laminar effects in self-propulsion test of propeller with low blade area.

A) Conduct a survey how ITTC members tackle this issue, and which scaling method they use for low blade area propellers.
B) Investigate the sufficiency of conduction two open water tests at different Reynolds numbers for full scale extrapolation. C) Review literature on the subject.
C) Suggest modification to recommended procedures.

7. Investigation of the issue of extrapolation of model tests with ducted propellers to full scale according to different Re-numbers. Identify the need and change relevant procedures if necessary.
8. Update of the Load variation test method in 7.5–0203–01.4 "1978 ITTC Performance Prediction Method"

A) Review of the Load Variation Test method, considering a wider range of resistance and develop a new method if necessary.
B) Review the effectiveness of shallow water effects in Load Variation Test method and develop of a new method if necessary.

9. Monitor the experience of ITTC members using CFD-based form factors and, if necessary, update the Recommended Procedures accordingly. This includes the correlation with sea trial data, numerical friction line, how to handle a submerged transom, the possibility to handle separation in model scale by deriving model and full scale form factors. Continue the comparative studies on CFD methods for form factor derivation.
10. Investigation of the requirements for the testing and numerical evaluation of high-speed marine vessels. Address the need of updating the relevant procedures.
11. Investigation into the use of CFD methods in scaling of model test results for a more precise speed-power prediction. The issues with high priority are:

A) Propeller open water scaling
B) Difference in Reynolds number at selfpropulsion and open water test, laminar effect in self-propulsion test
C) Effective wake scaling
D) Scaling of immersed transoms
E) Energy saving devices

12. Investigation of measurement and prediction methods for breaking waves.
13. Investigation of the scaling of sinkage and trim in deep water, as well as their effect on the form factor.
14. Investigation of the scale effects of ships advancing through shallow/restricted waters, in particular scaling of sinkage.
15. Developments in hull and propeller model manufacturing. Investigate the advances in additive manufacturing techniques and novel materials. Investigate the use of 3D scanning techniques to validate the model geometry in view of updating the procedures.
16. Guidelines for model testing of coatings; in particular, skin friction reducing and air lubrication systems, including scaling laws.
17. Review of CFD methods for roughness effects and recommend best practice; in particular, in terms of wall resolved as well as wall function methods.
18. Identify the necessity of guidelines for CFD methods, model tests and scaling for energy saving devices.
19. Investigation of the issue of powering and resistance for slower speed submerged vehicles due to the resurgence of UUV (Unmanned Underwater Vehicle) and AUV (Autonomous Underwater Vehicle). The UUV's and AUV's can be plagued by the added drag of appendages, sensors and addons. They can have much greater impact on performance (% wise) than typical submerged vehicles (torpedo/subs) since UUV's and AUV's typically operate at much slower speeds. The community would benefit with a better correction for Cf than the flat plate curve. Identify the need and, if necessary, update the procedures to better handle transition issues that would be present in these lower Re submerged vehicles.

Unfortunately, due to the limited resources of the R&P committee it was not possible to complete all actions and some have been recommended to be undertaken by the following committee.

2. STATE OF THE ART

2.1 New Benchmark Data

2.1.1 JoRes Project

One of the most significant sources of benchmark data in recent years is the "Joint Research Project: Numerical Methods Validation For Designing and Building More Advanced and Energy Efficient Ships". This is a €1.5M project, self-funded by the participants and contributors, which is a global initiative to develop validation cases.

The International Maritime Organisation (IMO) has set ambitious targets for the maritime sector to significantly reduce Greenhouse Gas (GHG) emissions. The IMO's goal of achieving net zero emissions by 2050 will require a combination of energy efficiency optimisation and the use of carbon-neutral fuels. The JoRes project noted that efficiency optimisation can only be achieved using digital simulations, which require validation.

The availability of appropriate full-scale data for comparison has long been an issue for both CFD validation and for making assessments of Correlation Allowance, hull fouling allowances and so on. The JoRes project aims to address this issue, by making a large dataset publically available. This phase of the JoRes project is already complete, and the project organisers have state that all the results and the geometry files will be made publically available on 1 December 2024 and will include trials data of:

- General cargo vessel
- Tanker
- Twin-screw RoRo ferry
- Cruise liner
- Tug boat
- Bulk Carrier

In addition to full-scale trials data, the project has also been collecting data on hull and propeller fouling, hull roughness, and other aspects which are considered critical to resistance and propulsion of ships.

2.1.2 GATERS project

The Gate Rudder System (GATERS) project has also published results of full scale trials data, which is of relevance to a number of areas of interest to the ITTC community. The objective of the GATERS project was to "Design, Manufacture and Install a Retrofit Gate Rudder System". Aimed at the retrofit market as well as for newbuilds, the Gate Rudder System (GRS) intends to improve the flow around an existing propeller, reducing tip losses and parasitic drag.

Full scale trials were conducted on vessels with both gate rudder systems and conventional rudder systems. As a retrofit system, the GATERS project believe that fuel savings of up to 10% are possible in calm water conditions, rising to 15% savings in a normal sea state, when compared to a conventional rudder system. If savings of even half this magnitude can be achieved in practice then it would be expected that this technology will become of significant interest over the next decade. It will be important for anyone conducting CFD simulations to design a GRS to have robustly validated their processes, as the cost-benefit analysis of whether to fit the system or not would be affected by the accuracy of the results. The availability of model and full scale data, both with and without a gate rudder system fitted could make this dataset particularly valuable, as it can be used to validate standard CFD processes as well as those applicable to this particular type of Energy Saving Device (ESD).

3. PROCEDURES

Three updated procedures were accepted by the Quality Systems Group of the 30th ITTC for publication at this time. These were:

- 7.5-01-01-01 Ship Models
- 7.5-02-03-01.8 Energy Saving Devices
- 7.5-02-05-01 High Speed Marine Vehicles

Corrections were minor in nature and focussed upon ensuring consistency with other Recommended Procedures and Guidelines.

A number of other procedures were deemed insufficiently complete by the Quality Systems Group and will be passed to the next committee for completion.

3.1 A REVIEW OF SCALING METHODS FOR SHIP WAKE FRACTION WITH PRE-SWIRL DEVICES

A comprehensive review was completed of Guideline 7.5-02-03-01.8 – *Scaling method for ship wake fraction with pre-swirl devices*.

The relevance of Energy Saving Devices (ESD), especially in the case of refitting of existing ships, is continuously increasing due to the need of comply with stricter requirements in terms of the efficiency and carbon footprint of ships. Typical ESDs are Pre- and Post- Swirl Stator (PSS), Pre-Swirl Ducts (PSD), Wake Equalizing Ducts (WED), Propeller Boss Cap Fins (PBCF), Vane Wheels, Contra-Rotating Propellers (CRP) and their possible combinations.

Among these devices, those exploiting the pre-swirling effect (PSS and PSD) appear to be the most promising, especially when applied to ships with high blockage coefficients. Although the performance varies according to ship type and operating condition, the energy reduction effect is estimated to be about 3% to 7% (Dang *et al.*, 2012, Lee *et al.*, 1992, Mewis and Guiard, 2011, Shin *et al.*, 2013, Kim *et al.*, 2015, Koushan *et al.*, 2020, Furcas and Gaggero, 2021, Gaggero and Martinelli, 2022, Nicorelli *et al.*, 2023). The working principle (the generation of a counter swirl flow to the propeller that corresponds to a local blade loading, a consequent reduction of the rate of revolution for the required thrust and the final reduction of delivered power) poses several questions concerning the extrapolation to full-scale. The original ITTC 1978 method was developed for conventional ships and showed limitations when applied to ships equipped with pre-swirl devices (Lee, 2015). The ITTC 1999 method adopted a different scaling procedure by distinguishing the axial and the tangential component of the wake to the propeller. However, it was never included in the recommended procedures and guidelines despite being introduced in the 22nd ITTC final report of the Specialist Committee on Unconventional Propulsors (ITTC 1999). Current ITTC recommended procedures and guidelines (ITTC 2021) adopt a modified extrapolation methodology to account in a more reasonable way for the angle of attack to the propeller based on the work of Kim *et al.* (2017). In this method, the axial and tangential velocity components are scaled separately: the axial wake (being viscous in nature) is scaled according to ITTC 1978, while the tangential component (being mainly potential in nature) following the assumptions of ITTC 1999, is not scaled:

$$w_{SS} = (t_{MS} + 0.04) + (w_{MS\,axial} - t_{MS} - 0.04)\frac{C_{FS} + C_A}{C_{FM}} + w_{MS\,tangential}$$

$$w_{MS\,axial} = w_{MO} + (w_{MS} - w_{MO}) \cdot F_x$$
$$w_{MS\,tangential} = (w_{MS} - w_{MO}) \cdot F_t$$

The most relevant modification, introduced by ITTC 2021, is the use of two weighting factors, F_x and F_t, to account for the importance of axial and tangential components of the velocity field to the propeller based on the type of the device.

Kim *et al.* (2017) suggested values for these weighting factors based on a limited number of ships and ESD types (KCS and KVLCC ships

equipped with a Pre-Swirl Stator and a Pre-Swirl Duct respectively), as shown in Table 1.

Table 1 - Factors of axial and tangential coefficients for ITTC 2021 scaling procedure. From Kim et a. (2017) and ITTC 7.5-02-03-01.8

ESD type	F_x	F_t
PSS	0.3	0.7
PSD	0.8	0.2

Some other recent studies widened the range of test cases and pointed out the necessity for systematic analyses, as suggested in the ITTC procedure, to refine the proposed extrapolation method.

Nicorelli *et al.* (2023) applied several extrapolation procedures (ITTC 1978, ITTC 1999 and ITTC 2021) to three devices specifically designed by a simulation-based optimization method for the Duisburg Test Case (DTC). The design was carried out at full-scale using a combination of BEM and RANSE analyses. Fully resolved RANSE analyses at both model and full scale allowed comparison with ITTC extrapolation methods. In the study, a PSD, a PSS and a WED were analysed in order to span over the entire range of pure axial/mixed/pure tangential functioning of the devices.

In addition, as one of the activities of the ITTC Resistance and Propulsion Committee, a similar analysis was extended to two additional PSS (a two- and a three-fins design), which geometries were available to the Committee. These devices were also designed using optimization based methodologies (Furcas and Gaggero, 2021) and model- and full-scale fully resolved RANSE analyses were employed for comparison with ITTC wake extrapolation procedures.

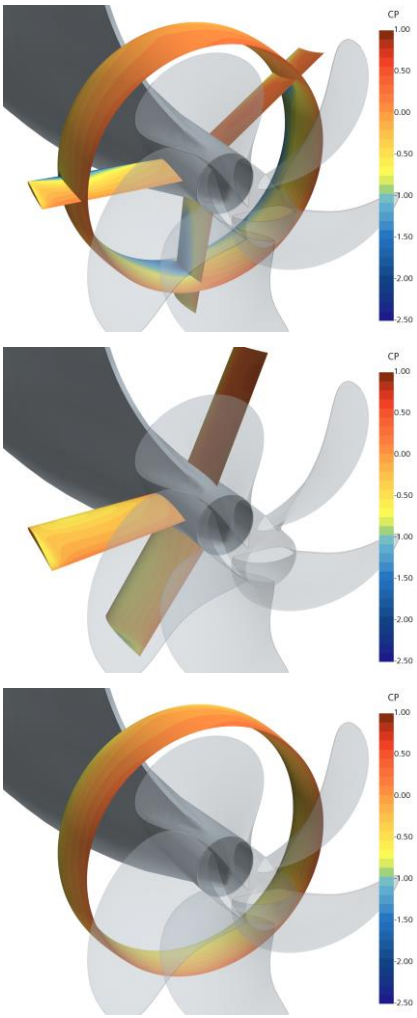

Figure 1 - Pre-Swirl Duct, Pre-Swirl Stator and Wake Equalizing Duct for the DTC hull from Nicorelli and Gaggero (2023)

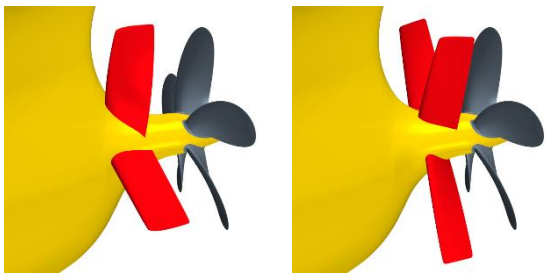

Figure 2 - Two- and Three-fins Pre-Swirl Stators for the JBC hull, from Furcas and Gaggero (2021)

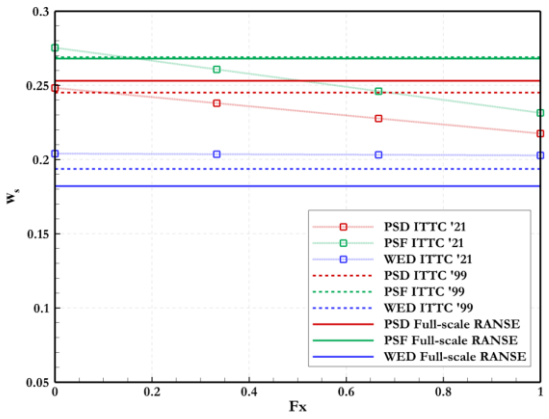

Figure 3 - Full-scale effective wake fractions (W_S) using several extrapolation methods compared to full-scale RANSE calculations; Influence of the axial/tangential coefficient of the ITTC 2021 procedure. DTC test case adapted from Nicorelli and Gaggero (2023)

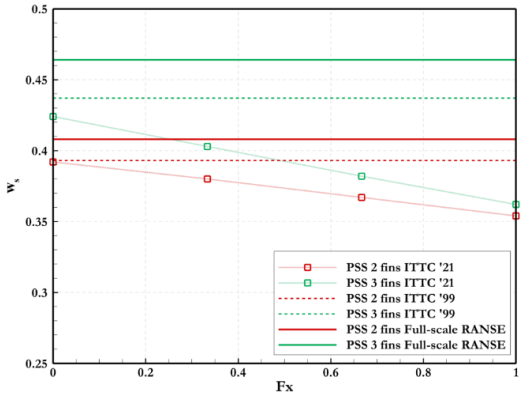

Figure 4 - Full-scale effective wake fractions (W_S) using several extrapolation methods compared to full-scale RANSE calculations; Influence of the axial/tangential coefficient of the ITTC 2021 procedure. JBC test case from ITTC Resistance and Propulsion Committee

The results of the CFD calculations showed that the coefficients suggested by the ITTC 2021 would benefit from further investigation. ITTC 2021 full-scale wake of DTC equipped with the pure swirling device (Pre-Swirl Stator) matches with the full-scale RANSE prediction with a weight of axial wake F_x equal to 0.18 (F_t = 0.82) compared to the 0.3 (and 0.7) suggested by the procedure. For the Japan Bulk Carrier, ITTC 2021 full-scale extrapolations are closer to fully resolved RANSE (Pre-Swirl Stator, regardless number of blades) when the axial component of the scaling procedure is set to 0. Mixed devices (Pre-Swirl Ducts) compare better with CFD when the axial component of the wake (which should be dominant due to the presence of the duct) is weighted by a factor equal to 0.1 (rather than the 0.7 of the procedure). Pure axial devices like the WED are substantially overestimated with respect to full scale RANSE analyses if compared to the results of the ITTC 1999 procedure.

Table 2 - Extrapolated and calculated full-scale wake fractions. (form factor = 0.094, C_A = 0, [1] F_X = 0.8, F_T = 0.2; [2] F_X = 0.3, F_T = 0.7; [3] F_X = 1, F_T = 0), DTC test case, from Nicorelli and Gaggero (2023)

	ITTC'78 (no ESD)	**ITTC'99 with ESD**
Reference	0.197	-
PSD 3p	-	0.245
PSS 3p	-	0.268
WED	-	0.194
	ITTC'21 with ESD	**Full-scale RANSE**
Reference	-	0.180
PSD 3p	0.224[1]	0.253
PSS 3p	0.262[2]	0.268
WED	0.203[3]	0.182

Table 3 - Extrapolated and calculated full-scale wake fractions. (form factor = 0.2, C_A = 0, [1] F_X = 0.3, F_T = 0.7), JBC test case.

	ITTC'78 (no ESD)	**ITTC'99 with ESD**
Reference	0.350	-
PSS 2p	-	0.414
PSS 3p	-	0.459
	ITTC'21 with ESD	**Full-scale RANSE**
Reference	-	0.313
PSS 2p	0.403[1]	0.408
PSS 3p	0.427[1]	0.464

Based on these results, which are not themselves conclusive due to the scarcity of configurations/combination of ESD and ship types, further investigations on the most appropriate extrapolation strategy for ship wakes affected by the presence of ESDs are recommended for future ITTC activities. Because of the difficulties of obtaining sharable geometries, a benchmark using available ships and non-commercial ESD designs would be preferred.

4. BENCHMARK STUDY ON THE EFFECT OR RE AT MODEL SCALE AND SCALING METHODS FOR FULL SCALE PREDICTION

The 28th ITTC initiated comparative CFD studies on conventional and unconventional (tip rake) propellers. A benchmark study, focusing on the effect of Re at model scale and on the scaling method for full scale, was proposed during the 29th ITTC as a task for the following ITTC. During the 30th ITTC, the benchmark was arranged and disseminated. Results collected by the Resistance and Propulsion Committee are collected in the following sections.

The two propellers adopted for the benchmark were, again, the VP1306 (aka PPTC) and the tip rake propeller P1727 (aka PPTC_2), kindly made available by SVA Potsdam (https://www.sva-potsdam.de/en/ittc-benchmark/). This choice was dictated by the availability of these geometries for easy sharing among participants. Additionally, several benchmarking activities have been already carried out on these propellers.

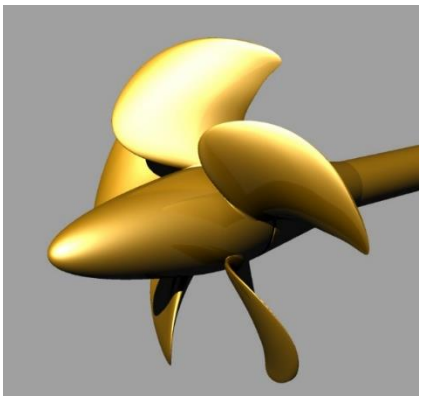

Figure 5 - 3D view of the PPTC propeller, "closed gap" version

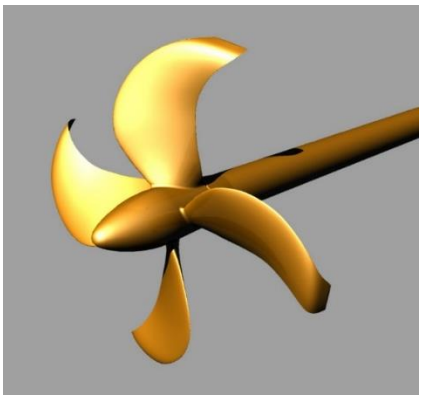

Figure 6 - 3D view of the PPTC_2 propeller, "closed gap" version

For the benchmark, contributors were requested to perform calculations at both model and full scale. Model scale results were collected for four different rates of revolution of the propellers, covering a relatively large range of testing conditions typical of towing tank/cavitation tunnel experiments.

Detailed instructions were provided to limit as much as possible uncertainties on the computational domain and numerical setup (domain size, use of transition sensitive turbulence model and turbulence intensity). Data were collected in dedicated questionnaires.

Table 4 - Functioning conditions – PPTC propeller

	Model Scale	*Full Scale*
Diameter [m]	0.25	3
rps	[10; 12.5; 15; 17.5]	4.33
Avg. Re $_{0.75r/R}$	0.6 to 1.05 $*10^6$	$36*10^6$

Table 5 - Functioning conditions – PPTC_2 propeller

	Model Scale	*Full Scale*
Diameter [m]	0.2386	7.5
rps	[12; 15; 18; 21]	3.21
Avg. Re $_{0.75r/R}$	0.36 to 0.64 $*10^6$	$86*10^6$

Only six institutions sent data. Since some of them performed analyses using different tools and setups (transition sensitive and fully turbulent models), in total 10 sets of results for the conventional and 8 for the non-conventional propellers are available. StarCCM+, Fluent,

CFX and OpenFOAM were the preferred computational tools for the analyses. MARIN used its in-house ReFRESCO code. Most of the calculations were presented using transition sensitive turbulence model (Gamma-based) with wall-resolved boundary layer (y+<<1) at model scale. Some participants sent data using only fully turbulent analyses at model scale, employing wall-functions (y+>40) and utilising only a limited number of prism layers. For transition sensitive analyses in most of cases the turbulence intensity was fixed equal to 1% on the propeller plane. For some participants, this was the value set at the inlet boundary, leading to a smaller value on the propeller plane due to decay. Other participants made use of decay controlling techniques (calibration of inlet value to achieve the required intensity on the propeller plane, turbulence intensity sources to counteract the turbulent decay). Only one participant performed calculations with a custom turbulence intensity (1.5%) based on its own experience.

Collected data were compared with model scale experiments (when available) and against each other. Scale effects were addressed by computing percentage differences of full-scale data ($_{fs}$) with respect to model scale ($_{ms}$) results:

The thrust and torque coefficient corrections are given by the following:

$$\Delta K_T = \frac{K_{Tfs} - K_{Tms}}{K_{Tms}}$$

$$\Delta K_Q = \frac{K_{Qfs} - K_{Qms}}{K_{Qms}}$$

The format of these formulae mean that a positive value of Δ corresponds to an increase in performance at full scale. Please note that this convention is opposite to what is typically assumed in ITTC procedures for scaling of the thrust coefficient.

Table 6 - Overview of the participants

Institute	VP1304	P1727
Samsung Heavy Industries	✓	✓
University of Genoa	✓	✓
INTA – CEHIPAR	✓	✓*
Akashima Laboratory	✓	✓
Japan Marine United Corporation	✓	✓
MARIN	✓*	

* not the entire set of rps

4.1 Results for the conventional propeller VP1304

The general trends of the results for the conventional propeller are similar to those observed by the 28th ITTC. By looking at the calculations at 15 rps, for which model scale experimental results are available from SVA POTSDAM, it is possible to observe a certain underestimation of thrust, which is more pronounced at higher advance coefficients. Calculations using transition sensitive models are generally closer to experiments while the few fully turbulent analyses tend to underestimate the thrust up to 10% at the design point (design advance coefficient of 1.269). Torque is generally better predicted. When transition sensitive models are employed the general trend is a slight overestimation at lower advance coefficients and a slight underestimation at high advance coefficients. Fully turbulent analyses under-predict the torque over almost the entire range of realistic conditions.

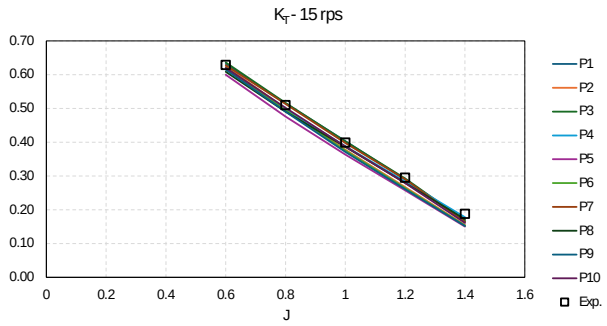

Figure 7 - Thrust coefficient at the rate of revolution (15rps) of experiments. Results for VP1304

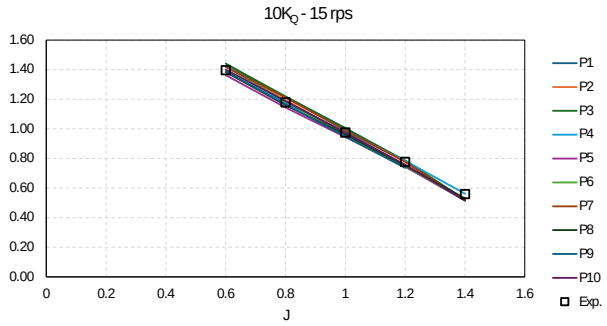

Figure 8 - Torque coefficient at the rate of revolution (15rps) of experiments. Results for VP1304

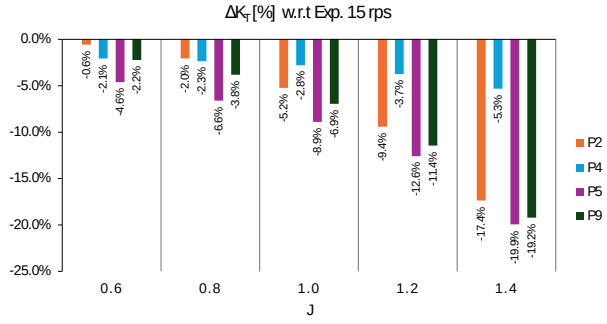

Figure 9 - Percentage difference (Thrust) with respect to experiments at 15 rps - fully turbulent analyses

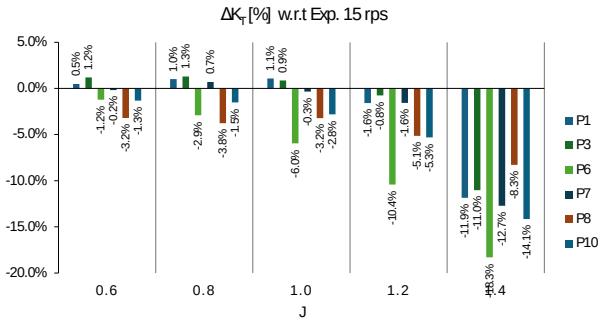

Figure 10 - Percentage difference (Thrust) with respect to experiments at 15 rps - transition sensitive analyses Results for VP1304

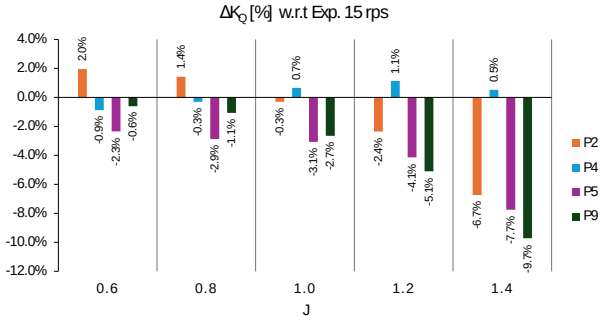

Figure 11 - Percentage difference (Torque) with respect to experiments at 15 rps - fully turbulent analyses

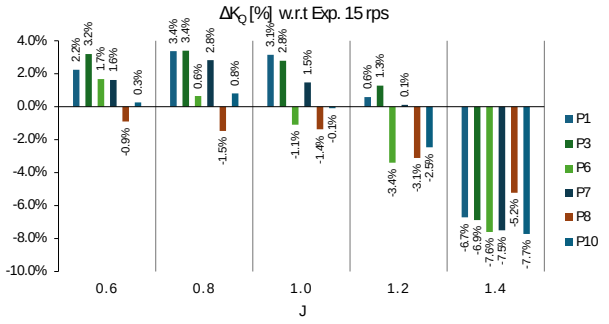

Figure 12 - Percentage difference (Torque) with respect to experiments at 15 rps - transition sensitive analyses Results for VP1304.

Full scale data seem to have less deviation for both thrust and torque, with the exception of two outliers (one significantly overestimated, one significantly underestimated).

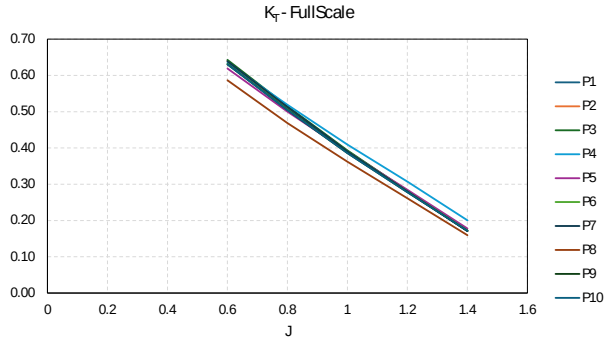

Figure 13 - Full-scale thrust coefficient of VP1304

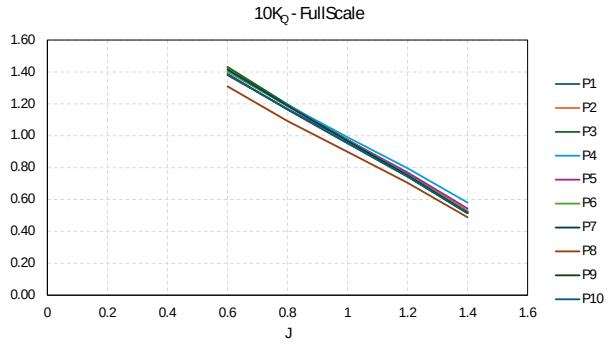

Figure 14 - Full-scale torque coefficient of VP1304

The resulting model-to-ship scaling is affected by non-negligible uncertainties, especially if the entire set of rotational rates is addressed. Two main features can be observed when relating data with the numerical models employed for the analyses. With the use of transition sensitive models (see data P1, P3, P7 and P8), model scale calculations, at most Reynolds numbers in the selected range, tend to predict values of model scale thrust and torque higher than those at full scale (using fully turbulent models). This results in scale corrections which are negative (based on the sign assumption of previous equations) for both thrust and torque. This is contrary to what is usually accepted (i.e. increased thrust and decreased torque at full-scale, due to the lower frictional coefficient). Reasons for this behaviour can be found in the "cambering effect" of radial streamlines, if laminar flow is occurring at model scale, which changes the lift coefficient of the blade sections. If significant laminar flow is present then abrupt separation characteristics can also cause a substantial increase in the sectional pressure drag. Transition sensitive calculations with the 1.5% turbulence intensity level (P10) mitigate this tendency, due to a large extension of the turbulent region at model scale, resulting in a model scale thrust that is more similar to the fully turbulent full scale data, at least for some loading conditions.

Scaling to full-scale, starting from model scale fully turbulent analyses, is in line with usual expectations, showing the generally accepted increase of thrust. Also, the values of torque are sometimes increased (whereas a decrease would typically be expected), but of a smaller amount compared to thrust, which then leads to an increase in the predicted open-water efficiency.

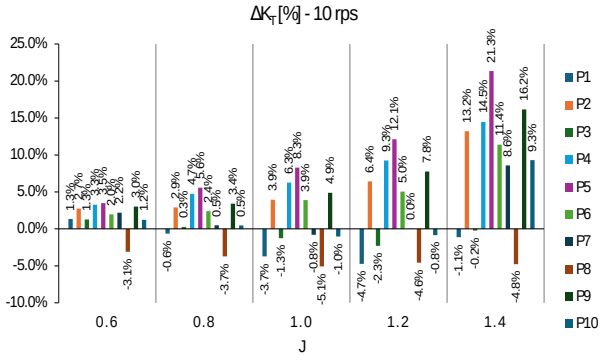

Figure 15 - Predicted scale effect (Thrust) for VP1304 at 10 rps (600 rpm)

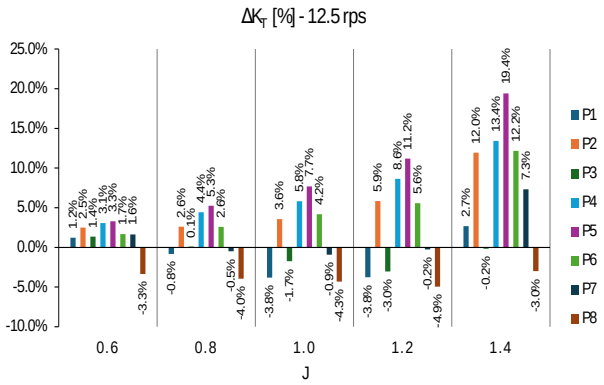

Figure 16 - Predicted scale effect (Thrust) for VP1304 at 12.5 rps (750 rpm)

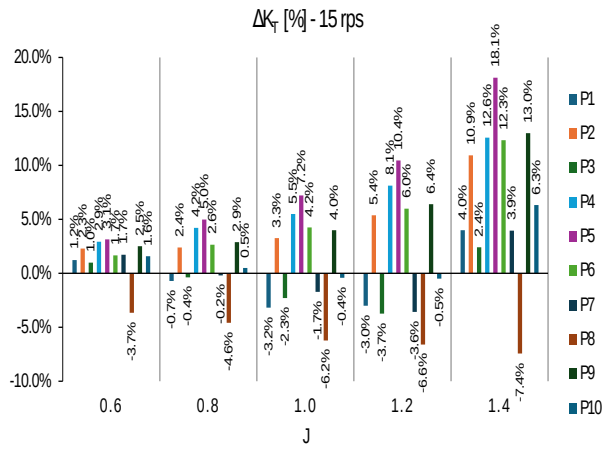

Figure 17 - Predicted scale effect (Thrust) for VP1304 at 15 rps (900 rpm)

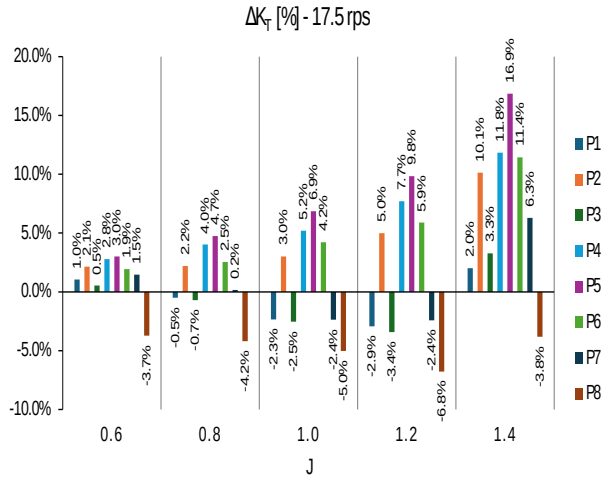

Figure 18 - Predicted scale effect (Thrust) for VP1304 at 17.5 rps (1050 rpm)

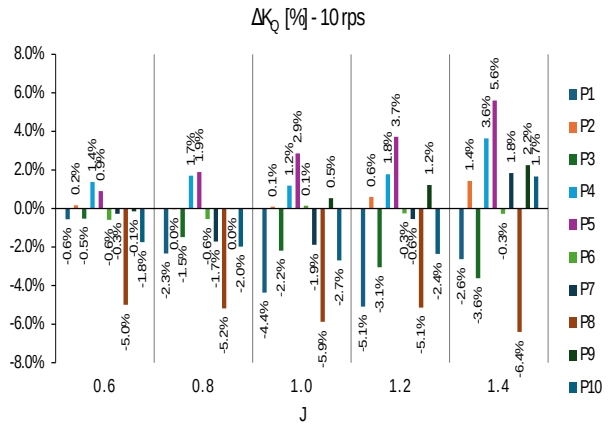

Figure 19 - Predicted scale effect (Torque) for VP1304 at 10 rps (600 rpm)

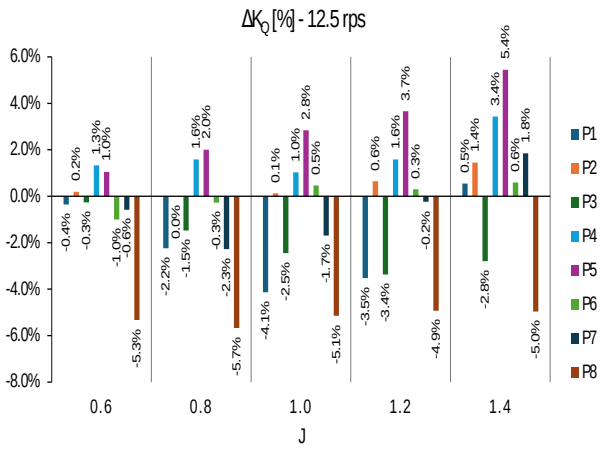

Figure 20 - Predicted scale effect (Torque) for VP1304 at 12.5 rps (750 rpm)

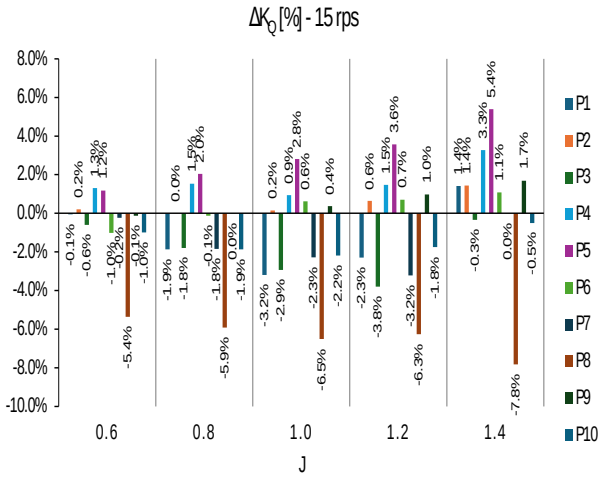

Figure 21 - Predicted scale effect (Torque) for VP1304 at 15 rps (900 rpm)

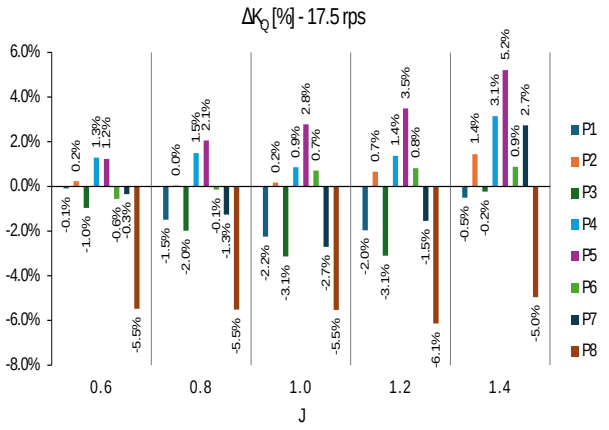

Figure 22 - Predicted scale effect (Torque) for VP1304 at 17.5 rps (1050 rpm)

Compared to usual ITTC-based scaling, CFD analyses generally overestimate the model-to-full scale effects by a significant margin. Regardless of the "sign" of the correction, numerical calculations predict variations between model and full scale of the order of 2-6%, on average, depending on J for both thrust and torque. ITTC '78 corrections are significantly lower, smaller than 0.2% (thrust) and 0.5% (torque) when computed using the suggested blade surface roughness of 30 x10^{-6} m (ITTC – Recommended Procedures and Guidelines - 7.5 – 02-03 – 01.4, effective date 2021 – rev. 05)

Also, when compared with data obtained having greatly reduced values of surface roughness (all the full scale CFD calculations were carried out using smooth surfaces, i.e. not employing roughness sensitive wall functions or corrections), the suggested scaled values from the ITTC procedure, especially for the thrust coefficient, are substantially lower than what is observed from the CFD calculations.

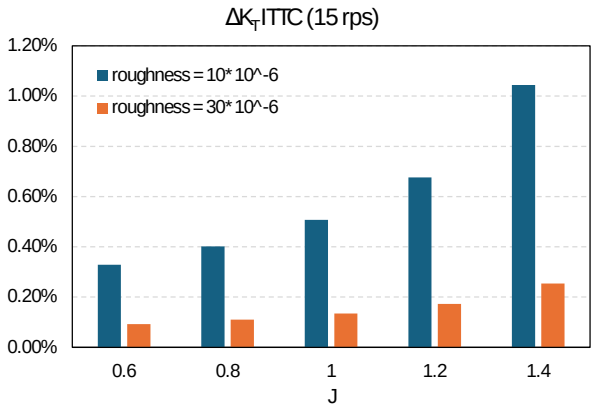

Figure 23 - ITTC scale effect (Thrust) for VP1304 at 15 rps (900 rpm)

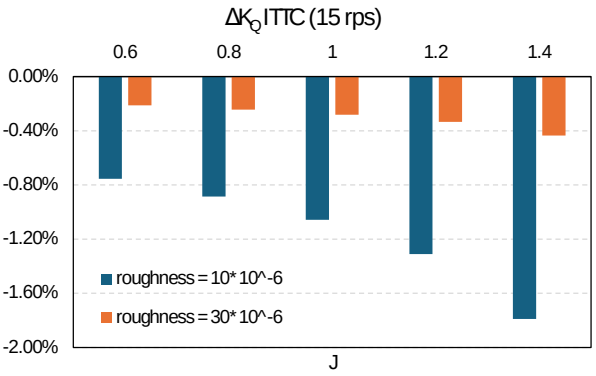

Figure 24 - ITTC scale effect (Torque) for VP1304 at 15 rps (900 rpm)

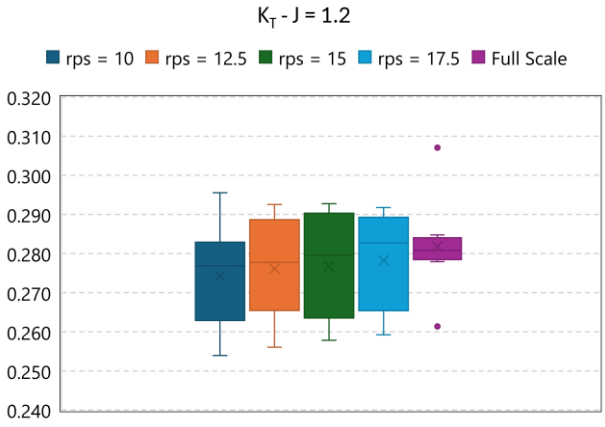

Figure 25 – Thrust coefficient statistics (mean/max/min/upper and lower quartile) at the design advance coefficient for VP1304

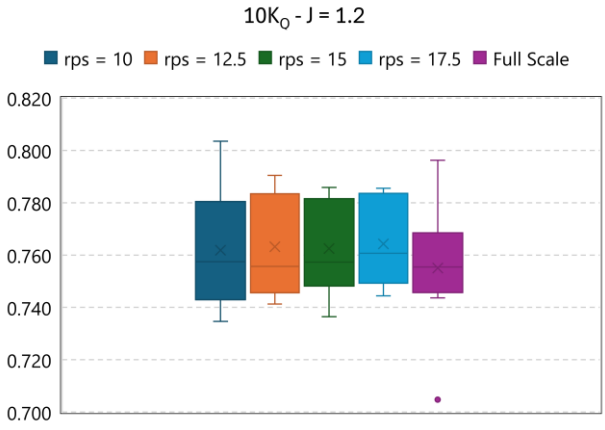

Figure 26 – Torque coefficient statistics (mean/max/min/upper and lower quartile) at the design advance coefficient for VP1304

4.2 Results for the unconventional propeller P1727

Results for the unconventional P1727 propeller confirm the trends observed for VP1304. Also, in this case, the comparison with the experimental data at 18 rps shows a certain deviation of calculations which, in this case, are equally over- and under- predicted. Overall, also for this propeller and its range of Reynolds numbers (lower than the previous tests case), calculations employing transition sensitive models are closer to experiments (1-2%) while fully turbulent calculations predict, on average, deviation up to 10% (underestimation) at the design point.

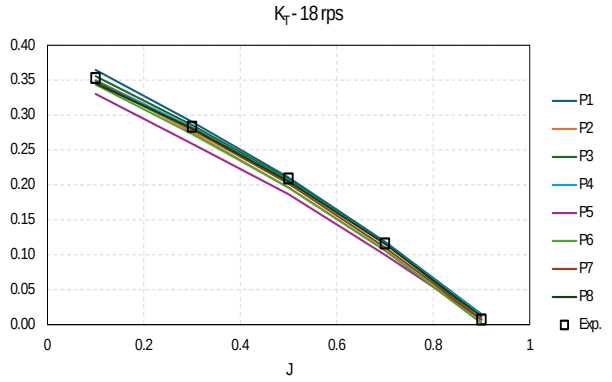

Figure 27 - Thrust coefficient at the rate of revolution (15 rps) of experiments. Results for P1727

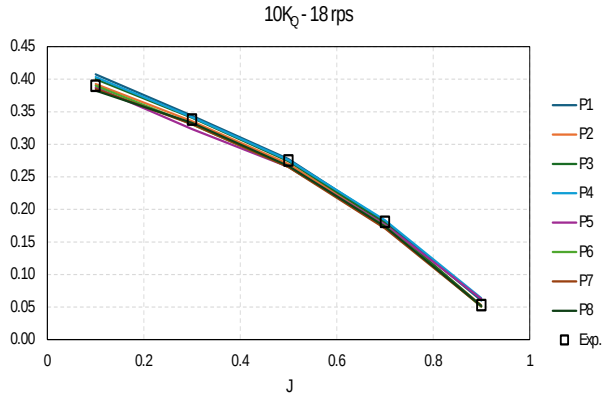

Figure 28 - Torque coefficient at the rate of revolution (15rps) of experiments. Results for P1727

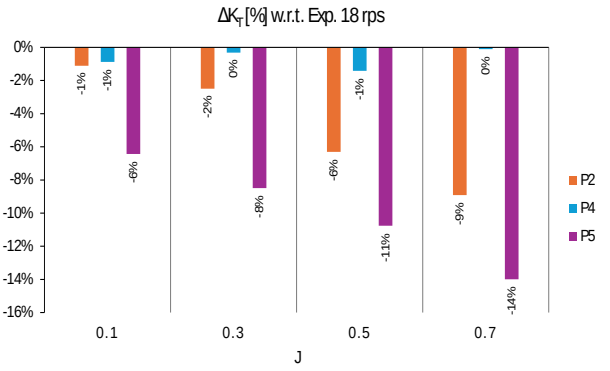

Figure 29 - Percentage difference (Thrust) with respect to experiments at 18 rps - fully turbulent analyses

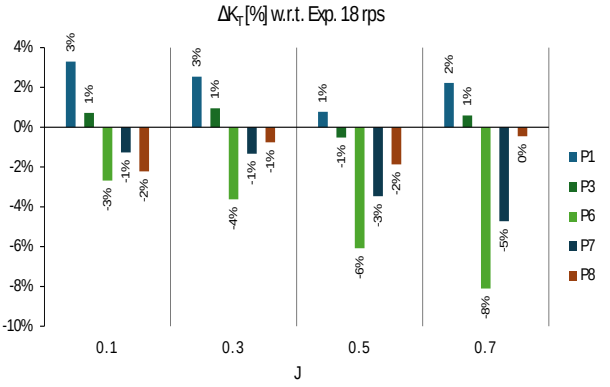

Figure 30 - Percentage difference (Thrust) with respect to experiments at 18 rps - transition sensitive analyses Results for P1727

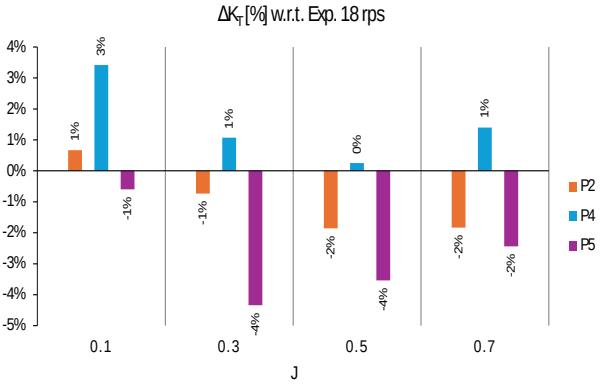

Figure 31 - Percentage difference (Torque) with respect to experiments at 18 rps - fully turbulent analyses

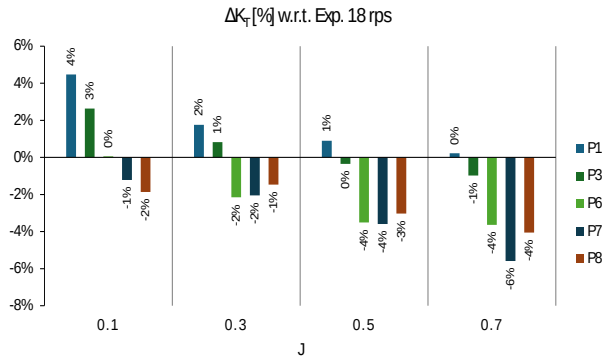

Figure 32 - Percentage difference (Torque) with respect to experiments at 18 rps - transition sensitive analyses Results for P1727

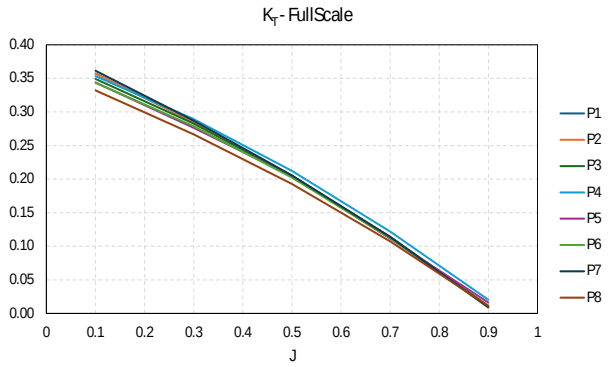

Figure 33 - Full-scale thrust coefficient of P1727

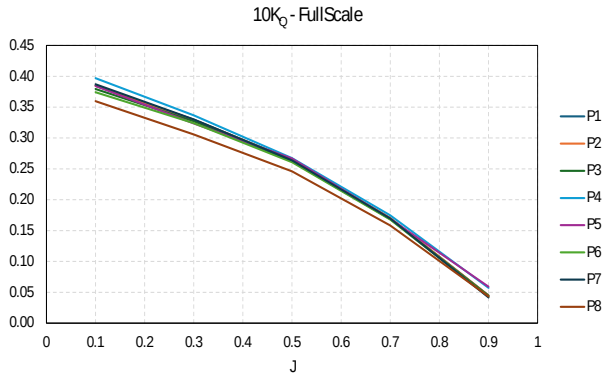

Figure 34 - Full-scale torque coefficient of P1727

In contrast, the full-scale data appear to be more scattered than what was observed for VP1304, which leads to even more complex trends. As a general statement, full scale scaling starting from fully turbulent model scale results shows increase of K_T and proportionally smaller Δ value (usually a decrease) of K_Q. Analyses with the transition sensitive models generally repeat the trends seen with VP1304. However, in some cases, it is possible to observe both decrease and increase of thrust correction from model to ship size as the advance coefficient varies, which is believed to principally due to the variation in Re as the rate of revolutions is varied..

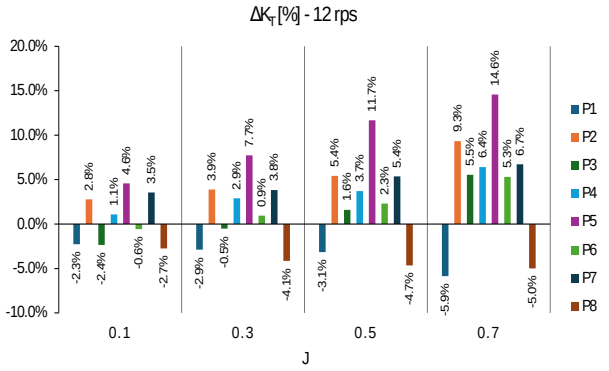

Figure 35 - Predicted scale effect (Thrust) for P1727 at 12 rps (720 rpm)

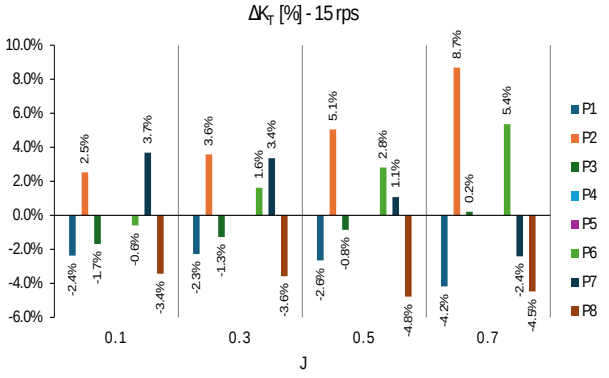

Figure 36 - Predicted scale effect (Thrust) for P1727 at 15 rps (900 rpm)

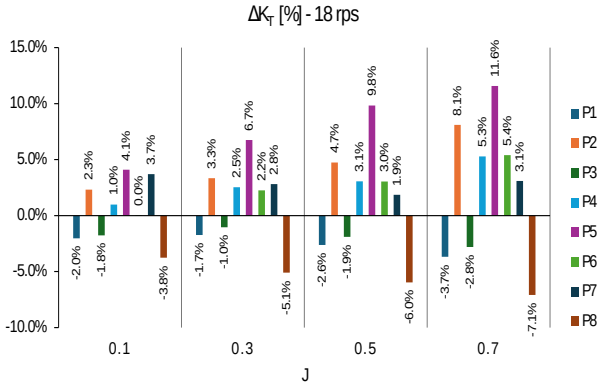

Figure 37 - Predicted scale effect (Thrust) for P1727 at 18 rps (1080 rpm)

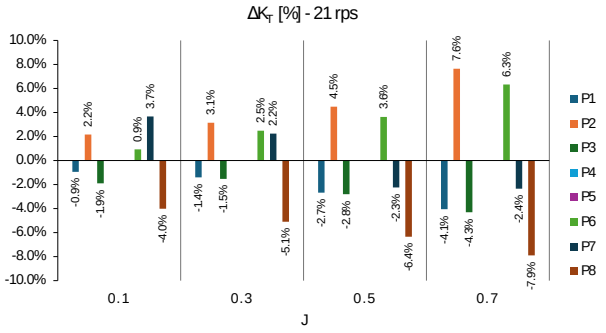

Figure 38 - Predicted scale effect (Thrust) for P1727 at 21 rps (1260 rpm)

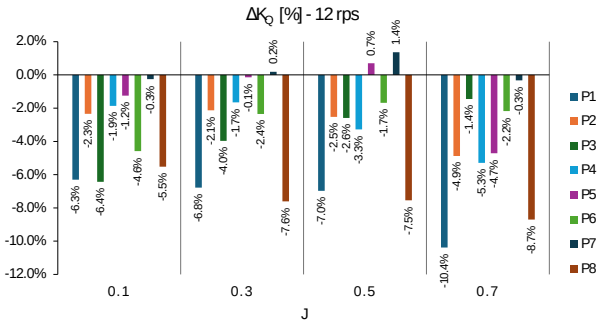

Figure 39 - Predicted scale effect (Torque) for P1727 at 12 rps (720 rpm)

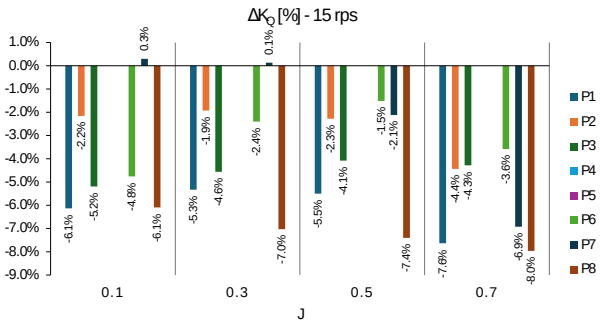

Figure 40 - Predicted scale effect (Torque) for P1727 at 15 rps (900 rpm)

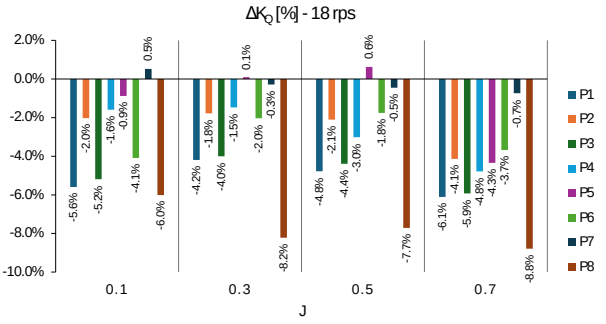

Figure 41 - Predicted scale effect (Torque) for P1727 at 18 rps (1080 rpm)

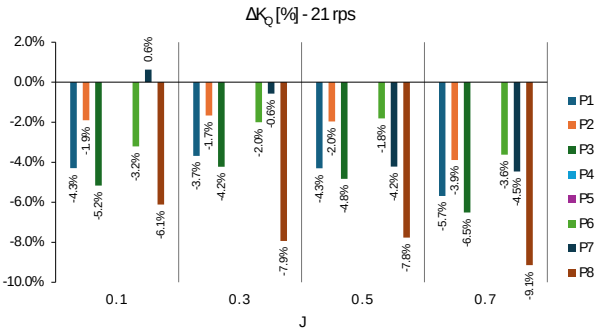

Figure 42 - Predicted scale effect (Torque) for P1727 at 21 rps (1260 rpm)

The comparison with the ITTC ’78 scaling method shows the same inconsistencies observed for the conventional propeller. CFD predicted scale correction are far higher than standard ITTC values which, even in the case of hydraulically smooth surfaces (closer to numerical calculations), are three or four times smaller.

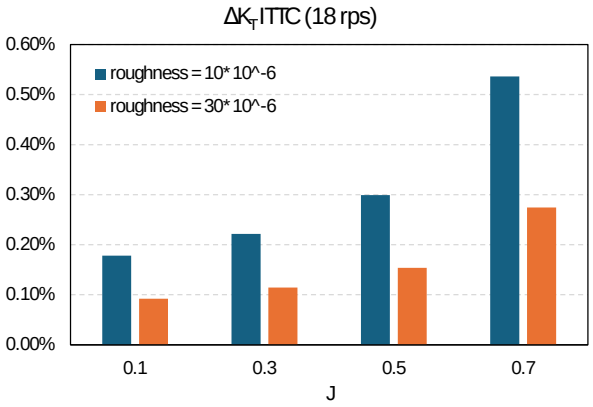

Figure 43 - ITTC scale effect (Thrust) for P1727 at 18 rps

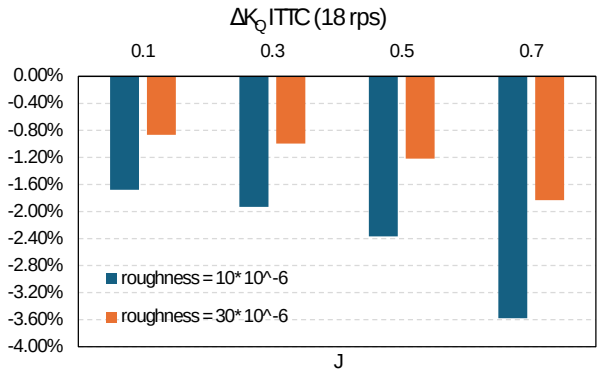

Figure 44 - ITTC scale effect (Torque) for P1727 at 18 rps

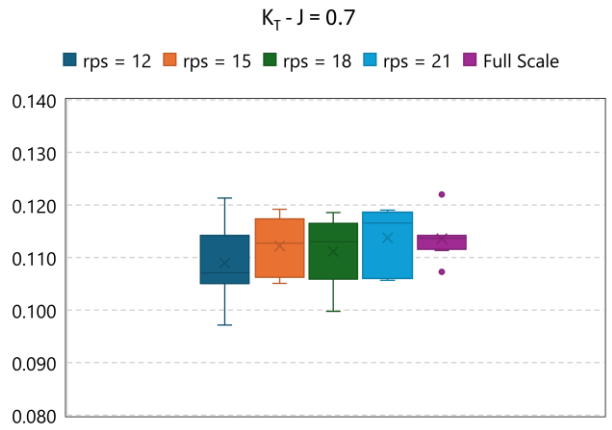

Figure 45 – Thrust coefficient statistics (mean/max/min/upper and lower quartile) at the design advance coefficient for P1727

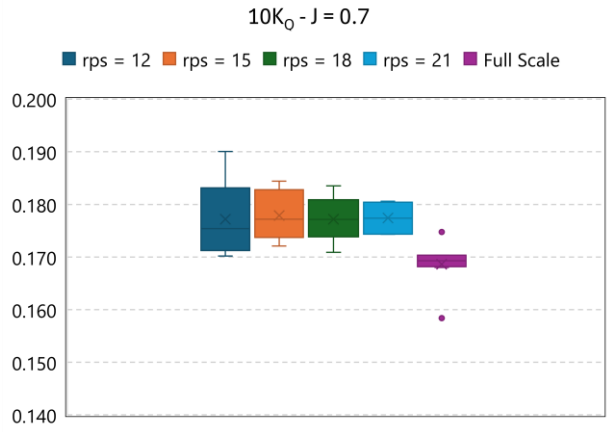

Figure 46 – Torque coefficient statistics (mean/max/min/upper and lower quartile) at the design advance coefficient for P1727

4.3 Final considerations

The analyses carried out for the geometries proposed by the benchmark show a certain number of small uncertainties, especially at model scale, that when taken in combination may lead to a significantly different assessment of the scaling effect. The use of transition sensitive calculations permits, in general, more accurate prediction of the model scale performance, since the underestimation of thrust and torque observed with fully turbulent analyses is substantially reduced. The high sensitivity to inflow conditions (not always available from experimental data) and the turbulence decay process (or how to control it), however, raise the question of whether an accurate full-scale prediction can be made from model-scale data (Kerkvliet *et al*. 2024) without knowing the results *a priori* (i.e. blade streamlines through paint flow tests or, more roughly, measured open water performance) for a calibration of the turbulence intensity parameters. The high sensitivity to turbulence intensity, shown in some additional calculations of the participants, as well as in recent papers (Gaggero, 2020, Rubino and Abdel Maksoud, 2024, Kerkvliet *et al*. 2024), may explain the unexpected behaviour of K_T and K_Q scaling behaviour when model scale calculations are performed at very low turbulence intensity and Re number without any feedback in terms of real behaviour of the flow over the blades. Slightly higher turbulence intensity may determine completely different scaling, moreover dependent on the propeller geometry, nullifying the efforts for a poorly calibrated numerically based scaling approach/tool. This makes the topic still worth of additional investigations. Better controlled model scale experiments to validate numerical tools (including measurement or recording of the inflow turbulence intensity level) may be useful. Fully-turbulent model scale measurements using non-intrusive tripping (Kerkvliet *et al*. 2024), on the other hand, may provide better characterization of the open water propeller performance thanks to the low numerical uncertainty and improved similarity with full-scale flow regimes.

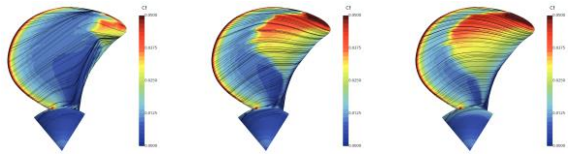

Turb. Int. = 1% Turb. Int. = 1.4% Turb. Int. = 1.8%

Figure 47 - VP1304 skin friction coefficient and streamlines at the design advance coefficient as a function of turbulence intensity (15 rps, from additional calculations of Participant 3).

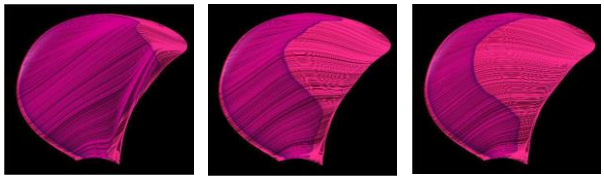

Turb. Int. = 1% Turb. Int. = 1.4% Turb. Int. = 2%

Figure 48 - VP1304 skin friction coefficient and streamlines at the design advance coefficient as a function of turbulence intensity (15 rps, from additional calculations of Participant 10).

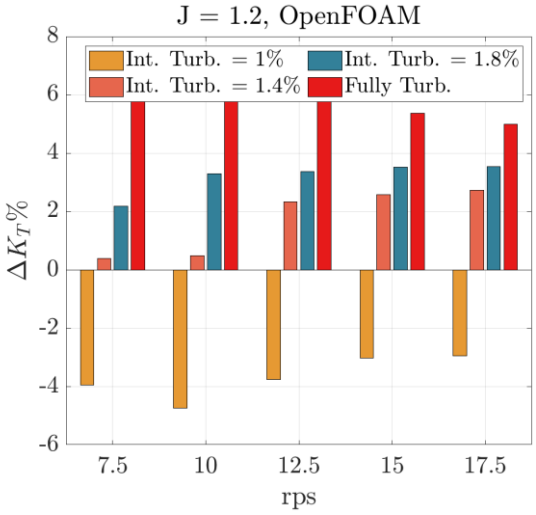

Figure 49 - Scale effect on thrust coefficient for VP1304 at the design advance coefficient as a function of rate of revolution and turbulence intensity at the propeller plane (from additional calculations of one of the participants).

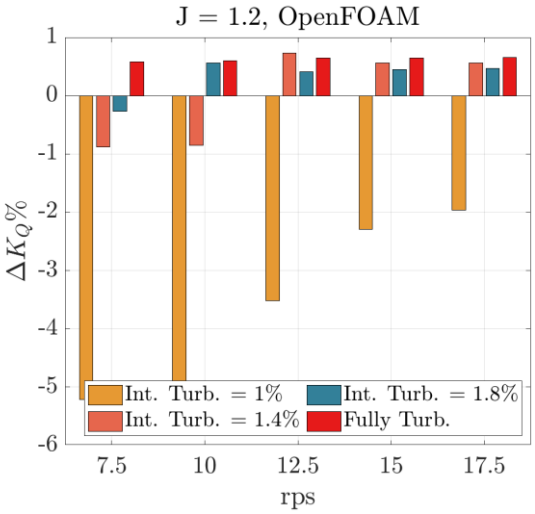

Figure 50 - Scale effect on torque coefficient for VP1304 at the design advance coefficient as a function of rate of revolution and turbulence intensity at the propeller plane (from additional calculations of one of the participants).

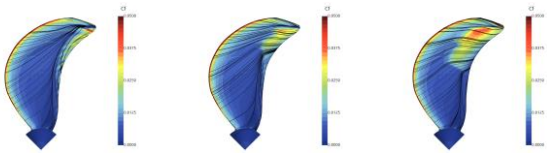

Turb. Int. = 1% Turb. Int. = 1.4% Turb. Int. = 1.8%

Figure 51 - P1727 skin friction coefficient and streamlines at the design advance coefficient as a function of the turbulence intensity (18 rps, from additional calculations of one of the participants)

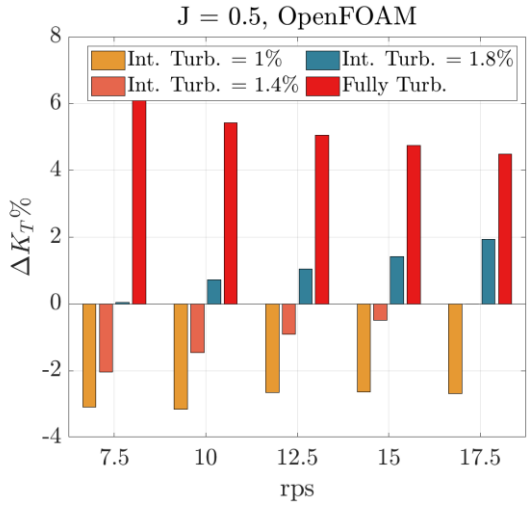

Figure 52 - Scale effect on thrust coefficient for P1727 at the design advance coefficient as a function of rate of revolution and turbulence intensity at

the propeller plane (from additional calculations of one of the participants)

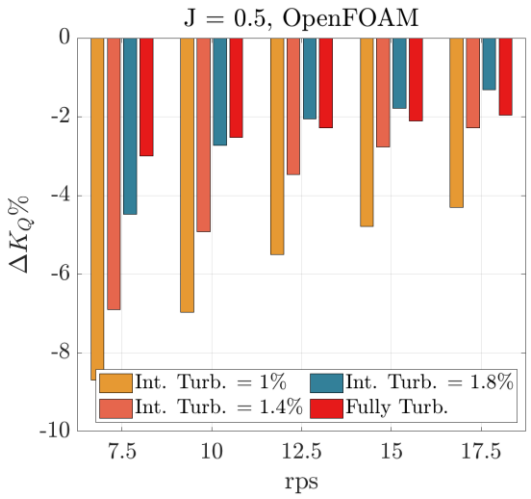

Figure 53 - Scale effect for P1727 at the design advance coefficient as a function of rate of revolution and turbulence intensity at the propeller plane (from additional calculations of one of the participants)

5. INVESTIGATION OF THE ISSUE OF LAMINAR EFFECTS IN SELF-PROPULSION TEST OF PROPELLER WITH LOW BLADE AREA

5.1 Introduction

Self-propulsion tests are often conducted at Reynolds Numbers (Re) lower than desirable, because many recent propellers have low blade area and short chord lengths in order to achieve high efficiency. The low Re can lead to an unexpected reduction in the calculated relative-rotative efficiency, η_R, which leads to difficulty when attempting to use the current scaling procedure as described in the ITTC '78 Performance Prediction Method.

While this is not a new problem, as there have been many discussions under previous ITTC committees, the trend towards low operating ship speeds and the pursuit of even smaller efficiency gains to reduce greenhouse gas emissions give this problem even greater importance in the current world.

Firstly, a survey was conducted to find out how ITTC members tackle this issue. Subsequently, a literature review was conducted, investigating how these low Re effects could be addressed.

5.2 Survey results

The committee conducted a survey on three topics: A) Self-Propulsion Test (SPT), B) Propeller Open water Test (POT) and C) Propeller scaling procedure. Fifteen organizations responded. The geographical region and organizational type of the respondents are shown below.

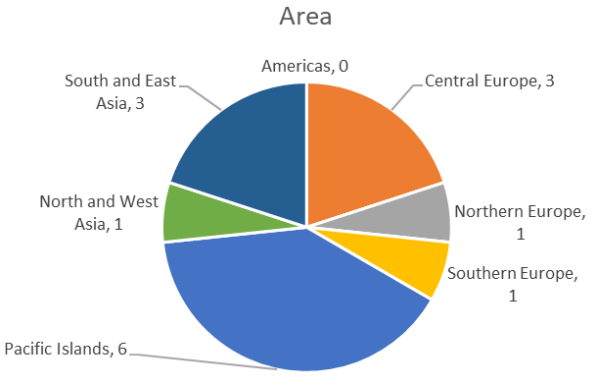

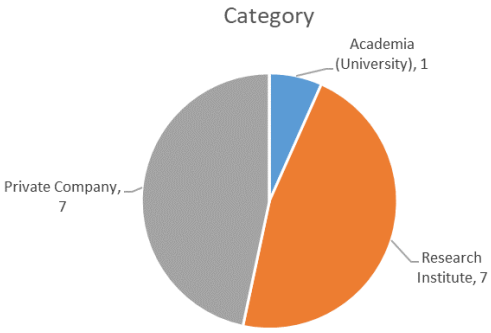

A. Self-propulsion test

A1. Have you ever had any problems with a self-propulsion test due to low Re?

- More than half of the respondents answered "YES".

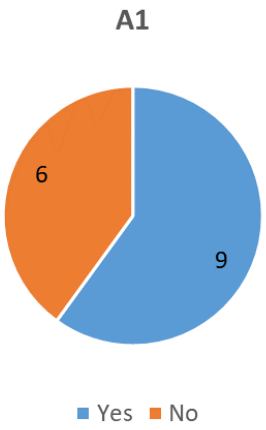

A2. Please let us know what problem you encountered and what Re was then.

- Self-propulsion factors, especially η_R, were unreasonable.
- Measurement values significantly scattered.
- Re was below 2×10^5.

A3. Please let us know how you dealt with the problem.

- Enlarge dimension of a ship model.
- Check with a conventional large blade area propeller.
- Check with a 2-POT method.
- The η_R obtained at the highest Froude number was used as a constant value.
- Apply a turbulent stimulator.

A4. Please let us know the typical value of length of the model ship, the diameter of the model propeller and the minimum speed of the model ship in a self-propulsion test, and whether a design propeller or a stock propeller was used.

- The length of model ranges from 4m to 12 m. Models of length 7 m to 8 m were most typical.
- The diameter of the model propellers range from 0.2 m to 0.3m.
- The minimum towing speed ranges from 0.8m/s to 2m/s. 1m/s being the most common.
- Most of the respondents use both stock and design propellers depending on the scale and extent of the testing programme.

A5. It is recommended in ITTC Recommended Procedure 7.5-02-03-02.1 that; *The propeller open water tests should be conducted at least at two Reynolds Numbers; one should be at the Reynolds Number used for the evaluation of the propulsion test, which should be not lower than 2×10^5 and the other should be as high as possible*. It is recommended that the open water characteristics at low Re are used to analysis the self-propulsion test. Do you follow the recommendation? If your answer is YES, please let us know which Re you select. (eg. The exact same as the self-propulsion test or specific value like 3×10^5 regardless of actual Re at self-propulsion test) If your answer is NO, please let us know the reason.

- Most of the respondents answered “No”.
- The flow in behind condition is assumed to be turbulent (i.e. different from POT).
- The database of model-ship correlations has been established based on the self-propulsion factors using the Propeller Open Water Characteristics (POWC) at the high Re.
- POT at multiple Re is expensive.
- The measurement values of the POW at the low Re are unsteady.
- There is no universal view which Re is appropriate to represent the behind condition.

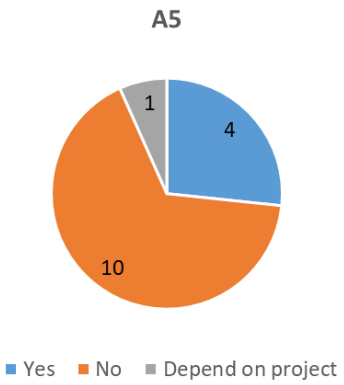

A6. Do you have any idea to solve problems with a self-propulsion test due to low Re?

- Carry out repeated tests and take longer measurements.
- Increase the size of a model ship.
- Use a 2-POT method.

- Use turbulence stimulators.
- Use a stock propeller with larger blade area.
- Carry out POT with simulated inflow turbulence (2-3% of turbulent intensity).

B. Open water test

B1. Have you ever had any problems with an open water test due to low Re?

- More than half of the respondents answered "NO".

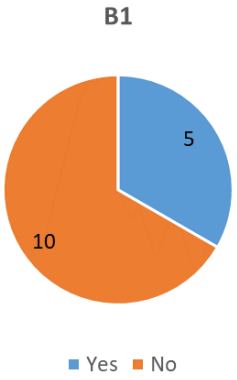

B2. Please let us know what problem you encountered and what the Re was.

- Poor reproducibility.
- Very different from the CFD simulation.

B3. Please let us know how you dealt with the problem.

- Use the most reasonable value from the repeated tests.
- Use turbulence stimulators.

B4. It is recommended in RP 7.5-02-03-02.1 that the open water characteristics at highest Re are used for full scale power prediction. Do you follow the recommendation?

- Most of the respondents answered "Yes".

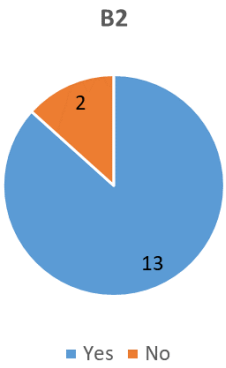

B5. Do you conduct an open water test at multiple Re each time in order to investigate the Re dependency?

- More than half of the respondents answered "Yes".

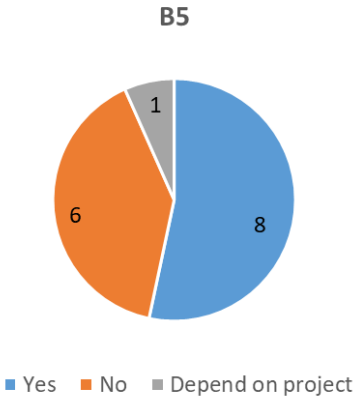

B6. Do you think the minimum Re, 2×10^5, in the present ITTC procedure is sufficient for obtaining the stable open water characteristics?

- More than half of the respondents answered "NO".
- Large laminar effect remains at Re of 2×10^5.
- The minimum should be higher than 5×10^5.
- Re should be above the transition from laminar to turbulent flow.
- A fixed value is not reasonable due to the plurality of different propeller designs.

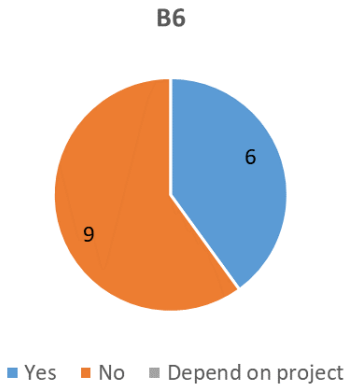

C. Propeller scaling procedure

C1. Do you scale an open water characteristics at model test for full scale power prediction?

- More than half of the respondents answered "NO".
- Model-ship correlation factors have been established based on the procedure using no scaled propeller open-water curve.
- There is no reasonable simple method considering the change of K_T.
- The propeller open-water curve at the highest Re can represent the full scale propeller open-water curve.

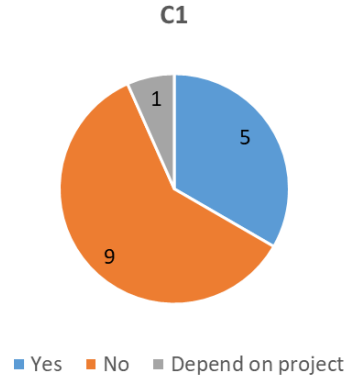

C2. Which kind of a scaling method do you use? (ex. ITTC-78, own procedure)

- All the respondents except one stated that they use the "ITTC '78 method".

C3. Please let us know on what Re is based when scaling.

- The highest Re

C4. Have you ever had any problems with scaling?

- Most of the respondents answered "NO".

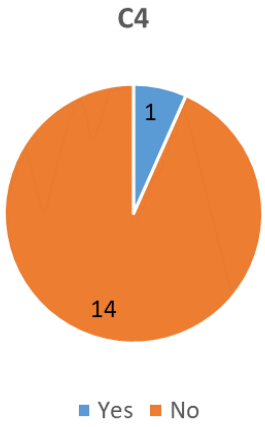

C5. Please let us know what problem you encountered and what Re was then.

- The scaled down propeller open-water curve did not correspond to the measured one at low Re.

C6. Please let us know how you dealt with the problem.

- Apply a 2-POT method.

Summary

According to the survey, more than half of the respondents have problems with the self-propulsion test, while not as many have problems with open-water test or the scaling method. Thus, the focus of the literature review was placed upon investigating the problems with the self-propulsion test. The problems that many organizations consider are as follows.

- Self-propulsion factors obtained, especially η_R, are unreliable.
- Measurement accuracy is reduced due to small measurement quantities.

Because the latter is highly dependent on the facility's dynamometer specification, the literature regarding the former was reviewed. The

problem arises from an inconsistence in the propeller characteristics, i.e. the boundary layer regime on the blade surface, between open water and behind condition.

Thus, the direct solution to this problem is to make the open water characteristics used for self-propulsion factor analysis as similar as possible to the behind condition.

There are two approaches. One is to use a 2-POT method and the other is to use turbulence stimulation techniques.

5.3 2-Propeller Open-water Test method

The 2-POT method uses the propeller open-water curve at the same or similar Re as the self-propulsion test for analysis of the model-scale self-propulsion data and then uses the high Re propeller open-water curve data to make the full-scale powering predictions. This method is based on the assumption that the flow characteristics on the blade in the behind condition are similar to those in the open water condition at the same or similar Re. In contrast, a 1-POT method uses the same high Re propeller open-water curve for both the self-propulsion analysis and the full-scale powering predictions.

The effectiveness of the 2-POT method has long been studied. One of the earliest studies was by Tamura et al (1977). They concluded that the 2-POT method is preferable to the 1-POT method to obtain reasonable self-propulsion factors, i.e. effective wake ratio and η_R, by observing the flow patterns on the blade in both the open water and behind conditions and by comparing the results against self-propulsion factors analysed using propeller open-water curve using turbulent stimulators.

More recent studies by Hasuike et al. (2017) and Lücke et al. (2017) were introduced in the report of the 29th ITTC Resistance and Propulsion committee (2021). They performed CFD calculations to investigate the flow on the blade, in addition to the paint tests included in many previous studies, and clearly showed the mixed state of laminar and transitional flow at model-scale, which is different from fully turbulent flow at full-scale. The superiority of the 2-POT method over the 1-POT method was confirmed by highlighting similarities in the flow regime between open water and behind conditions at low Re.

Li et al. (2019) investigated transitional flows and their impact on performance prediction. Similar to the studies by Hasuike et al. (2017) and Lücke et al. (2017), their study included propeller open-water test, self-propulsion test, paint flow visualisation tests and CFD analysis on three propellers: one with a small blade area and two with large blade areas. An unexpected decrease in η_R was only observed for the propeller with the smallest blade area when analysed using the 1-POT method. Although high turbulence intensity and inhomogeneous propeller inflow in behind condition may stabilize the flow on the blade, thereby delaying or preventing flow separation, they were probably insufficient to prevent separation for the smallest blade propeller, which had a steeper negative pressure gradient at the trailing edge than the large blade propellers. Analysing η_R using the propeller open-water curve at high Re with reduced flow separation could result in an unexpected reduction in η_R. They concluded that the reason for the too low η_R was not only the difference in Re between the propeller open-water test and the self-propulsion test, but also the difference in the degree of flow separation. The 2-POT method can be a solution to the issue of too low η_R, but they noted that careful calibration work is needed to identify an appropriate Re for the self-propulsion analysis, as Lücke et al. (2017) used propeller open-water curve data at 40% higher Re, considering the difference in flow characteristics between propeller open-water test and self-propulsion test.

Although various studies have shown the effectiveness of the 2-POT method, and it being recommended in the ITTC Recommended Procedure 7.5-02-03-02.1, many organizations don't use it for the reasons outlined in the survey results.

One of the reasons is the assumption that the flow in behind condition is fully turbulent, unlike in open water. However, this is not clearly supported by the aforementioned studies.

Challenges related to measurement precision for small quantities and inconveniences associated with changes in model-ship correlation factors may also contribute to the reluctance to use the 2-POT method. In addition, an unusual drop of η_R is not evident in all cases. As shown in Lücke et al. (2017) and Li et al. (2019), whether or not the reduction in η_R occurs depends heavily on the particular design of the propeller, e.g. blade area, section profile and chord width load distribution.

However, when the reduction in η_R does occur, the application of the 2-POT method can be highly beneficial. Therefore, it is recommended to perform the propeller open-water test at multiple Reynolds numbers, particularly for propellers with a low blade area ratios and short chord length sections.

5.4 Turbulence Stimulation

The second potential solution is a turbulent stimulator. Turbulence stimulation aims to create similar flow patterns on the blades in both open water and behind conditions and both at model-scale and full-scale conditions, i.e. encourage a fully turbulent flow regime.

As well as the 2-POT method described previously, the effectiveness of turbulence stimulation is well established and proven. The 14th ITTC Propeller committee (1975) investigated the influence of turbulence stimulation on self-propulsion factors and recommended as follows;

"*As mentioned above, not only the correlation method but also the test technique used in testing propellers are important to obtain good correlation between the ship and model. For that the propeller surface should have turbulent flow. Since it is difficult to perform the propeller open water test at a sufficiently high Rn, turbulence stimulation should be introduced for the propeller blades. Considerable work on turbulence stimulation has been devoted to model ships, but very little to model propellers. Cooperative work may be needed to obtain a standard method for stimulating turbulence on the propeller surface. Also, flow survey will be necessary on the propeller surface in the self-propulsion tests.*"

Around the same time as the 14th ITTC (1975), various research was conducted on turbulent stimulators, e.g. Suzuki(1974), Tamura et al. (1977), Tsuda et al. (1978), Ishii et al (1983). They reported the successful transition from a laminar flow to turbulent flow by applying trip wires, sand roughness and studs near the leading edge. Turbulent stimulators can stabilize values of η_R by ensuring consistent flow regime between the open-water test and the self-propulsion test and by mitigating changes in propeller open-water curve with Re. Contradicting these results, studies by Boorsma (2000) and Lücke et al. (2017) suggested that the presence of stimulators did not significantly alter the flow compared to conditions without them, remaining predominantly laminar. They showed that artificial roughening at the leading edge does not consistently induce turbulent flow at model scale. These contradictory results indicate the difficulty in determining the optimal size and location of turbulators, which are highly dependent on the propeller geometry. In addition to the uncertainty associated with making the flow turbulent, a significant decrease in efficiency due to turbulators themselves poses a practical obstacle to their use.

Addressing this issue, Bart Schuiling et al. (2024) introduced a novel turbulent stimulator as shown in Figure 54.

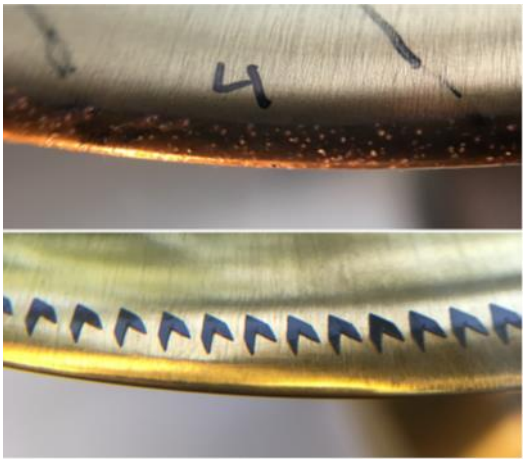

Figure 54 - Sand roughness (top) and novel turbulators (bottom), Bart Schuiling et al. (2024)

It is believed that this method can efficiently trip the flow from laminar to turbulent by generating vortices which resembles the hairpin-like vortical structures crucial to the boundary layer transition process, and with minimal additional drag. As shown in Figure 54 arch-shaped seals made from vinyl foil were attached discretely at the leading edge. Contrary to sand roughness widely used as stimulators on propulsors, the geometry of the turbulators can be accurately defined using CAD, which ensures precise and easy application. The paint test, which utilized also a novel technique using ultra-violet photography, revealed that applying the novel turbulators could successfully trip the flow as shown in Figure 55. They confirmed that the turbulators could mitigate the laminar flow separation for a small blade area propeller, resulting in a smaller change in efficiency as Re was varied. The parasitic drag of the elements was also investigated by varying the height of the element and it was found that penalty on both open water efficiency and thrust coefficient were typically of the order of 0.1% to 0.6%. Although not mentioned in the paper, the novel turbulence stimulators are expected to solve the problem with the prediction of too low η_R.

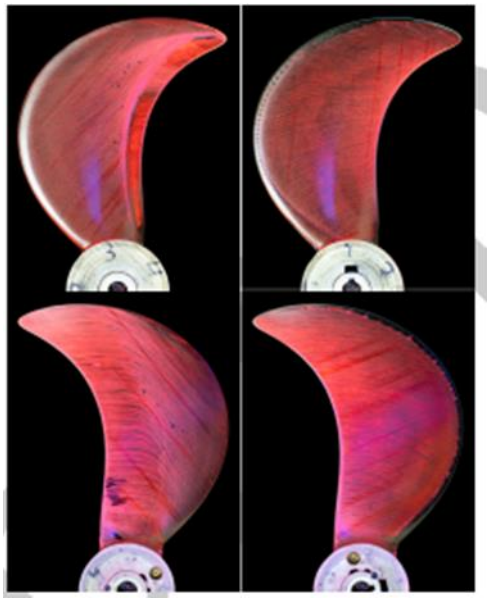

Figure 55 - Comparison of flow patterns without turbulators (left) and with turbulators (right), Bart Schuiling et al. (2024)

The introduction of a new technique is challenging because it requires a change in the model-ship correlation factors that each test facility has accumulated over time. However, accurately predicting full-scale performance and developing the most efficient full-scale propeller is crucial if the IMO's targets on reducing greenhouse gas emissions are to be met. MARIN, the organisation where Schuiling & Kerkvliet work, is running a Joint Industrial Project called "Tripping" to develop new scale corrections for propellers using their novel turbulators. According to the website of Tripping (2024), this project will involve extensive model testing and CFD simulation. This project is in line with the aforementioned recommendation by 14th ITTC Propeller committee (1975) and therefore deserves particular attention in the near future.

6. INVESTIGATION OF THE ISSUE OF EXTRAPOLOATION OF MODEL TESTS WITH DUCTED PROPELLERS TO FULL SCALE ACCORDING TO DIFFERENT REYNOLDS NUMBERS

Studies on the extrapolation to full scale of the performance of ducted propellers are particularly scarce. Only a few studies, based on CFD

calculations, are available (Bhattacharyya *et al.*, 2015, 2016a, 2016b) and are limited to propulsors equipped with accelerating nozzles (Nozzle 19A and Nozzle 37). No published data are available for decelerating nozzle configurations.

As one of the activities of the Resistance and Propulsion Committee, some additional CFD analyses on both accelerating and decelerating type ducted propulsors were carried out. Following the guidelines of the benchmark on open propeller performance scaling, the investigation accounted for the influence of turbulence models, turbulence intensity and model scale rate of revolution for two geometries available within the Committee and taken from the EU Funded BESST Project (Gaggero *et al.* 2013).

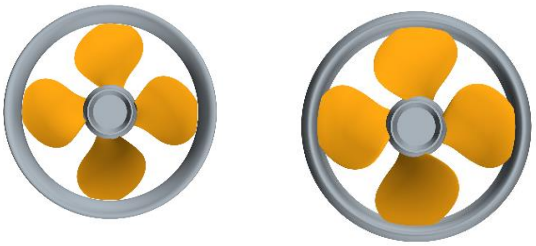

Figure 56 - Accelerating (left) and decelerating (right) ducted propellers

Analyses were repeated at model scale using the fully turbulent SST k-ω turbulence model and the γ-Reθ turbulence sensitive method (three levels of turbulence intensity at the propeller plane). Four advance coefficients at five different choices of rate of revolutions were considered to investigate the influence of propeller loading in a range of functioning conditions typical of model scale experiments. Full-scale values were obtained only using the fully turbulent model.

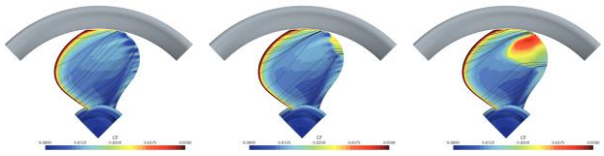

Turb. Int. = 1% Turb. Int. = 1.4% Turb. Int. = 1.8%

Figure 57 - Accelerating ducted propeller: skin friction coefficient and streamlines at the design advance coefficient as a function of the turbulence intensity (15 rps)

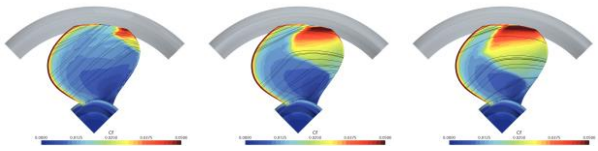

Turb. Int. = 1% Turb. Int. = 1.4% Turb. Int. = 1.8%

Figure 58 - Decelerating ducted propeller: skin friction coef-ficient and streamlines at the design advance coefficient as a function of the turbulence intensity (15 rps).

The limited analyses on ducted propellers show very similar trends and the complexity of phenomena observed for the open propellers. Also, in this case there is a strong influence of the inflow conditions on the model scale predicted performance which make the realization of robust scaling methodologies based on model scale CFD a very demanding task and require, first of all, detailed and accurate model scale measurements to understand the role of flow turbulence.

For this choice of geometries, the accelerating ducted propeller seems less prone to transition to turbulence, even at relatively high values (1.8%) of turbulence intensity estimated in correspondence of the propeller disk. This corresponds, as in the case of open propellers, to computed values (transition sensitive models) of thrust realized by the propulsor blades that are substantially higher at model scale than at full scale.

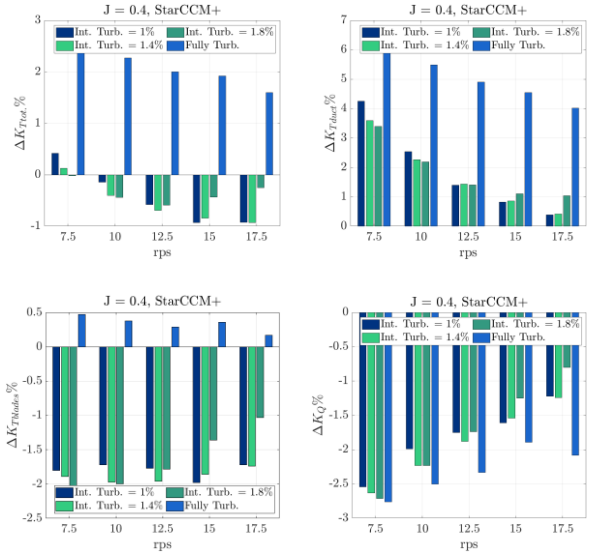

Figure 59 – Scale effect at J = 0.4 for the Accelerating ducted propeller (total thrust, thrust of the duct alone, thrust of the blades alone, total torque)

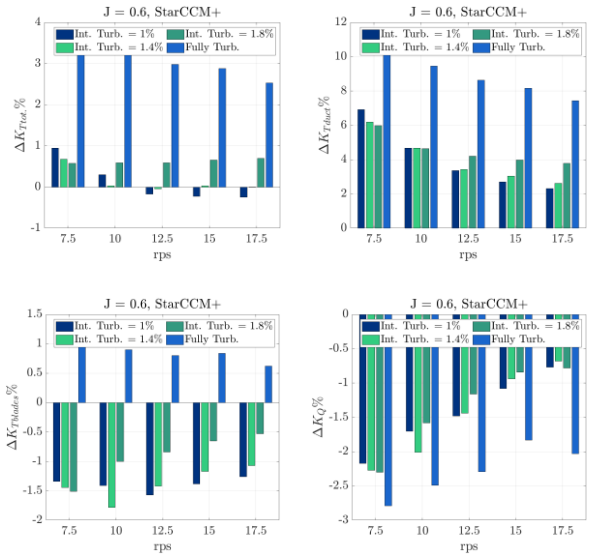

Figure 60 – Scale effect at J = 0.6 for the Accelerating ducted propeller (total thrust, thrust of the duct alone, thrust of the blades alone, total torque)

This trend is less evident for the decelerating ducted propeller, for which a reduction of the delivered thrust is observed only for combinations of very low turbulence intensity levels at highly loaded conditions (low J). In contrast, at high J values, when the decelerating nozzle produces a resistance and the increase of the static pressure inside the duct is higher, the scaling of torque change signs.

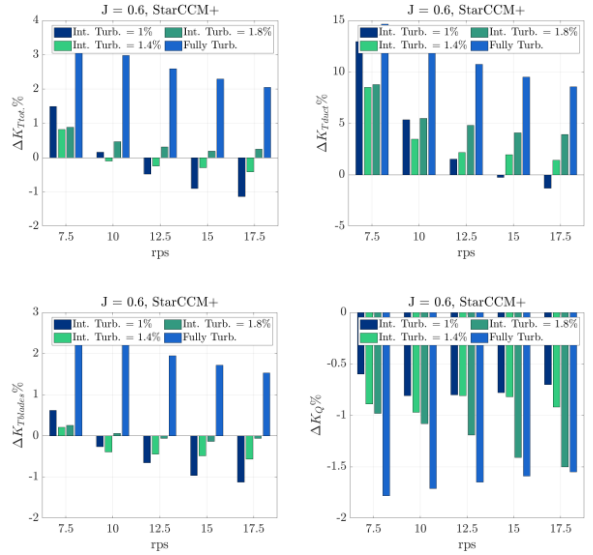

Figure 61 – Scale effect at J = 0.6 for the Decelerating ducted propeller (total thrust, thrust of the duct alone, thrust of the blades alone, total torque)

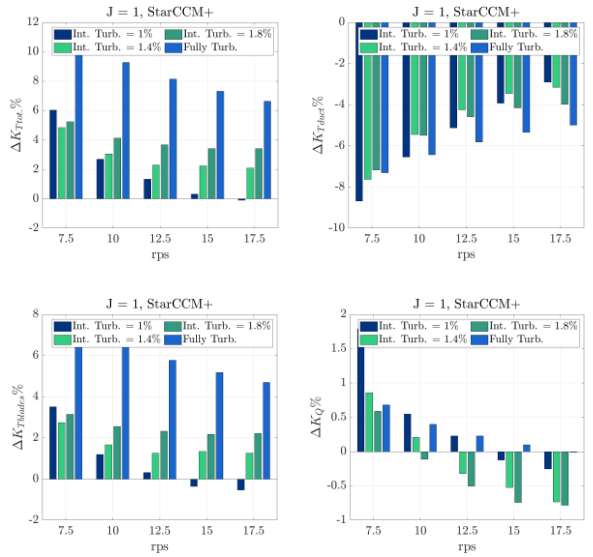

Figure 62 – Scale effect at J = 1.0 for the Decelerating ducted propeller (total thrust, thrust of the duct alone, thrust of the blades alone, total torque). Note that at J = 1 the duct produces a drag

7. UPDATE OF THE LOAD VARIATION TEST METHOD IN 1978 ITTC PERFORMANCE PREDICTION METHOD

7.1.1 Introduction

The Load Variation Test is carried out to assess the variation of propulsion performance such as the efficiency, speed of revolution, propeller torque and thrust due to a change of the ship's resistance for a particular speed.

In the current procedure 7.5-02-03-01.4, the rate of revolutions is varied to provide a self-propulsion point corresponding to the calm water resistance plus an additional allowance of between -10 to +20%. However, there is concern that this range may be insufficient, according to the new Minimum Propulsion Power requirements of the IMO. It is suggested that the appropriate range may be different according to the application fields and ship type, size and draft. Therefore it is necessary to re-examine the recommended range of the Load Variation Test.

The results of Load Variation Test can be applied to the following scenarios.

- Speed/power trials
- Operational performance
- IMO Minimum propulsion power
- IMO EEDI f_w

The characteristics of the application fields are summarized in Table 7. In this review, the most appropriate range for the Load Variation Rest is investigated in the speed/power trial condition.

Table 7 - Characteristics of application fields for load variation test

Application fields	Speed	Environment	Testing stage	Analysis
Speed/power trials	65~100% of MCR	BF5~6	Sea Trials	Real seas -> calm water
Operational performance	Operation range	Depends on operation area	Sea Trials	Real seas -> calm water
Minimum propulsion power	2knots	BF7~8	Design stage	Calm water -> real seas
EEDI fw	≒design speed	BF6	Design stage	Calm water -> real seas

7.1.2 Methodology

The speed and power trial study investigated 19 ships across 4 different types and a range of appropriate sizes, as shown in Table 8. Design and ballast drafts were selected as test conditions at each trial speed corresponding to NCR.

Table 8 - Ship types and sizes

Type	Size (Δ or capacity)
Bulker	10, 60, 176 k Te
Tanker	37, 50, 75, 115, 157, 320 k Te
Container	3600, 8600, 11000, 20000 TEU
Gas Carrier	4, 12, 80, 138, 174, 200 k Te

For environmental disturbance, wind and wave loads were considered. The detailed conditions of environmental load calculation are summarized in Table 9.

Table 9 - Conditions of environmental load calculation

Item	Value
Significant wave height	Visual observation limit*
Modal wave period	Statistics on North Pacific ocean (Bales, 1983)
Wave direction	0~180deg
Wave spectrum	ITTC spectrum
Irregular wave type	Long crested
Added resistance formula	STAWAVE2*, SNNM*
Wind speed	Statistics on North Pacific ocean (Bales, 1983)
Wind direction	0~180deg
Wind resistance coefficient	ITTC chart

*Recommended ITTC Procedure 7.5-04-01-01.1

When using the SNNM formula in the range $\lambda/L < 0.3$, the value of the added resistance coefficient at $\lambda/L = 0.3$ was used instead of the value from original formula. This was done because it is difficult to validate the empirical formula for $\lambda/L < 0.3$ due to limitations on measurement accuracy. Furthermore, the full-scale values of added resistance coefficient at short wavelengths can be lower than that measured at model-scale (Sigmund and Moctar (2018)), as illustrated in Figure 63.

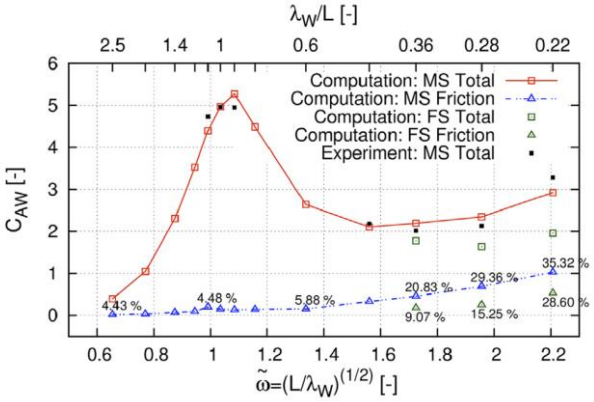

Figure 63 Computed and measured coefficients of total and frictional added resistance at model and full-scale (Sigmund and Moctar, 2018).

7.1.3 Results of speed & power trials investigation

The calculation results are shown in Figure 64 to Figure 67 and Table 10 to Table 11. Although there are differences depending on the type of ship and the method of analysing the added resistance in waves, the maximum added resistance ratio is typically about 30% and the minimum added resistance ratio is typically about -3.5%. In these tables R_0 denotes the resistance in calm water.

Table 10 – Max. added resistance ratio ($\Delta R_{max}/R_0$)

Method		Range [%]	Avg. [%]
Wind	Wave		
ITTC chart	STAWAVE-2	16~36	27
ITTC chart	SNNM	19~40	32

Table 11 – Min. added resistance ratio ($\Delta R_{min}/R_0$)

Method		Range [%]	Avg. [%]
Wind	Wave		
ITTC chart	STAWAVE-2	-7.3~-1.5	-4.1
ITTC chart	SNNM	-5.7~1.3	-3.0

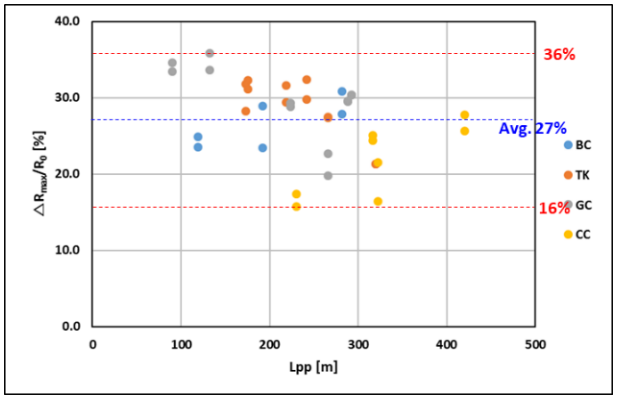

Figure 64 Max. added resistance ratio (STA-WAVE-2)

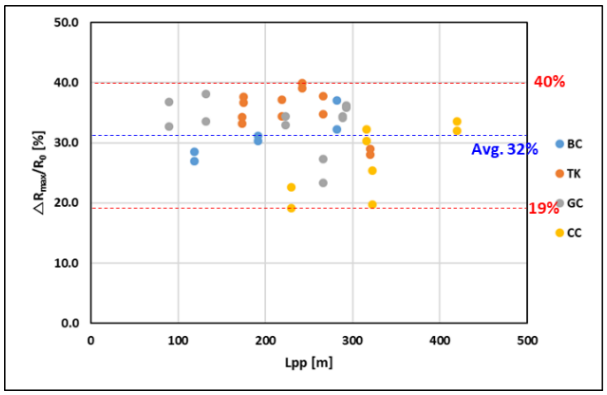

Figure 65 Max. added resistance ratio (SNNM)

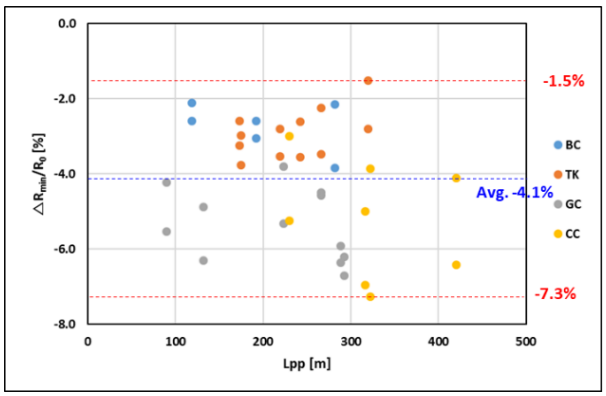

Figure 66 Min. added resistance ratio (STAWAVE-2)

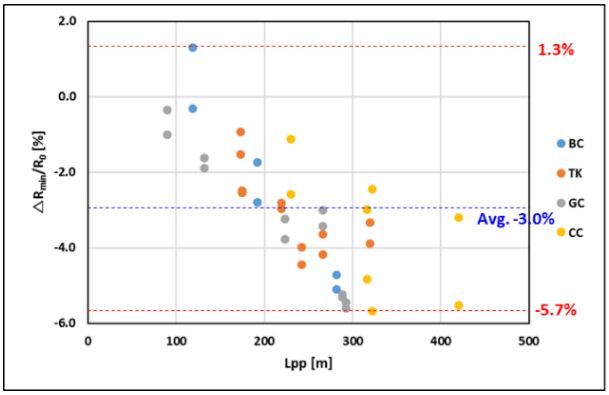

Figure 67 Min. added resistance ratio (SNNM)

There is no clear trend in the maximum added resistance according to the length of the ship. This is because as the length of the ship increases, the significant wave height and wind speed determined by the visual observation limit also increases. The difference due to a change in draft of a vessel does not appear to be particularly large, because, as draught reduces from the design condition to the ballast condition the windage area increases by a corresponding amount. The resulting increase in the wind resistance compensates, to some degree, for the decrease in the added resistance in waves.

7.1.4 Conclusion

The range of the Load Variation Test in Procedure 7.5-02-03-01.4, when applied to the analysis of speed/power trials, should be adjusted so that its maximum limit is 40% of the resistance in calm water.

7.2 Investigation of Self-propulsion Factors for Evaluation of Minimum Propulsion Power in Adverse Conditions

7.2.1 Introduction

IMO MEPC has been regulating the minimum propulsion power by providing a guideline to ensure safe operation of ships in adverse conditions since 2013, when EEDI began to be applied. The guideline has been revised several

times and the adverse conditions are defined according to the length between perpendiculars of the ship, as shown in Table 12.

Table 12 - Definition of adverse conditions

Ship length [m]	H_S [m]	T_P [s]	V_W [m/s]
Less than 200	4.5	7.0 to 15.0	19.0
200 ≤ L_{PP} ≤ 250	Linear interpolation		Linear interpolation
More than 250	6.0		22.6

*H_S is significant wave height, T_P is peak wave period, and V_W is mean wind speed.

The guideline suggests two assessments:

- Assessment level 1 – minimum power lines assessment
- Assessment level 2 – minimum power assessment.

If it fulfils either of these assessments then the ship is considered to have sufficient power. These assessments are applied to bulk carriers, tankers and combination carriers with a size equal to or greater than 20,000 DWT.

In assessment level 2, the default conservative values for self-propulsion factors are provided as $w = 0.15$ and $t = 0.1$. These values were suggested by China, as shown in in Figure 68 (see reference IMO MEPC 72/5/9), and adopted to the guideline at MEPC 76. To check whether the default conservative values are reasonable, the model test was performed in KRISO, through the following method.

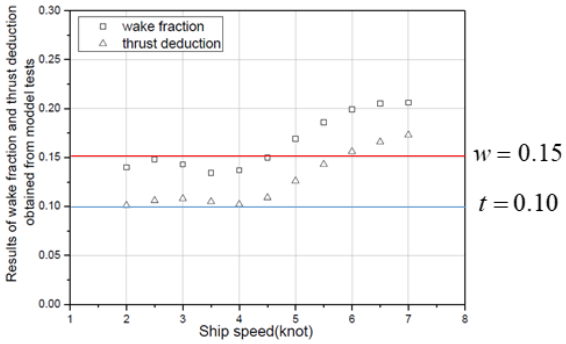

Figure 68 - Model test results of wake fraction and thrust deduction factor at low speeds (IMO MEPC 72/5/9, 2018)

7.2.2 Test conditions of self-propulsion for minimum propulsion power assessment

Test conditions for evaluating minimum propulsion power are similar to load variation test in that they evaluate propulsion performance considering realistic seaway, but the degree of load change and advance speed are significantly different. And the results of load variation test are normally used for speed/power trial correction, which converts propulsion performance from real seas to calm water. However, evaluating minimum propulsion power has the opposite process of converting from calm water to real seas.

Table 13 - Comparison of test conditions

	Load variation test	Minimum propulsion power
Advance speed	Normally corresponding to 65% ~ 100% MCR	2knots
Load range ($\Delta R/R_0$)	-10 ~ 20%	≫1,000%
Conversion	From real seas to calm water	From calm water to real seas

The model test under low speed of 2 knots and highly overload condition is similar to the model test in ice condition. For the evaluation of minimum propulsion power, the model test is carried out through the overload test defined in

ITTC Recommended Procedures 7.5-02-04-02.2 (Propulsion Tests in Ice).

7.2.3 Method to obtain self-propulsion factors

For the evaluation of minimum propulsion power, self-propulsion factors of full-scale ships are required. The self-propulsion factors of model-scale are obtained from the model test results with the advance speed applying Froude similarity and extrapolated to full-scale.

By the following assumptions, it can be obtained the self-propulsion factors of full-scale at 2 knots.

- The correlation between towing force (F_X) and thrust (T_M) is linear. The towing force measured during self-propulsion is equal to the resistance of the model ship when the measured propeller thrust is zero at low speed range.
- The flow characteristics of the propeller blade in self-propelled condition is defined only by the propeller Reynolds number, ignoring the turbulent flow characteristics developed along hull surface.
- The thrust deduction factor is considered as constant for the variations of the propeller loading.
- As advance speed decreases, the boundary layer thickness increases due to the decrease of Reynolds number and the effect of ship wave can be ignored.

To find the self-propulsion point, the following equation is used to calculate the towing force considering the skin friction correction and the additional resistance.

$$F_X = F_{D,skin} - \frac{R_{Add}}{\lambda^3}\frac{\rho_M}{\rho_S} \quad (1)$$

In the above equation, R_{Add} is the added resistance of full-scale at 2 knots. The value is calculated from the guideline for minimum propulsion power. The added resistance in adverse conditions is, in general, significantly larger than the calm water resistance at 2 knots.

The thrust deduction factor is obtained according to 1978 ITTC method.

$$t = \frac{T_M + F_X - R_C}{T_M} \quad (2)$$

Using the assumptions, the thrust deduction factor also can be obtained using linear relation of the thrust and the towing force.

$$t = 1 + \frac{\Delta F_X}{\Delta T_M} = 1 + 1/\left(\frac{\Delta T_M}{\Delta F_X}\right) \quad (3)$$

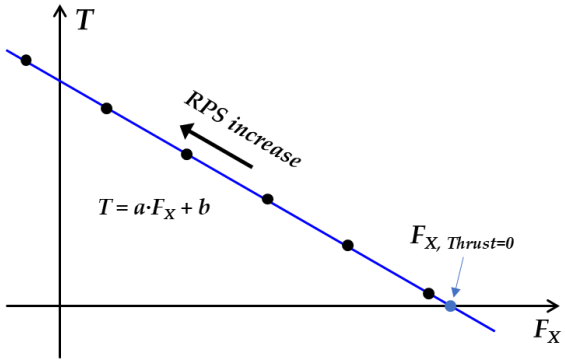

Figure 69 - Correlation between towing force and thrust

When calculating wake fraction of model-scale, it shall be used that the test results of propeller open water with propeller Reynolds number same as that in self-propulsion test. Propeller Reynolds number is defined in ITTC Recommended Procedure 7.5-02-03-02.1 (Open Water Test).

$$Re_{0.7} = \frac{c_{0.7}\sqrt{V_A^2 + (0.7\pi nD)^2}}{\upsilon} \quad (4)$$

For calculating propeller Reynolds number in self-propulsion test, the wake fraction is assumed initially and then an iterative calculation is performed until the wake fraction and propeller Reynolds number converge. In the iterative calculation process, test results of propeller open water with various propeller Reynolds number and advance ratio are also used.

The wake fraction in full-scale is obtained according to 1978 ITTC method with w_{TM} and t.

7.2.4 Characteristics of self-propulsion factors in adverse conditions

To investigate the characteristics of self-propulsion factors, KVLCC2 (300,000 DWT tanker) and KSUPRAMAX (66,000 DWT bulk carrier) were used. Propeller Open Water (POW) tests at various blade Reynolds numbers were performed, and the characteristics of wake fraction were analysed using two different POW results. One is the POW results with the high propeller Reynolds number (High $Re_{0.7}$), which is normally used for the extrapolation to full-scale. The other is that of the lower Reynolds number ($Re_{0.7}$) matched with the Reynolds number of the self-propulsion point during the propulsion test.

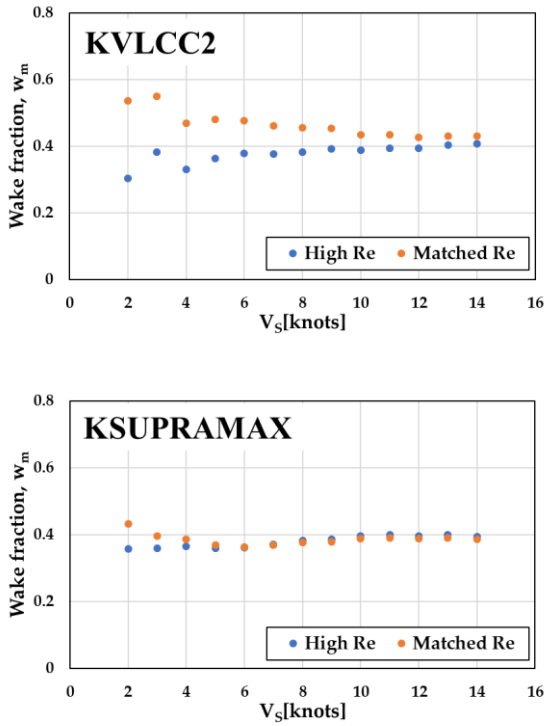

Figure 70 - Calculated wake fraction at model-scale

From the results of Matched $Re_{0.7}$ in Figure 70 it was confirmed that the wake fraction in model-scale increased at low speed range, which was consistent with the previous assumption.

To evaluate the minimum propulsion power, the self-propulsion factors calculated by the results of Matched $Re_{0.7}$ are extrapolated to full-scale.

As shown in Figure 71, the wake fraction and thrust deduction factor showed the same tendency in full-scale. As the speed decreased, the self-propulsion factors also decreased. However, comparing the results with the values at 2knots suggested in the guideline, the wake fraction is higher than $w = 0.15$ and the thrust deduction factor is lower than $t = 0.1$.

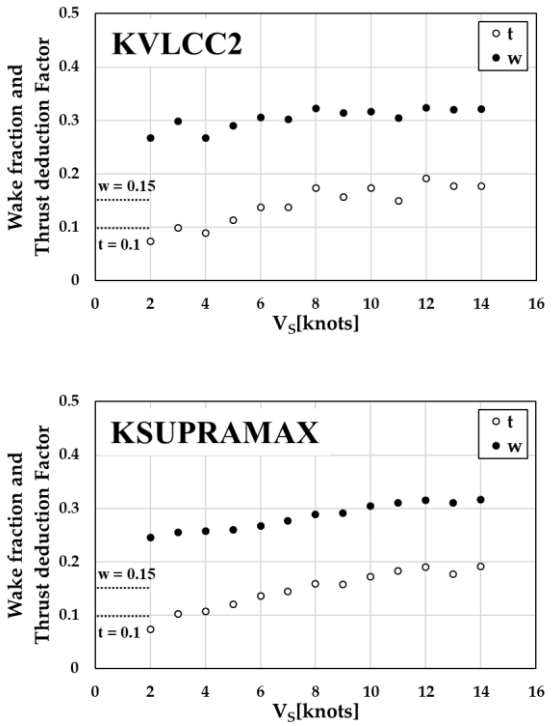

Figure 71 - Calculated wake fraction at full-scale

As shown in Table 8~9, the minimum propulsion power was evaluated using the self-propulsion factors from model test. And the assessment result was compared with that of the self-propulsion factors from the guideline. The required brake horsepower deduced from the model tests less than that of the guideline by about 5% in the both ships.

Table 14 - Minimum propulsion power assessment for KVLCC2

Item [unit]	Guideline	Model test	Diff.
X_S [kN]	35	35	
X_W [kN]	339	339	
X_d [kN]	824	824	
X_r [kN]	40	39	
X_T [kN]	1,238	1,237	
EHP [kW]	1,274	1,273	
J [-]	0.123	0.109	
w [-]	**0.150**	**0.268**	
t [-]	**0.100**	**0.075**	
η_O [-]	0.193	0.171	
η_H [-]	1.059	1.264	
η_R [-]	1.000	1.000	
η_D [-]	0.205	0.216	
RPM	43.1	42.2	-2.2 %
T [kN]	1,375	1,337	-2.8 %
Q^{req} [kN-m]	1,391	1,347	-3.2 %
P_B^{req} [kW]	**6,282**	**5,949**	**-5.3 %**

Table 15 - Minimum propulsion power assessment for KSUPRAMAX

Item [unit]	Guideline	Model test	Diff.
X_S [kN]	15	15	
X_W [kN]	188	188	
X_d [kN]	334	334	
X_r [kN]	18	17	
X_T [kN]	555	555	
EHP [kW]	571	571	
J [-]	0.114	0.103	
w [-]	**0.150**	**0.246**	
t [-]	**0.100**	**0.074**	
η_O [-]	0.171	0.155	
η_H [-]	0.159	1.228	
η_R [-]	1.000	1.000	
η_D [-]	0.181	0.190	
RPM [rev/min]	76.6	75.0	-2.1 %
T [kN]	617	599	-2.9 %
Q^{req} [kN-m]	398	386	-3.0 %
P_B^{req} [kW]	**3,191**	**3,031**	**-5.0 %**

8. INVESTIGATION OF THE REQUIREMENTS FOR TESTING AND NUMBERICAL EVALUATION OF HIGH-SPEED MARINE VESSELS

The Committee discussed the requirements for testing and numerical evaluation of high-speed marine vessels and addressed the need to update the relevant procedures.

Attention focussed on specific needs associated with properly manufacturing, measuring and reporting the transom radius geometry. Namely, the Committee reviewed synergetic experimental and computational studies (see Lee et al., 2021) highlighting the effect that the transom radius has upon the running trim and sinkage of the model. In this regard, it was found useful to recommend that the model manufacturer should pay particular attention, when finishing the model, to ensure that geometric features including boundaries of transom sterns remain well-defined with sharp edges. It was also recommended that the model documentation should include details of transom sterns and record the transom radius.

Accordingly, revisions were made to the relevant procedures, namely ITTC Recommended Procedure and Guidelines 7.5-01-01-01 Ship Models and 7.5-02-05-01 High Speed Marine Vehicles Resistance Test.

9. INVESTIGATION OF MEASUREMENT AND PREDICTION METHODS FOR BREAKING WAVES

9.1 Introduction

Even though ship resistance in calm water can be well predicted, it is still challenging to accurately resolve the flow field, especially for the breaking wave phenomenon of high-speed surface ships. For a large-scale ship, the bow wave is usually unstable and irregular, which is

often accompanied by wave breaking and intense water-air mixture. Therefore, the problem of bow wave breaking is one of the main focuses (Li et al. (2022b)).

As shown in Figure 72, depending on the shape of a bow and for sufficiently high ship speeds, spilling and/or plunging breaking occurs, inducing vortices and scars. The waterline entrance angle and ship speed are thought to have a considerable impact on the breaking type of bow waves. Depending on the appearance of stability at the crest, the breaking waves can be classified as plunging breaking waves or spilling breaking waves (see reference Olivieri et al. (2007), Jin (2022)).

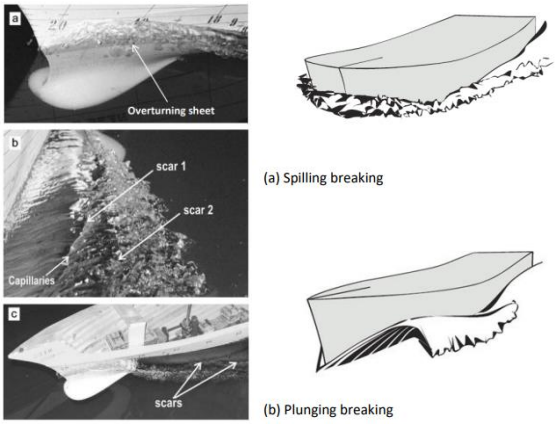

Figure 72 - Bow breaking waves & Classification of the bow wave breaking, Olivieri et al. (2007), Jin (2022)

For task 13 of the 30th ITTC Resistance & Propulsion committee, a literature study was undertaken to investigate the measurement and prediction methods for breaking waves. The literature search focused on resistance and propulsion papers published in the last 5 years containing keywords; 'breaking waves', 'bow wave', 'ships', etc.. The reviewed papers were broken down into two categories; experimental observations and numerical simulations.

9.2 Experimental observations

Vera Hengelmolen et al. (2022) studied the effect of bow wave breaking on added resistance by combining visual observations with resistance tests. Their research introduced a dynamic waterline detection method involving stereo vision, to capture the relative wave elevation in the bow region of the ship. By placing stereo camera arrangements inside the hull of a semi-transparent ship, the waterline can be tracked using an edge detection algorithm at each moment in time. By performing resistance tests on the Delft Systematic Dead rise Series ship model no. 523, the added resistance was observed to be proportional to the relative wave height squared. Figure 73 shows the experimental setup of relative wave height measurements and Figure 74 shows the example of the waterline detection and waterline mapped to be plotted on the 3D hull model.

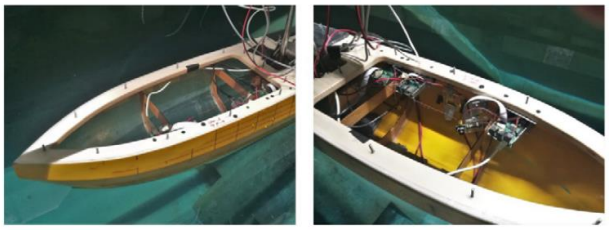

Figure 73 - Experimental setup of wave height measurement, Vera Hengelmolen et al. (2022)

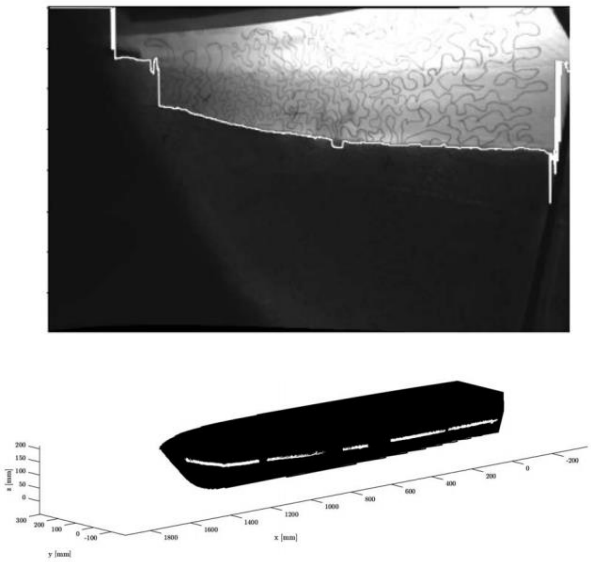

Figure 74 - Waterline detection, Vera Hengelmolen et al. (2022)

Mallat et al. (2022) summarized the breaking wave bubble measurement around ship model

using an optical probe measurement and PIV technique. Using an optical probe they locally measured the size and the velocity of the bubbles generated by breaking waves around a ship model in calm water and regular waves in a circulating flume tank. They also performed a comparison with more classical bubble detection results obtained using image tracking methods. They suggested that the two methods provide complementary results for bubble characteristics. Figure 75 shows the experimental setup of the bubble measurement study by using optical probe and PIV cameras. Figure 76 show a time sequence of images of the same taken over one wave period viewed from the bottom of the circulating flume tank. The tip of the optical probe is visible on these figure (green circle).

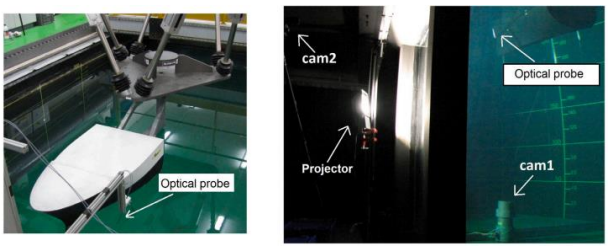

Figure 75 - Experimental setup, Mallat et al. (2022)

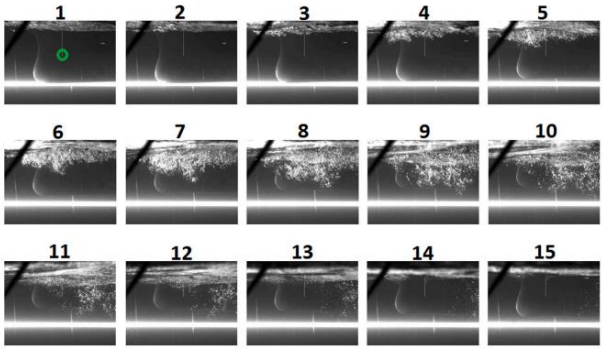

Figure 76 - Images in the (x,z) plane from camera for a wave period with bubbles, Mallat et al. (2022)

Jacobi et al. (2022) presented velocity measurements using PIV, together with a reconstruction of hydrodynamic pressures for the analysis of fast ships. Stereoscopic PIV measurements with a towed underwater PIV system were conducted during towing tank tests to obtain the velocity field in the bow region of a fast ship at speeds up to Fr=0.8. Figure 77 shows the ship model mounted to a hexapod next to the stereoscopic PIV system.

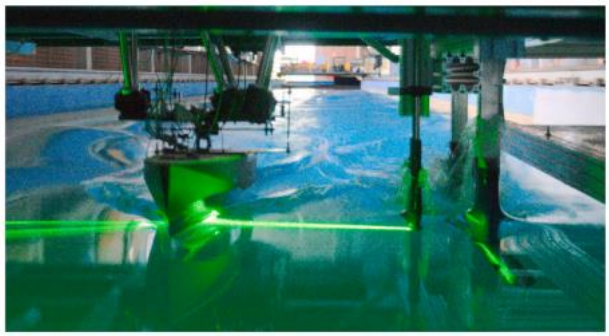

Figure 77 - Experimental setup, Jacobi et al. (2022)

They implemented the post-processing procedure for the pressure reconstruction, including the solution of the Poisson equation, into the open-source CFD package OpenFOAM. Their results show that the PIV method is capable of capturing the flow characteristics in the bow region of a fast ship and, in addition, that it can be used together with the pressure Poisson equation to obtain the hydrodynamic pressure field. The pressure fields reconstructed from the velocity field captured by the PIV system are presented in Figure 78, where they are compared to the numerical results for three selected time-steps during the downward motion of the ship hull.

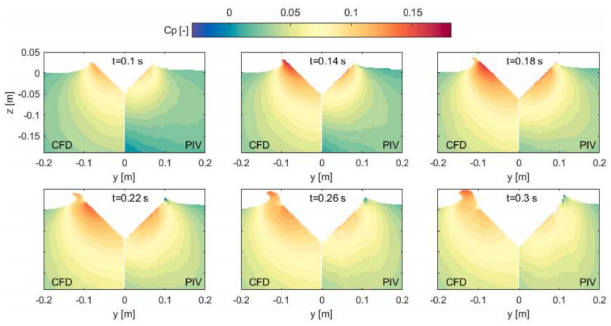

Figure 78 - Distribution of phase-averaged pressure fields at six selected time instants during the downward motion of the ship model, performing oscillatory motions at f = 1 Hz with an amplitude of a = 0.035 m. Comparison of experimental with numerical results, Jacobi et al. (2022)

Regarding the wider range of flow kinematics in breaking wave, systematic analysis to in-

vestigate the effects of breaking waves impacting on marine structures has been of recent interest in green water research. Fontes et al. (2022) presented an experimental investigation of the kinematics of consecutive green water events generated with incident wave trains, particularly during their formation and interaction with the bow of a fixed structure. These events include Plunging-Dam-Break (PDB) and Hammer-Fist (HF) types of green water. These event types were also reported by Greco et al. (2007) in experiments using regular wave trains in a wave flume but did not include flow kinematics.

The experimental campaign by Fontes et al. (2022), consisting of incident wave trains of different steepness, was carried out using a fixed, rectangular bow installed in the wave flume of the Institute of Engineering at the National Autonomous University of Mexico. In the experiments, each wave train consisted of consecutive wave cycles that approached the bow of the structure, thus generating consecutive green water events. The flow kinematics during the formation of representative PDB and HF types of consecutive green water events, were experimentally investigated using Particle Image Velocimetry (PIV) methods. The evolution of the kinematics of PBD and HF type events was analysed to understand the flow behaviour as they are generated at bow of the structure. Figure 79 illustrates the flow kinematics during the generation of HF type green water events.

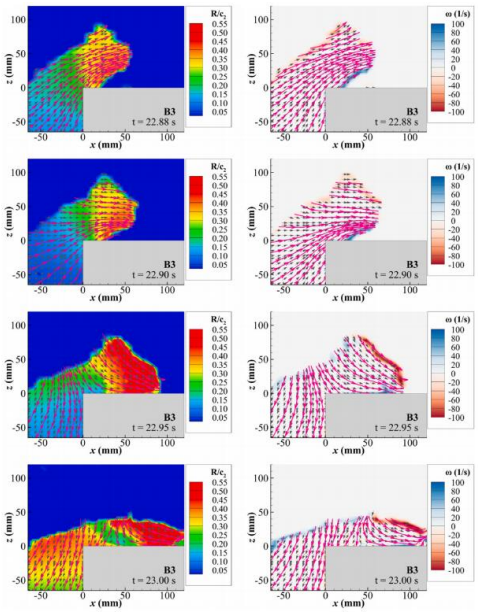

Figure 79 - Evolution of flow kinematics during the generation of a representative HF type green water event, Fontes et al. (2022)

9.3 Numerical approaches

Focusing on the wave-breaking phenomena of high-speed ships, Wang et al. (2020) performed numerical simulations to investigate the wave breaking phenomenon around high-speed ships. To resolve the flow field around a KRISO Container ship (KCS) model, they used both, Unsteady Reynolds-Averaged Navier-Stokes (URANS) simulations and Delayed Detached Eddy Simulation (DDES) approaches. Additionally, they used high-resolution, Volume of Fluid (VOF) techniques in OpenFOAM to capture the free surface. In their paper, the breaking wave phenomena was resolved by both URANS and DDES for Froude numbers greater than 0.35. The predicted URANS and DDES bow wave results were compared with experimental measurements conducted at the China Ship Scientific Research Center (CSSRC).

Figure 80 shows the comparison of the simulated wave patterns in high-speed conditions with the experimental measurements.

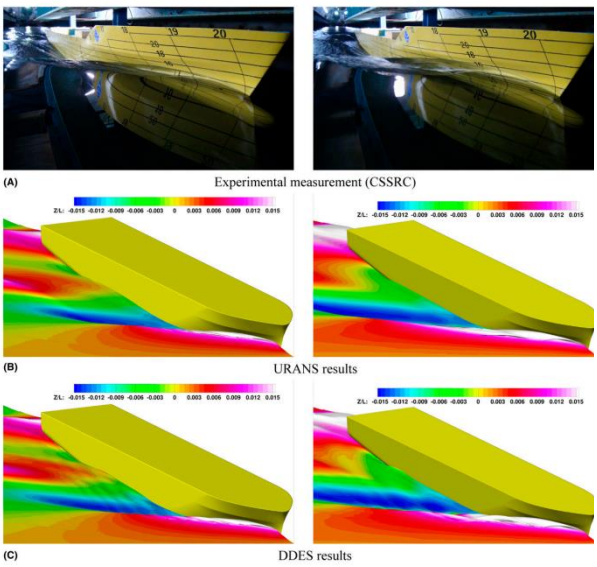

Figure 80 - Comparison of wave patterns (left column: Fn=0.35, right column: Fn=0.40): (A) Experimental measurement (CSSRC); (B) URANS results (C); DDES results, Wang et al. (2020)

The Fn = 0.40 cases shows more violent breaking bow waves more consistent with the experimental results. The DDES results provided more complex results illustrating the process of the overturning and breaking bow wave, and also captured some small-scale free surface features.

They presented axial vorticity distributions at different transverse cross sections to illustrate the different predictions of the breaking bow waves made using URANS and DDES methods. Five sections with x/Lpp equal to 0.05, 0.10, 0.15, 0.20, and 0.25 are presented in Figure 81 to illustrate the breaking wave phenomena.

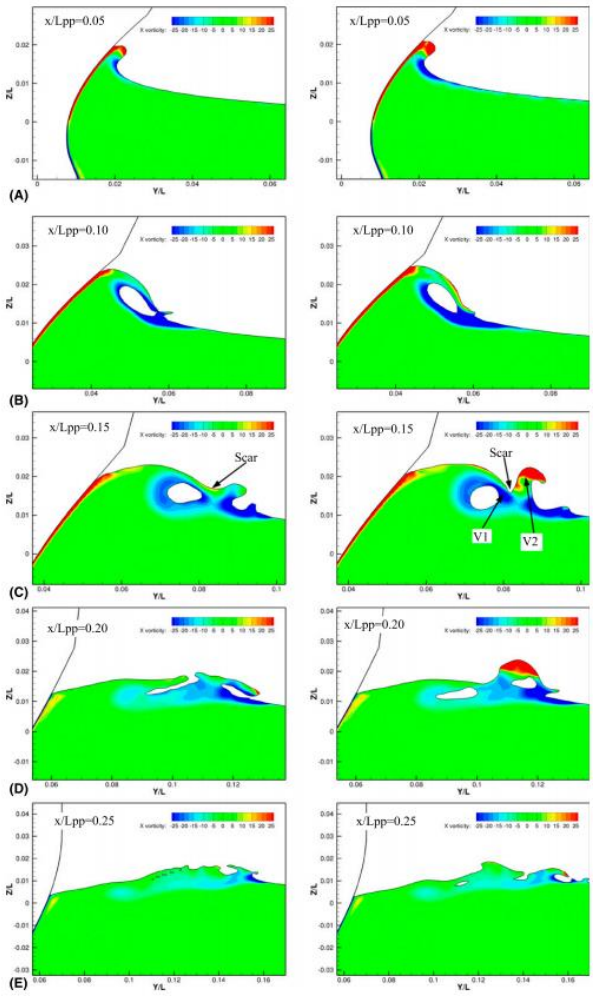

Figure 81 - Axial vorticity distribution (left column: URANS results, right column: DDES results), Wang et al. (2020)

The variation between the URANS and DDES wave fields and vorticity were mainly concentrated near the free surface. As shown in Figure 81-A, the initial plunger was generated because of the interaction between gravity and inertial forces when the hull blocks the inflow. A second plunger can be seen in Figure 81-C (x/Lpp=0.15), where it can be seen that the axial vorticity distributions predicted by DDES and URANS show significant differences. These differences are the main cause of the different shapes of breaking waves. Scars can be observed in the bow wave region from both URANS and DDES results due to counter-rotating vortex pairs (V1 and V2). In the far field region of Figure 81-C (x/Lpp=0.25), dissipation of the vorti-

city in the URANS results is noticeable compared with the DDES results. Consequently, the free surface is smoother in the URANS computations.

Another publication focusing on breaking waves by Wu et al. (2021) studied the breaking bow wave of the David Taylor Model Basin (DTMB) surface combatant model under different trim angles at Fr = 0.35 using Delayed Detached Eddy Simulation (DDES). The approach was adopted to study the breaking bow wave features, such as plunging jet and air entrainment. DDES was chosen because it has been shown that RANS methods average the N-S equation by time, smoothing out the turbulent pulsations in the flow field (Wilson et al., 2007). Wu's research delves into the influence of hull trim angle on breaking bow waves through simulations of different trim conditions (1 degree trim by bow, a model test condition, and 1 degree trim by stern). They compared and analysed the wave contour, free surface outline, vorticity field and velocity field at several transverse cross sections. Figure 82 shows the numerical representation of the bow waves generated by different trim angles.

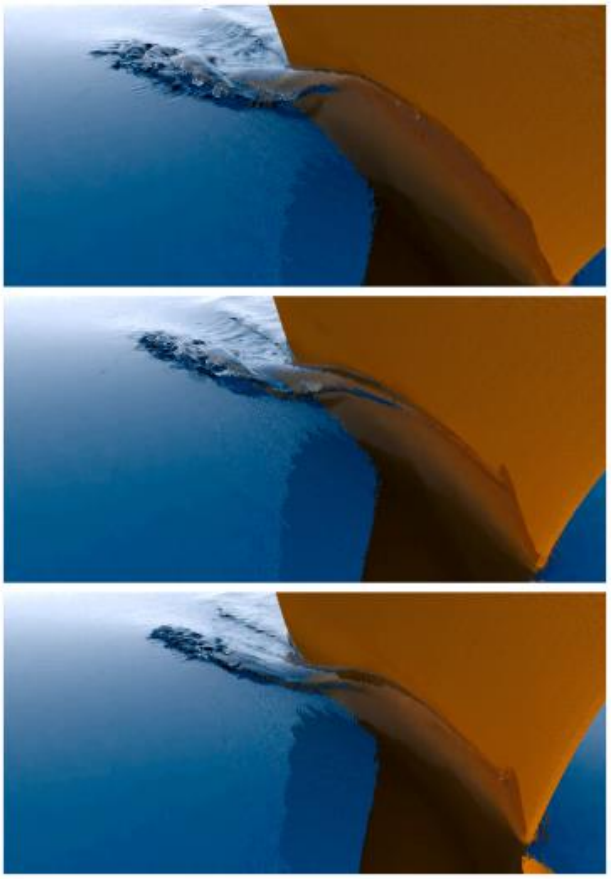

Figure 82 - Close-up view of the bow waves in the three cases (top; 1 deg. trim by bow, middle; model test condition, bot-tom; 1 deg. trim by stern), Wu et al. (2021)

Their results showed that trim by the bow makes free surface steeper and wave amplitude larger in the breaking bow wave region. They presented that the reason is that trim by the bow enlarges the attack angle of the bow, thus energizing the bow wave and generating a more violent free surface on the breaking bow wave.

To accurately capture the complex free surface of the breaking waves, it has been suggested that higher order two phase solvers in numerical simulations are needed. Jin (2021) presented a new two-phase flow solver for the analysis and prediction of complex ship flows through an investigation of breaking bow waves and built an air-water boundary layer model to overcome the discontinuity over the two-phase

interface in his PhD thesis. He developed a combined Volume of Fluid (VOF) and immersed boundary method to simulate two-phase flows with high density ratio. The interface was captured using the VOF method, and a new boundary layer was built on the lighter phase side by an immersed boundary method. The new solver was used to study breaking bow waves generated by a wedge-shape bow and the KRISO Container Ship (KCS). Jin (2021) showed this method improves the robustness and stability of two-phase flow simulations, and higher accuracy can be obtained on a relatively coarse grid compared to the original VOF method.

Li et al. (2022a) introduced another interface capturing method to simulate the ship-induced breaking waves with high-accuracy VOF (volume of fluid) schemes using the un-structured THINC (tangent of hyperbola for interface capturing) type scheme. Particularly, an extension version of THINC/QQ (THINC method with quadratic surface representation and Gaussian quadrature), namely, THINC/QQ-SF (THINC/ QQ extended for split-face unstructured cells) was used in their works. By numerical simulation for model DTMB 5415 under Fn=0.35, they showed that the combination of THINC/QQ-SF and HRIC can better capture the wave breaking details with less numerical diffusion, and the reliability of the resistance prediction is higher, compared with original VOF-HRIC. Figure 12 shows the comparisons of the breaking wave interface near the DTMB 5415 bow with the original VOF-HRIC scheme and the new scheme illus-trating the benefit of the combination VOF scheme of THINC/QQ-SF and HRIC (high-resolution interface capturing).

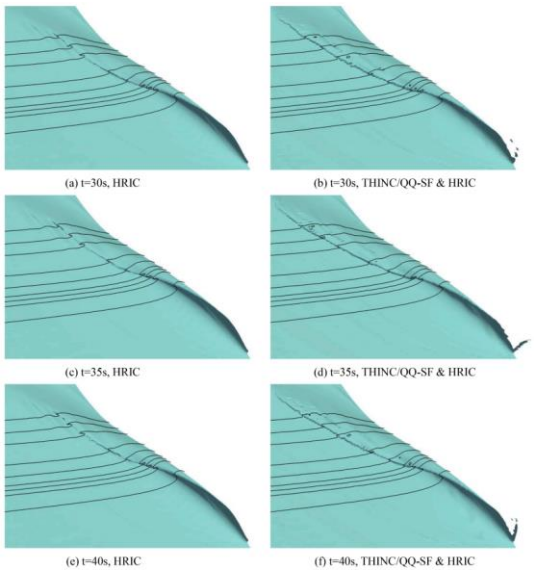

Figure 83 - Comparisons of the interface near the DTMB 5415 bow, Li et al. (2022a)

Figure 12: Comparisons of the interface near the DTMB 5415 bow, Li et al. (2022a)

Wang et al. (2023) investigated nonlinear ship waves by implementing the Longitudinal Cut Method (LCM) and Wake Survey Analysis Method (WSAM) in a computational fluid dynamics (CFD) simulation. LCM is wave pattern analysis by and the wake survey analysis method (WSAM) is the viscous resistance measurement method. The wave pattern resistance (Rwp) prediction of the LCM method was validated using a Series 60 Cb= 0.6 ship model. WASM was performed on a wall-sided model, incorporating the local adaptive mesh refinement (LAMR) and surface tension models to capture nonlinear bow waves. Far and near-field wave patterns and momen-tum loss resistance (RML) were compared with the experiment as shown in Figure 84.

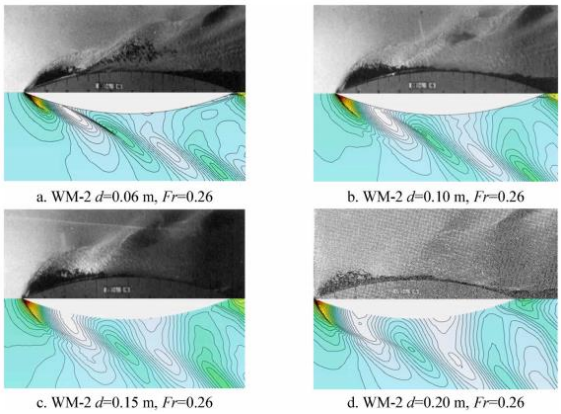

Figure 84 - Measured (top) and computed (bottom) wave patterns of WM-2 at Fr = 0.26 , Wang et al. (2023)

In their paper, they stated that it is meaningful to evaluate the nonlinearity in ship waves (Rn_w) by numerical simulation, considering the high-cost and complexity of conducting such an experiment. Their paper focuses on the analysis and evaluation of the resistance due to the nonlinearity of the waves and consequently provides some insights to evaluate the nonlinearity in ship waves to further understand their underlying mechanisms.

9.4 Concluding remarks

Breaking waves are important to ship engineers. Violent breaking bow waves, including spray, foam and bubbles, have significant impact on many aspects of ship design, such as increased hull resistance, inaccurate prediction of the added resistance in waves, and a substantial additional source of radar signature for naval craft. It also directly affects the motion and dynamic response of ships, local structural strength, and also ship manoeuvrability. The understanding of how waves break around the bow of a ship is important to the design of advanced 'green' ships, the development of energy saving techniques, structural safety, vibration reduction and noise control. To gain a better understanding of the physical phenomena for high-speed ships, extensive experimental studies have been conducted worldwide to try to explain the mechanism of breaking waves and to provide abundant computational fluid dynamics (CFD) validation data (Li at al.(2022b)).

In previous studies, the features of breaking bow waves are observed via experiment method. Experimental observations on bow waves mainly focused on the wave height or the velocity fields by using surface visualization techniques (aluminium powder and tracking particles), capacitance wires, 5-hole pitot tubes, underwater cameras etc. Recently, thanks to the development of the high-speed camera, video equipment can now be used to record the process of wave breaking, to capture the typical flow structures and to record the locations of bow wave run-up. PIV technology can also be employed to measure the velocity/pressure field and to determine the evolution of vortical flow fields around the ship.

The hydrodynamic phenomena involved in ship flows are usually discovered by experimental observation and then investigated further by conducting numerical simulations. Experimental measurements are still considered to be the most reliable methods to evaluate the breaking bow wave, however, there are many limitations with experimental measurements.

The experimental measurements are highly dependent upon experimental conditions and involve time consuming procedures for test measurement system preparation and experiment execution. Due to the high cost in both money and time, the observation is usually limited to benchmark ships or simplified geometries (Jin (2021)).

Traditionally, ship wave systems are described by potential flow theories without taking in to account the influence of viscosity. Nonlinear potential flow methods are suitable for modelling steep waves up to the point of breaking but have limited ability to capture the spray and bubbles associated with breaking waves.

In recent years, with the rapid development of High-Performance Computing (HPC) systems, Computational Fluid Dynamics (CFD) approach are widely used to conduct flow field simulations. Most of the previous numerical studies are based on the Reynolds-Averaged Navier-Stokes (RANS) equations. Using RANS codes, the overturning of bow wave and jet splashing can be captured while details of the turbulent flow field cannot be well resolved due to the time-averaging operator. Therefore, the Delayed Detached Eddy Simulation (DDES) approach, combined with a higher order two-phase solver to accurately capture the free-surface, has been prevalent in the simulation of breaking bow waves. However, the high computational cost of this approach limits its widespread use. Therefore, simulation with adaptive mesh refinement may be a good approach, which can greatly improve the computational efficiency of massively parallel computations of two-phase mixed flow (Li et al. (2022b)).

10. DEVELOPMENTS IN HULL AND PROPELLER MANUFACTURING

In the age of Artificial Intelligence, Autonomous Vehicles and other '4th Industrial Revolution' technologies, there have also been developments in Additive Manufacturing (AM) which are potentially applicable in the production of ship and propeller models. Physical model testing requires the manufacture of low volume or bespoke parts to extremely tight tolerances, which can be challenging to achieve in a cost-effective manner and drives up testing costs. With no need for moulds or fixed tooling, each part produced by AM can be unique, which lends itself perfectly to the manufacture of bespoke components. In recent years, the introduction of large scale / large format AM machines allows ever larger components to be manufactured, including the production of complete ship models.

10.1 Developments in Additive Manufacturing (AM) processes for metals

10.1.1 Background

GE Aviation started conducting research into AM techniques in the early 1990s and by 2012 its work with Morris Technologies enabled it to manufacture a radical new injector nozzle, which would have been extremely difficult and uneconomical to produce using conventional manufacturing techniques. GE realised the significance of its new manufacturing capability and decided to bring future development in-house and bought out its collaborator. By 2015 GE Aviation had improved its AM techniques and processes sufficiently that they could be used to produce over 25% of its new 'Catalyst' turboprop engine. The technology born from Rapid Prototyping had evolved into a fully-fledged production capability, capable of forming high precision parts from complex metal alloys suitable for use in safety critical aviation components.

In 2010 the American Society for Testing and Materials (ASTM) released a set of standards which split up the range of AM processes into seven categories [ASTM standard F2792-12; Standard Terminology for Additive Manufacturing Technologies;2012], covering methods of manufacture for both plastics and metals. In 2015 the ASTM standard was incorporated into ISO/ASTM 52900, which uses the same seven categories of AM processes (ISO/ASTM 52900:2021).

In 2017, the world's first class approved 3D printed propeller was unveiled at Damen Shipyards in the Netherlands. The 1.35 m diameter propeller, named WAAMpeller, was manufactured by Rotterdam Additive Manufacturing Lab (RAMLAB) and was a collaborative project between RAMLAB, Damen shipyards group, Promarin, Autodesk and Bureau Veritas. The first propeller was manufactured for demonstration purposes, but the second propeller was tested on a tug and passed all acceptance criteria.

The propeller was subsequently accredited by Bureau Veritas for use on Damen's Stan Tug 1606 class, making it the first AM propeller to be accredited for operational use. 3D printing of the 'WAAMpeller' is shown in Figure 85.

Figure 85 - Printing WAAMpeller (courtesy RAMLAB)

Another benchmark research project was conducted in South Korea by Det Norske Veritas (DNV), Hyundai Heavy Industries (HHI), Korea Institute of Industrial Technology (KITECH) and SY Metal Co. Ltd. (SYMETAL). A report on the project was published by Govindaraj et al (2021). SYMETAL manufactured a 2 m diameter 4-bladed propeller and a 0.7 m long sacrificial propeller blade using the WAAM process. Both the propeller and the single test blade were subjected to dye-penetrant testing with no flaws being detected. Four test coupons were subsequently cut from the sacrificial blade; two aligned with the build layer direction and two perpendicular to the build layer direction. The four coupons were subjected to material composition and mechanical properties tests, and the results showed were highly consistent. Both material properties and composition control exceeded DNV Ship Rule requirements and DNV accepted WAAM as a method suitable for the manufacture of Ship Propellers. DNV updated their 'Rules for Classification of Ships' in July 2021 (effective 1 Jan 2023), with the inclusion of a new section on Additively Manufactured Materials.

The 'Realisation and Demonstration of Advanced Material Solutions for Sustainable and Efficient Ships' (RAMSSES) project also used WAAM to produce a hollow propeller blade and is currently ongoing. Testing was conducted on a samples of a number of materials, including Cupro-Aluminium and Martensitic or Duplex Steels. The materials testing again showed that the WAAM method produced more consistent material properties than traditional casting methods (which typically vary through thickness of the casting).

Det Norske Veritas (DNV) released an updated version its metal Additive Manufacturing Standard DNV-ST-B203 in 2022. It covers qualification and production requirements for the most established metal AM processes, including Directed Energy Deposition (DED), Powder Bed Fusion (PBF) and Binder Jetting (BJT).

A comprehensive review of different materials and techniques was presented by Bergsma et al at the High Performance Marine Vehicle (HIPER) conference in 2016 [3D-Printing and the Maritime Construction Sector, Bergsma, van der Zalm, Pruyn, HIPER 2016, Cortana, Italy]. An overview of a limited number of relevant processes and developments to metal 3D printing is given below.

10.1.2 Wire Arc Additive Manufacturing, also known as DED-Arc

The use of WAAM in the shipbuilding industry was summarised by Tasdemir and Nohut (2021).

Wire Arc Additive Manufacture (WAAM) was developed from welding processes and uses an electric arc as the heat source and the metal wire as the raw material. The part is built up sequentially by adding material using a robotic arm. WAAM is now also referred to as Directed Energy Deposition – Arc (DED-Arc) in accordance with the ISO/ASTM naming convention.

WAAM can achieve a high deposition rate compared to many other AM techniques and the material properties are considered excellent, partly because the high temperature deposition of new material heat treats the layers deposited previously. However, tight tolerances are not currently possible, so it is necessary to build the part oversize and then use conventional subtractive machining strategies (i.e. CNC milling) to achieve necessary tolerances.

WAAM offers the potential for cost and lead time reductions for Ship's propellers, together with increased material efficiency, since it is able to produce very near net shape preforms without the need for complex tooling, moulds or dies. However, WAAM can currently only produce "near net shape" components, and CNC machining is required to produce the final geometry to acceptable tolerances. While WAAM could be used for model scale propellers, the relatively small cost of the raw material billet relative to the total manufacture cost and the fact that 3 or 5-axis CNC machining is required to complete the propeller mean that it is unlikely to have significant advantages at model scale.

10.1.3 Powder Bed Fusion (PBF)

Powder Bed Fusion (PBF) creates the part in a basin filled with metal powder, which is melted using a high energy source to build the solid structure layer-by-layer. A variety of different energy sources are currently used to melt the powder, which include Laser (L) and Electron Beam (EB). The excess powder is then recycled. L-PBF is also known as Selective Laser Melting (SLM) or Direct Metal Laser Sintering (DMLS),

These two methods (L-PBF and EB-PBF) are two of the manufacturing techniques pioneered by GE Aviation. GE Aviation state that L-PBF can produce complex parts with complex geometries to exceptional levels of precision. EB-PBF is stated by GE Aviation as being able to produce dimensionally accurate parts that need to be produced quickly and efficiently, while delivering parts with low residual stresses (the part is usually heat treated in the printer after printing to remove residual thermal stresses). Both these methods are potentially suitable for model scale production of finished propellers and components, however the cost of the machines and powders is high and it is considered difficult to get parts right first time.

In 2022 DNV reported that a joint project between Kongsberg Maritime and SLM Solutions produced a hollow thruster blade with a titanium internal honeycomb structure. The blade is currently undergoing fatigue testing, which is a known concern relating to parts produced using PBF methods.

10.1.4 Blown Powder Technology (BPT)

BPT uses a similar theory to PBF, but instead of forming the part in a basin full of powder, the powder is transported to the melt pool by adding it to the inert gas flow used to shield the arc.

A relatively new technique, BPT has the advantage of being able to change metallurgy through the deposition process, so that different layers of metals can be laid down which are well bonded to one another. This technology enables multi-layered components to be fabricated which would be impossible with conventional manufacturing techniques.

10.1.5 Binder Jetting

Binder Jetting Technology (BJT) is another AM technique which can produce metallic parts, however it cannot produce parts with the same structural properties as WAAM, PBF or BPT. Porosity and structural integrity are considered significant considerations when considering BJT, as is shrinkage of the part during sintering.

BJT produces parts using metal powder within a basin and a printing head (similar to an ink-jet printer) applies the binding agent to bond the powder particles together. After all layers have been laid down, the part can be sintered at

high temperature to fuse the metal particles together. However, the sintering process can cause shrinkage of up to 20% and can sometimes also result in warping or sagging. Control of dimensional tolerances is therefore difficult its applicability to parts requiring tight tolerances may be limited.

10.2 Developments in Additive Manufacturing processes for plastics

In comparison to AM processes for metal components, those for plastics are relatively well developed and are already commonly used in hydrodynamic model testing. As far back as 2016 the Ship-Technology.com website reported that Hamburg Ship Model Basin (HSVA) used 3D printers to create vessel appendages and energy saving devices and HSVA stated that "it's quite widespread in the model basins". A straw poll of the R&P committee members showed that while a large number of different techniques are currently being used to produce hull models, a significant number already use 3D printing to produce appendages such as rudders, fin stabilisers, transom wedges, waterjet housings etc. Member organisations have also been experimenting with coating components, in order to improve surface finish and also the structural integrity of the component. Treatments include coating with epoxy, or thermal spraying of metallic coatings, though little work has been published to date.

A number of member organisations are currently investigating 3D printing manufacturing techniques for the production of ship hull models, even for relatively large models of up to 10 m in length. While the manufacturing tolerances appear in line with ITTC guidelines, members have also expressed concern that model stiffness may not be as good as that of traditional model manufacturing techniques. To provide additional structural stiffness, two different organisations have 3D printed material around aluminium beam reinforcement, which has apparently worked well.

One of the most advanced attempts at 3D printing an entire ship model has been conducted at the Naval Surface Warfare Center, Carderock Division (NSWCCD). A detailed description of their work is provided below:

10.3 Applications of AM in model and component manufacture for hydrodynamic testing.

10.3.1 Hull manufacture capability development by Naval Surface Warfare Center Carderock Division

Mosqueda et al (2024) presented results from a new model fabrication technique illustrating the effectiveness of a large-scale additively manufactured hull model.

The hull form used was a representative geometry of the Arleigh Burke Class Destroyer during its Pre-Contract design phase, the geometry of which will be better known to the ITTC community by its original design designation DTMB 5415. This geometry was previously used by the ITTC for comparative resistance testing by the hydrodynamic community and has also been used for a number of computational workshops, such as the Gothenburg 2000 CFD workshop (Larsson et al, 2003). This geometry exists in the public domain, allowing for future studies and validation tests to be conducted with open-source data within the naval hydrodynamics and tow tank testing communities.

Models 5617 and 5796 were manufactured and tested to evaluate the feasibility of using an additively manufactured model for future experimental testing purposes at the Naval Surface Warfare Center Carderock Division (NSWCCD). The models were used to conduct a resistance test to determine if the additively manufactured model can withstand the structural stresses of a carriage test and reproduce results from a traditionally manufactured fiberglass model. AM technology provides the potential for significant cost and time savings to be

achieved from a construction, rigging, and testing standpoint.

Tests were be conducted in August and September, 2023 at the David Taylor Model Basin (DTMB) on Carriage 1 located in West Bethesda, Maryland.

The AM hull was fabricated under contract by Airtech International using a Large-Scale Additive Manufacturing (LSAM) machine developed by Thermwood, Inc., which is shown in Figure 86.

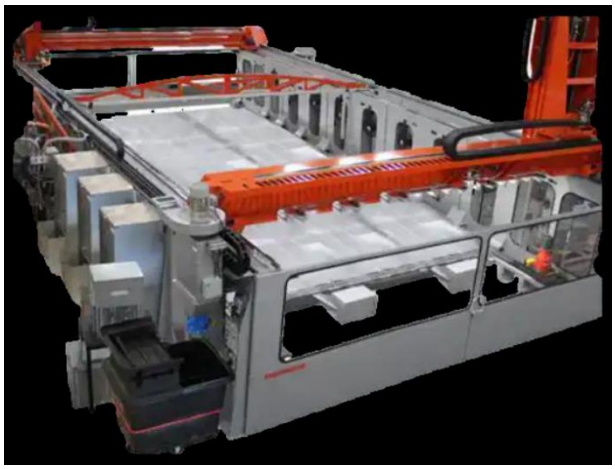

Figure 86: LSAM 1540 additive and subtractive machine (https://www.thermwood.com/lsam_home.htm)

This technology features both additive and subtractive capabilities allowing for large-scale, tight-tolerance parts to be created quickly and at a low per part cost. LSAM uses a "Near Net Shape" approach to part production where the part is first printed at high speed slightly larger than needed, then trimmed to the final size and shape using a 5-axis milling head on the same machine. LSAM can process parts from virtually any thermoplastic composite material, including high temperature materials that are ideal for moulds and tooling that must operate at elevated temperatures. A number of recycled materials are also available. LSAM's unique printing system produces parts that are solid, fully fused, vacuum tight and virtually void free, due to the compression roller that compacts the layers together after material deposition. LSAM systems can print in three orientations:

- Horizontal Layer Printing (HLP). Standard printing from the machine table.
- Vertical Layer Printing (VLP) option. Vertical Layer Printing allows parts to be printed that are as long as the machine table.
- Angle Layer Printing (ALP) option. Angle Layer Printing is the ability to print at a 45-degree angle.

Each print orientation has advantages and limitations for a particular part design. The ability to perform all three options using the same machine provides maximum print flexibility.

The objective of the presented work was to assess the feasibility of using an additively manufactured model for future model making and testing purposes. Specifically, they compared results from a LSAM model (5796) to a geometrically-similar fiberglass model (5617). , both constructed to a dimension ratio of 1:24.824.

The assessment included the hydrodynamic performance characteristics through calm water resistance tests, the geometric accuracy and repeatability of model fabrication, and assessment of rudimentary level material characteristics during testing. The material characteristic assessment included model/material water intake/absorption, hull crack development, and the presence and magnitude of hull deformation while testing.

The model appendage suite consists of a bow sonar dome, bilge keels, skeg, struts, and twin rudders with rudder shoes. Of the listed appendages, removable components include the bilge keels, struts, and rudders, which were fabricated using Stereolithography (SLA) 3D printing technology out of Accura 60 resin, and the dummy prop shafting which was fabricated using a 5/8 inch diameter hollow brass tube. Detailed dimensional characteristics of Model

5617 and Model 5796 were provided with waterline lengths of 18.77 feet (5.721 m) and a draught of 0.81 feet (0.247 m).

Turbulence tripping was achieved by installing 1/8th inch diameter by 1/10th inch projected length cylindrical studs placed approximately 0.5%*LPP aft of the stem spaced one inch apart. Studs around the sonar dome were placed in the transverse plane at the area of maximum sonar dome breadth.

Model 5617, originally built in 2002 by NSWCCD , was constructed of a fiberglass outer hull with mahogany internal structure, plywood bulkheads, and RenShape medium-high density polyurethane mounting pads. A photograph of Model 5617 is provided in Figure 87.

Figure 87: Photograph of Model 5617.

Model 5796 was built in 2022 by Airtech Int. for the current effort. The bare hull model was 3D printed using LSAM technology with a modified ABS material with 20% carbon-fiber infill reinforcement published by Airtech International (2021). The hull was printed using the ALP orientation at a 45-degree angle as shown in Figure 88.

Figure 88. Angled Layer Printing (ALP) LSAM Model 5796.

The build was completed in three separate sections and subsequently bonded together prior to final machining due to the complexity of the overhanging geometries. Section 1 is the forward part of the hull from the tip of the bow to approximately station 0.5, section #2 a small region on the lower forward part of the sonar dome, and section #3 is the remaining bulk geometry of the hull, from station 0.5 to the end of the stern. A photograph of Model 5796 as delivered from Airtech Int. showing the different sections is provided in Figure 89.

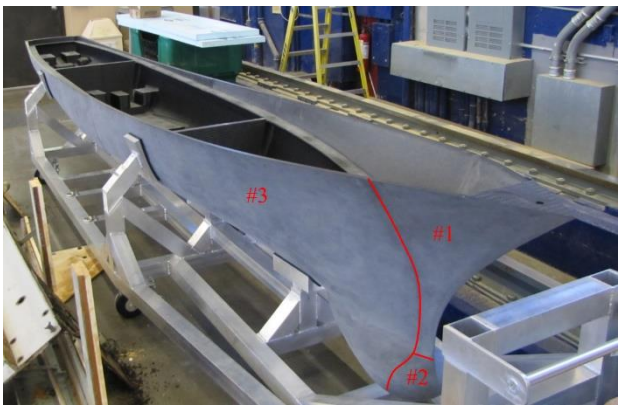

Figure 89. Model 5796 as delivered showing different sections.

After delivery of Model 5796, NSWCCD, installed the appendages (bilge keels, rudders, struts, propeller shafting), painted the outer hydrodynamic surface and sealed the joints between the hull sections. A photograph of Model 5796 after all additional work was completed is provided in Figure 90.

Figure 90. Photograph of Model 5796.

Laser scans of both models were conducted by the NSWCCD metrology department. Model 5617 was scanned, prior to testing, in an inverted orientation while resting on a layup table with elevated pedestals. Model 5796 was scanned in this same orientation, in a right-side-up orientation while in its cradle prior to testing, and again after testing in the inverted orientation. The intent of these scans was to ensure that LSAM technology can produce a model that is geometrically as accurate, if not more accurate, than historical model fabrication practices.

When constructing a model using LSAM technology, it is recommended to incorporate a flat-machined surface on the model that can be easily referenced as a datum plane when comparing point cloud metrology surface measurements to the source geometry. This technique allows for a more accurate assessment of the model geometry and the information can be used to guide future design decisions when building models for experimental testing purposes. The results of the surface deviation contour plots are shown in Figure 91 and Figure 92.

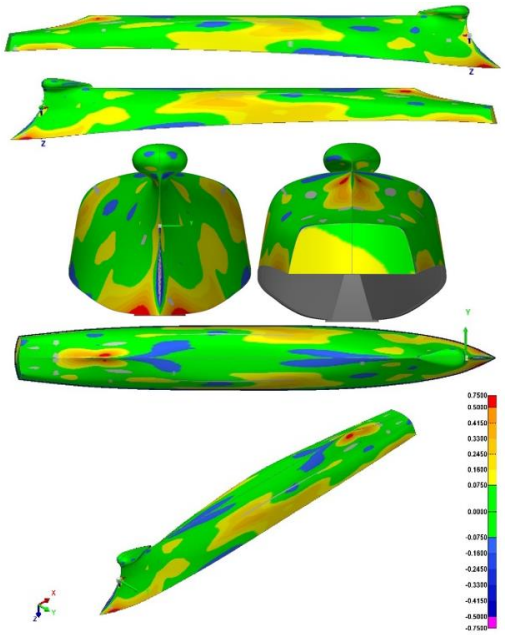

Figure 91. Model 5617 (GRP) – Pre-test Inverted. Contour plots of model surface deviation using best-fit method at 60% acceptance criteria.

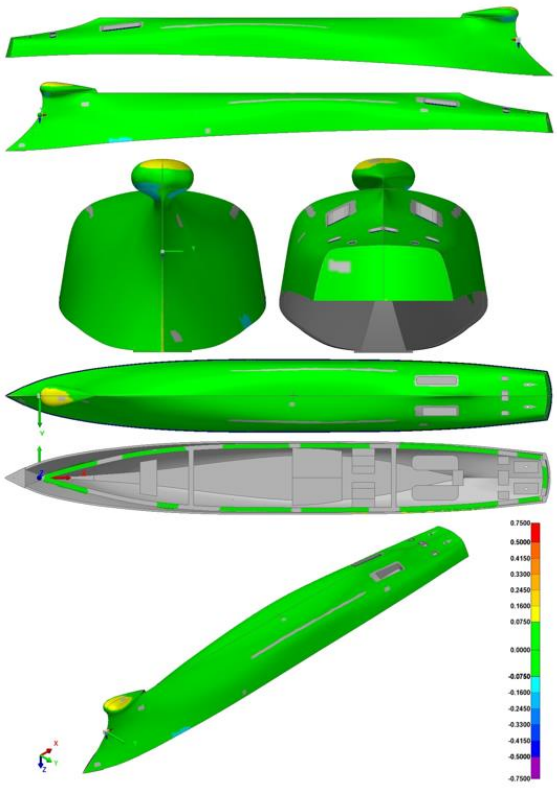

Figure 92 - Model 5796 (LSAM) - Post-Test, Inverted, Contour plots of model surface deviation using best-fit method at 60% acceptance criteria

The contour plot levels range from ±0.75in but show that the geometric accuracy of the hydrodynamic surfaces of the LSAM Model 5796 was far superior to that of the fiberglass Model 5617 and passed all scanning tolerance criteria, with measurements falling within ±0.075 in. The author suggested that additional hull form measurements be conducted periodically over the next several years and/or decades to assess the impacts on the model of long-term exposure to changing temperatures and humidity in the stored environment. Although, considering the low build cost and the ability to recycle the build materials, storing models for long durations may not be necessary.

Both Models 5617 and 5796 were outfitted with the same set of resistance testing and deflection measurement instrumentation. The resistance and the side force of the models were measured using linear transducer block gauges positioned at the forward tow point below the heave staff. The predicted full-scale effective power (EHP) indicated good agreement between both models as well as with historical data from Borda, G. G., et al. (1984) and Longo and Stern (1998). The deviation between the predicted EHP for the LSAM and the fiberglass model is shown in Figure 93.

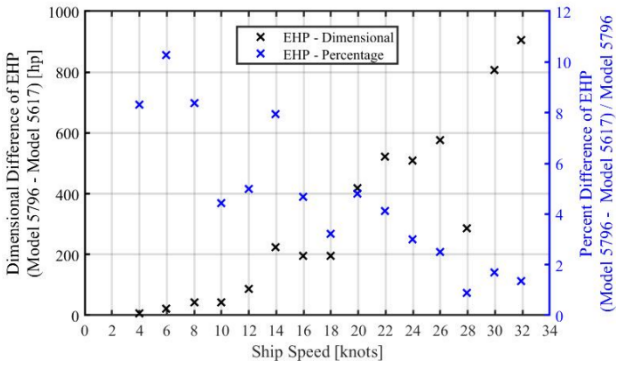

Figure 93. Deviation of EHP between LSAM and fiberglass models

The ship rise at L/LPP = 0.3, 0.5, and 0.7 and trim indicated acceptable underway model attitude was achieved with minimal impact on resistance measurements. The predicted ship rise for each model is shown in Figure 94.

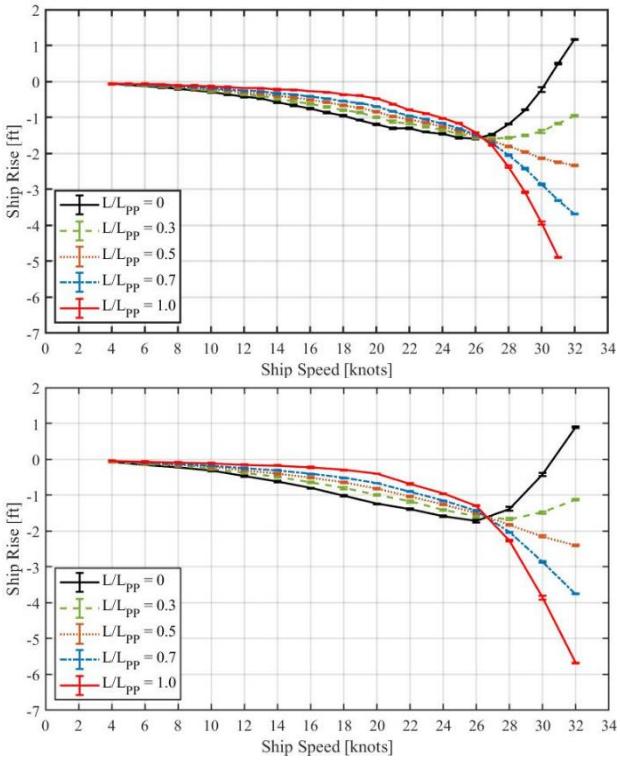

Figure 94. Prediction of ship rise for LSAM (top) and fiberglass (bottom) models

To quantify any deflection, or model hogging/sagging at various speeds while underway, the deflection of both models was determined by using a set of vertical and horizontal string potentiometer measurements positioned along the length of the hull. There were 5 vertical string potentiometers at the longitudinal positions indicated in Figure 94. These included two required for measuring running sinkage and trim at FP ($L/L_{pp}=0$) and AP ($L/L_{pp}=1$), and an additional 3 located nominally at the two internal bulkhead locations of Model 5796 and at the longitudinal center of gravity (LCG). Three horizontal string potentiometers were used to measure the deflection across the breadth of the model, at the top of the gunwhales. The measurements for both models were within the uncertainty of the string potentiometer sensors, however it was observed that the variance of measurements on Model 5796 were narrower than those measured on Model 5617 as shown in Figure 95.

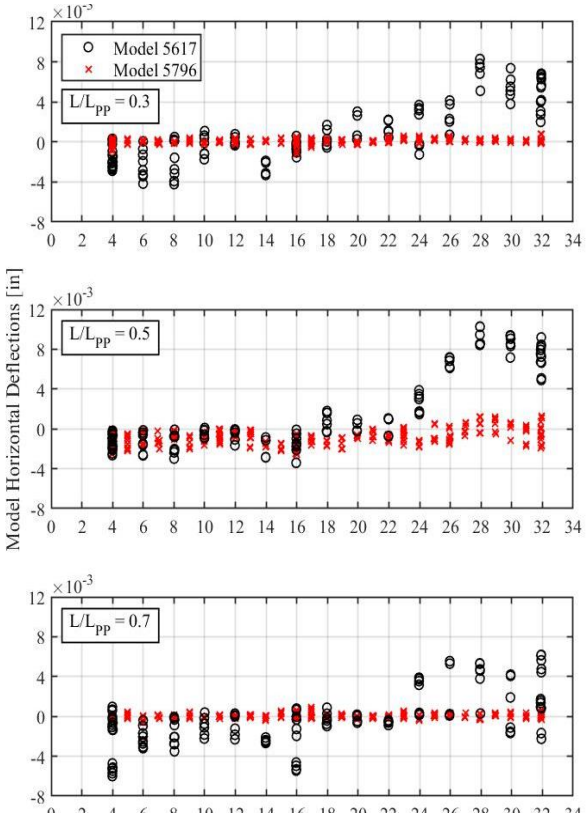

Figure 95. Model horizontal deflections at L/LPP = 0.3, 0.5, 0.7 AFP.

Additionally, water absorption and/or hull crack development were assessed throughout the duration of testing by weighing and inspecting the model at the start and end of each testing day. These measurements resulted in insignificant findings for water absorption but deflection measurements illustrated a more flexible fiberglass model as shown in Figure 96.

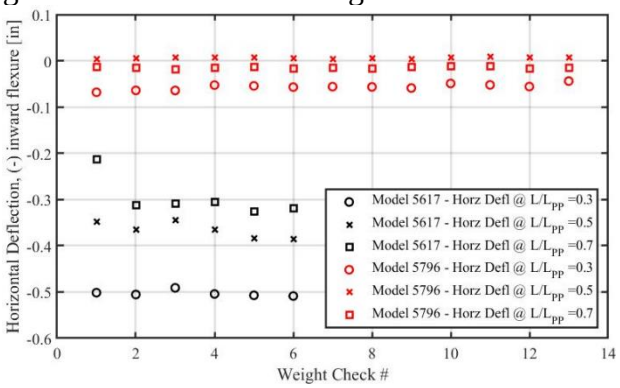

Figure 96. Horizontal deflections during model weight checks.

As the model was lifted to measure the weight it was found that the fiberglass model deformed inward from the lifting straps significantly relative to the LSAM model. Horizontal deflection measurements at L/LPP = 0.3, 0.5, and 0.7 suggest that the LSAM Model 5796 was slightly more rigid than Model 5617, however due to the differences in the age of the two models and the designs of the as-tested internal structures, it cannot be stated conclusively that an LSAM model is an improvement in this regard.

Based on the experience of using an LSAM model, the author included a list of design considerations for future LSAM model fabrication efforts as follows;

- All mounting holes, reference planes, scribe markings, etc. should be completed during initial model construction while model is in the original LSAM coordinate system.
- Coat the inner hull with an epoxy/hardening compound to protect against scratches and scrapes.
- Install metal threaded inserts, suitable for plastic materials, into all holes for all critical bolted joints, or for joints where repeated disassembly is required.
- During model construction phase, scribe a centerline along length of hull and mark all known or anticipated markings on hull while model is in original LSAM coordinate system.
- Include a flat plane relative to keel at the bow and stern of the model to provide measurable reference planes relative to the keel.
- Include a common reference plane along the length of the model to provide a datum plane for alignment of laser scan point cloud for geometry verification measurements.
- Hull geometry should be constructed without hollow voids to avoid spaces that could retain water without awareness.

- Design sufficient internal structure (bulkheads and longitudinals) to provide desired stiffness for your application.

- For models used in dynamic measurements (i.e. seakeeping and manoeuvring tests) consider a hull design for a near target dynamic mass property configuration with minimized total displacement.

Provided the quantitative and qualitative information, the author stated the overall feasibility of an additively manufactured surface ship model was deemed acceptable for tow tank resistance testing in calm water. A significant savings in cost and time-to-procure the model was achieved and is expected to improve further over time as lessons are learned and recommended design suggestions are employed.

10.3.2 Manufacture and testing of a 3D printed propeller at University of Genoa

Cilia et al (2019) conducted a cavitation test using a propeller printed in stainless steel and compared the results with data for the same propeller manufactured from bronze. The purpose of the programme was to determine whether a printed propeller could be accurate enough and strong enough that it would be suitable to conduct a cavitation experiment.

Initially they assessed material suitability for the production of the test propeller, considering a range of plastics and metals. Their preliminary assessment concluded that all the plastics would be insufficiently stiff and that tip deformation would not be expected to remain within ITTC guidelines. They also concluded that all the metals would be considered suitable for manufacture.

10 stainless blades were printed using a Renishaw AM-250 printer, and six were selected for metrological assessment. Limited 'high precision' measurements were obtained for each blade (three sections, twenty points per section) to determine the accuracy to which the manufacture had been achieved. They noted that:

- There was a generalized lack of material in the printed blades.
- Tip geometry fell far outside ITTC tolerances, with a high standard deviation.
- The worst measurement points were at the leading and trailing edges, which is also partly due to the difficulty in measuring these locations.
- The printed blades were less consistent than the machined blades.

They noted that the propeller blades did not conform to accepted ITTC tolerances, but considered that it was still worthwhile to conduct a cavitation inception test on the printed propeller, to determine what degree of difference would be found relative to their baseline historic data. Differences in hydrodynamic performance were found to be significant, with notable reduction in K_T, K_Q and η_O. They also showed that the propulsive coefficients were significantly different even at low load conditions, indicating that differences may be due to the as-manufactured geometry and not to deflections under load.

When conducting cavitation inception assessments, they noted that the 3D printed blades showed significant variation in cavitation inception indices. They attributed most of this variation to the lack of consistency in blade geometry, such as flat spots, squared leading edges with knuckles, incorrect surface curvature etc.

Overall, they concluded that they had identified a number of critical issues with their manufacturing process which had affected the accuracy of their printed propeller and would need to be resolved in future attempts.

10.3.3 AM manufacture and testing of 3D printed plastic and metal propellers at University of Naples Federico II

Staiano et al (2018), at the University of Naples, manufactured three propellers using AM

techniques and conducted open water propeller tests. Two were printed from engineering grade plastics using Fused Deposition Moulding. The third propeller was manufactured using Direct Metal Laser Sintering (DMLS / L-PBF) from AlSi10Mg Aluminium alloy. Data were compared with benchmark data of INSEAN.

A comprehensive assessment of build accuracy was undertaken using both a high-resolution Laser scanner, together with surface roughness measurements. The standard deviation of the distance between measured point cloud data and the nominal CAD data surface was found to be 0.14 mm for the DMLS propeller. Assuming a normal distribution of points around the mean, this would mean that more than 30% of the measurement points showed discrepancy in excess of 0.14 mm. The plastic propellers showed even greater discrepancy from the design intent, particularly around the blade tips, with a standard deviation in excess of 0.50 mm. They attributes some of the discrepancy to thermal stresses and shrinkage of the plastic as it cooled. They also noted that the DMLS propeller showed rotational symmetry in its error characteristics, indicating that the geometrical errors were consistent between blades, whereas the plastic propellers showed rotational asymmetry. A key factor noted by the authors was that the DMLS propeller had a significantly higher level of surface roughness than is typically seen with conventional manufacturing techniques.

The authors reported that the propulsive coefficients presented showed significant differences to the benchmark data. They stated that future work will be undertaken to study the effect of roughness on the hydrodynamic performance of propellers. No comments were made on the corrections used when processing the data.

10.4 Conclusions

Significant advances in Additive Manufacture have been made over the last 10 years, with the development of many techniques which can now be considered suitable for use in model manufacture for hydrodynamic model testing.

The Additive/Subtractive LSAM system developed by Thermwood and demonstrated by NSWCCD shows very exciting promise, achieving tolerances which easily meet ITTC guidelines. The structural integrity of the complete model also appears to be at least equal to conventional manufacture techniques. Full exploitation of such a build technique would require some rethinking of conventional build approaches, to include the printing of all mounting points for propulsion and data acquisition equipment (dynamometers, force gauges etc). This new manufacturing methodology has the potential to significantly reduce model build and fit-out times, if the high initial cost of purchase of the machine can be overcome.

Additive manufacturing techniques for propellers are less well developed, although there are some methods which show promise. Some of the techniques already accredited by Classification Societies have significant advantage at full scale, where custom moulds and casting formers are needed. At model scale, however, the availability of high-quality solid billets of the necessary size and material renders some of these techniques (e.g. WAAM) redundant, since 5-axis machining is also required to produce the final part. The PBF family of AM methods are considered by the AM industry to be the most mature technologies and also have the largest market share. However, DMLS (L-PBF) machines can be difficult to operate and a process of trial and error is sometimes required before producing accurate and functional parts. To be cost-effective in hydrodynamic model testing it is required that a propeller model is created right-first-time, which makes new technologies difficult and costly to implement. Nonetheless, developments are rapidly continuing in this field and it must be considered only a matter of time before some of these new techniques are ready and cost-effective for the manufacture of bespoke model-scale propellers. Future developments in this field should be closely monitored.

11. GUIDELINES FOR MODEL TESTING OF COATINGS

11.1 Model testing of coatings to evaluate the hydrodynamic frictional performance

There are several options to investigate the hydrodynamic frictional characteristics of coating surfaces by model testing, e.g., velocity profile method, rotating disk method, towed plate method and so on. In any of those cases, it is necessary to obtain the roughness function for the coating surface at actual ship scale roughness Reynolds number, in order to evaluate the frictional characteristics of the coatings when they are installed to actual ships.

The mean velocity profile near the smooth wall surface has logarithmic region which is given by equation (1). The surface roughness causes a downward shift ΔU^+ in log-law which is so-called roughness function given in eq. (2). The roughness function is a function of roughness Reynolds number k^+ which is defined as $k^+ = u_\tau k_S/\nu$ where k_S is the roughness length scale. Once $\Delta U^+ = \Delta U^+(k^+)$ is obtained for a given rough surface, we can estimate the additional frictional resistance due to surface roughness, by using the boundary layer similarity law or by conducting CFD calculations with wall-function based boundary condition considering roughness function.

$$U^+ = \frac{1}{\kappa}\ln(y^+) + B \qquad (1)$$

$$U^+ = \frac{1}{\kappa}\ln(y^+) + B - \Delta U^+ \qquad (2)$$

11.1.1 Velocity profile method

The velocity profile method directly measures the mean velocity profile in turbulent boundary layer of coated rough surface and obtains the roughness function by determining the frictional velocity in some way. Schultz and Myers (2003) measured the velocity profile of flat plate flow using LDV in a closed-circuit water tunnel. Fig.1 shows the schematic of the flat plate test fixture. In their study, the friction velocity, u_τ, for the smooth surface was obtained by Clauser chart method, and for the rough surfaces, u_τ was obtained using a procedure based on the modified Clauser chart method given by Perry and Li (1990).

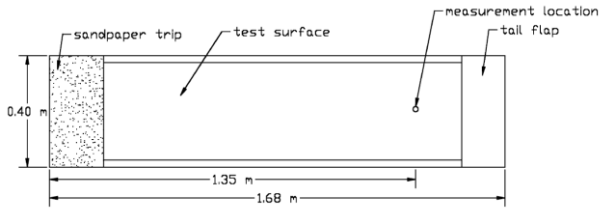

Figure 97 - Schematic of the flat plate test fixture for the velocity profile method by Schultz and Myers (2003)

11.1.2 Rotating disk method

Schultz and Myers (2003) conducted rotating disk experiments and obtained the roughness functions for several rough surfaces. A schematic of the rotating disk facility is shown in Fig. 2. This method measures the torque coefficients C_m for the smooth and rough disks for various rates of revolution and the roughness functions are calculated indirectly using the similarity law analysis of Granville (1982). This procedure involves comparing the C_m values of smooth and rough disks at the same value of $Re_R(C_m)^{1/2}$. The resulting equations for k^+ and ΔU^+ are given in eq. (3) and (4), respectively.

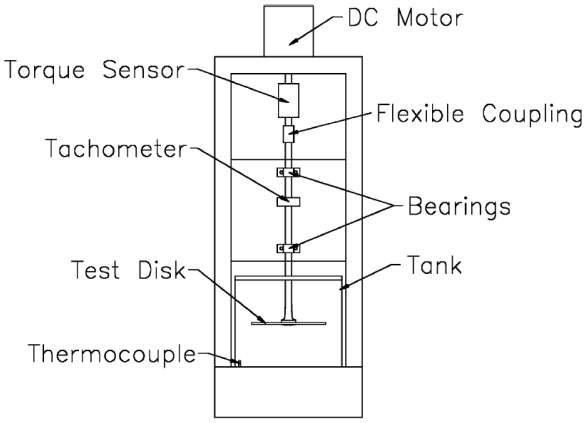

Figure 98 - Schematic of rotating disk test apparatus by Schultz and Myers (2003)

$$k^+ = \left(\frac{k}{R}\right)\sqrt{\frac{5}{8\pi}}Re_R\sqrt{C_m} \times \left\{1 - \left[\frac{2}{\kappa} - \Delta U^{+\prime}\right]\left(\frac{C_m}{40\pi}\right)_R\right\} \quad (3)$$

$$\Delta U^+ = \sqrt{\frac{8\pi}{5}}\left[\left(\frac{1}{\sqrt{C_m}}\right)_S - \left(\left(\frac{1}{\sqrt{C_m}}\right)_R\right)\right] + \frac{\Delta U^{+\prime}}{5} \quad (4)$$

11.1.3 Towed plate method

The towed plate method measures the frictional resistance coefficientsC_F of flat plate with smooth and rough surfaces. Figure 99 shows the experimental setup of Schultz and Myers (2003) research. The roughness functions for the towed plate data are calculated using the similarity law analysis of Granville (1987). This procedure involves comparing the C_F values of smooth and rough plates at the same value of $Re_L C_F$. The resulting equations for k^+ and ΔU^+ are given in eq. (5) and (6), respectively.

$$k^+ = \left(\frac{k}{L}\right)\left(\frac{Re_L C_F}{2}\right)\left(\sqrt{\frac{2}{C_F}}\right)_R \times \left[1 - \frac{1}{\kappa}\left(\sqrt{\frac{C_F}{2}}\right)_R + \frac{1}{\kappa}\left(\frac{3}{2\kappa} - \Delta U^+\right)\left(\frac{C_F}{2}\right)_R\right] \quad (5)$$

$$\Delta U^+ = \left(\sqrt{\frac{2}{C_F}}\right)_S - \left(\sqrt{\frac{2}{C_F}}\right)_R - 19.7\left[\left(\sqrt{\frac{C_F}{2}}\right)_S - \left(\sqrt{\frac{C_F}{2}}\right)_R\right] - \frac{1}{\kappa}\Delta U^{+\prime}\left(\sqrt{\frac{C_F}{2}}\right)_R \quad (6)$$

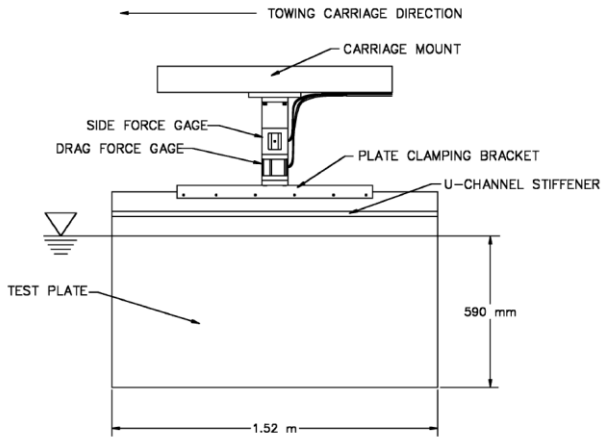

Figure 99 - Schematic of the flat plate test fixture for the towed plate method by Schultz and Myers (2003)

Schultz and Myers (2003) have compared three roughness determination methods which are velocity profile method, rotating disk method and towed plate method for two types of sandpaper and epoxy surface. Figure 100 shows the measured roughness functions for each of the test surfaces using the three determination methods and the comparison with the Grigson's

and Schlichting's roughness functions. The authors concluded as follows, "The results for the velocity profile and towed plate methods show good agreement for all surfaces, with the epoxy surface following a Colebrook-type roughness function and the sandpaper surfaces following a Nikuradse-type roughness function. Although the tests using the rotating disk method were carried out at much higher Reynolds numbers, the results for the sandpaper rough surfaces agree within their uncertainty with a Nikuradse-type roughness function in the fully rough regime, while the results for the epoxy surface agree with a Colebrook-type roughness function."

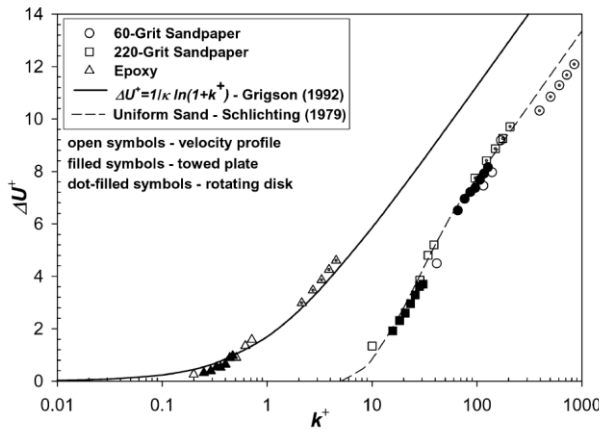

Figure 100 - Roughness function for the test surfaces obtained using the three methods by Schultz and Myers (2003)

Schultz also investigated the frictional resistance of antifouling coating systems by towed plate method. The roughness function for the un-fouled coatings shows reasonable agreement with a Colebrook-type roughness function when $k_S = 0.17R_a$ ($R_a$is a simple multiple of the centreline average height) is used as the roughness length scale shown in Figure 101.

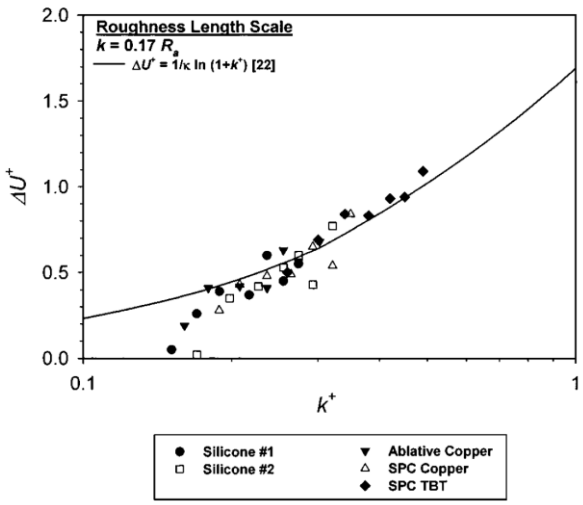

Figure 101 - Roughness function for the AF test surfaces in the cleaned condition. (Schlutz 2004)

Demirel et. al. (2014) calculated frictional resistance of smooth and rough surface flat plate using CFD in the same condition with Schultz's experiments (2004). The Colebrook-type roughness function of Grigson (1992) was employed in the wall-function of the solver and the roughness length scale was set in $k_S = 0.17R_a$ as Schlutz recommended. The calculated frictional coefficients showed good agreement with experimental results. This indicates that the roughness function and roughness length scale for antifouling (AF) coatings shown by Schultz are appropriate for use at model scale. Demirel *et al* also calculated the frictional resistance coefficients of flat plate at ship scale Reynolds number. The percentage increase in frictional resistance coefficients due to the AF coatings' roughness varies between 3.77% and 6.10%.

Yeginbayeva and Atlar (2018) presented experimental data on the boundary layer and drag characteristics of antifouling coating systems with different finishes. The coating types investigated were linear-polishing polymers, foul-release and controlled-depletion polymers. Their method is so-called velocity profile method which uses LDV in a large circulating water tunnel. The Krogstad's method was used to estimate the friction velocity, which is required to obtain the roughness functions for each coating surface. The measured roughness functions of

tested surfaces displayed a monotonic behaviour of Colebrook-type Grigson's roughness function against the roughness Reynolds number. The range of roughness Reynolds number is relatively higher than the other experimental results. The roughness length scales defined by the peak-to-trough height ($k_S = 0.14R_t$) and combination of root mean square roughness and spatial distribution of height parameters ($k_S = 0.4R_q(1+\lambda_a)^{0.05}$) presented a satisfactory correlation with ΔU^+ in the transitionally rough flow regimes. (Fig. 6, 7)

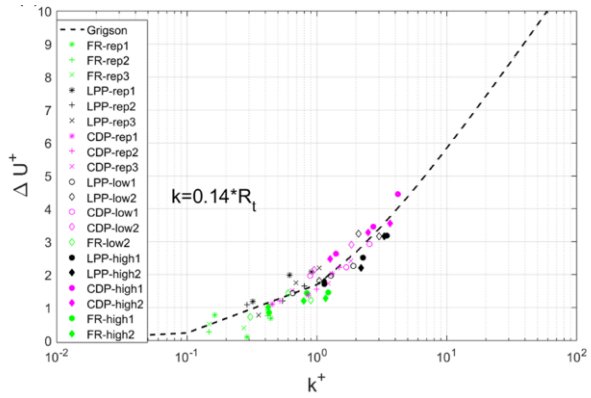

Figure 102 - Roughness function results for FR, LPP and CDP types with normal and mimicked hull finishes by using R_t. (Yeginbayeva and Atlar 2018)

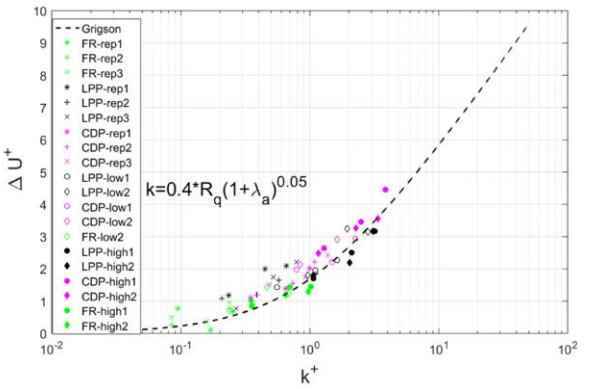

Figure 103 - Roughness function results for FR, LPP and CDP types with normal and mimicked hull finishes by using a correlation based on R_q and λ_a (Yeginbayeva and Atlar 2018)

As mentioned above, frictional characteristics have been investigated in detail at model scale. However, the behaviour of the roughness functions for coating surfaces at actual ship scale roughness Reynolds number region is still not sufficiently clear. As pointed out by Schlutz (2004), in order to obtain the roughness functions at higher roughness Reynolds number region, the rotation disk method is appropriate. Therefore, it is needed to investigate the frictional characteristics of coating surfaces in detail at higher roughness Reynolds number region using rotating devices, such as rotating disk and rotating cylinder (Katsui et. al. 2018) for the more accurate estimation of actual ship's frictional resistance.

11.2 Frictional drag reduction by air lubrication systems

The attempt to reduce the hydrodynamic frictional resistance such as ships and pipelines by air lubrication systems has a long history. Murai (2014) reviewed the research history of this topic comprehensively and exposited recent understandings of drag reduction mechanism.

According to Murai, the air lubrication-based drag reduction techniques are categorized into three kinds, which are bubble drag reduction (BDR), gas layer drag reduction (GLDR) and gas cavity drag reduction (GCDR). BDR works with action of dispersed bubbles inside the boundary layer. GLDR relies on replacement of highly shearing liquid with gas in the form of froths or long gas films. GCDR occurs when backward step provides a large gas single-phase space. Fig. 8 shows the schematic of three kinds of air lubrication.

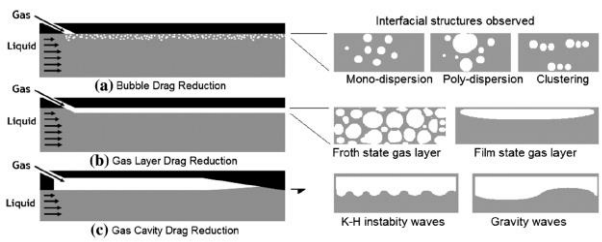

Figure 104 - Three types of frictional drag reduction enabled by gas injection. a Bubble drag reduction, b Gas layer drag reduction, c Gas cavity drag reduction (Murai 2014)

In order to apply the air lubrication-based drag reduction systems to engineering applications, it is necessary to understand the physical mechanism of drag reduction, including the scale effects. However, as Murai pointed out, "Understanding of the mechanism of transition allows reasonable design of drag reduction and improved performance. Unfortunately, the mechanism in use of bubbles is not explained by a couple of dimensionless parameters. What we see from data available today is a series of correlations among the liquid flow speed, gas flow rate, mean bubble size, and drag reduction ratio for a number of different flow configurations." Figure 105 represents a rough sketch of a drag reduction mechanism diagram as proposed by Murai. The parameter "G" in this figure is the sensitivity of the drag reduction per unit void fraction which is defined in eq. (7).

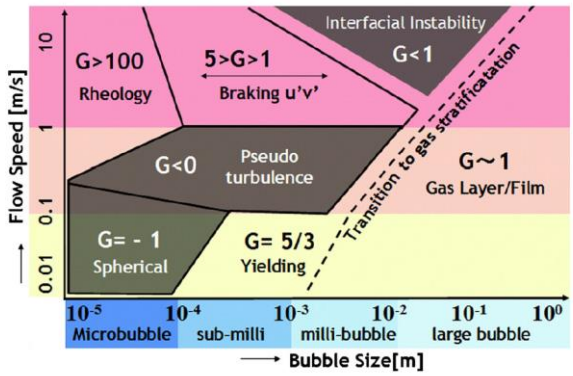

Figure 105 - Transition diagram of the drag reduction mech-anism owing to bubble injection (Murai 2014)

$$G = \frac{\frac{\Delta D}{D}}{\alpha} = \frac{1}{\alpha}\left\{1 - \frac{C_f}{C_{f0}}(1-\alpha)\right\} \qquad (7)$$

Where, ΔD, D, and α are original drag without air injection, reduced drag with air injection, and void fraction respectively. The lines that separate the domain into seven regions are determined from experimental data. Thus, the lines can be termed as transition lines of the dominant drag reduction mechanism.

On the other hand, the air lubrication system has been already installed to the actual ship and its energy-saving effects were confirmed by sea trial test (Mizoguchi et. al. 2010). The size of the ship is 162m in length, 38m in breadth and 4.5/6.37m in draft. The achieved net energy-saving effect was 12% at the maximum air blow-off rate. Although, we have to know the scaling law of drag reduction rate by the air lubrication system to estimate the actual ship performance from the model experiments accurately, we still don't have sufficient understanding on it. Therefore, it is important to accumulate the experimental data at ship scale Reynolds number using large sized model to investigate the scaling law for the drag reduction by air lubrication method.

Tanaka et. al. (2022) investigated the frictional drag reduction by bubble injection by means of model experiments using a 36 m length flat-bottom model ship. The towing speed is up to 8.0 m/s, with which Reynolds number reaches $2.9*10^8$. The resistance of the model ship and the distribution of the local wall shear stress on the entire bottom plate was measured. They have found out that the local wall shear stress has a profile that decays with the downstream distance depending on the air flow rate. Considering this feature, they have presented a formula describing the streamwise transition of the ratio of the friction coefficient and proposed a method of predicting the drag reduction for a full-scale ship.

It is still needed to accumulate the experimental data on drag reduction by air lubrication at ship scale Reynolds number to find out the behaviour of the air. If the air behaviour in turbulent boundary layer at full scale can be modelled, we can also utilize CFD technique to estimate the actual ship performance.

12. TOR18 – REVIEW CFD METHODS FOR ROUGHNESS EFFECTS

12.1 CFD methods for roughness effects using wall-function method

This procedure uses the relation between velocity and surface shear stress, the so-called log-law including roughness effects shown in eq. (1) at the 1st layer cell center point from the surface. And once the friction velocity is known, the value of k and omega are defined based on asymptotic behaviour at the near wall, eq. (2) and (3) (Wilcox 2006). ΔU^+in eq. (1) is called the roughness function, which represents a downward shift in the log-law caused by to the momentum deficit in the boundary layer due to roughness. The roughness function is generally defined as a function of roughness Reynolds number $k^+ = u_\tau k_s/\nu$ and has logarithmic behavior in terms of k^+ for usual sand-grain roughness. k_s means roughness length scale and it is defined to be the roughness height for the sand-grain roughness. In ship hydrodynamics, t hull surface roughness is mainly split into two categories: painted surface roughness and roughness due to bio-fouling. The characteristics of those two types of roughness are different from sand-grain roughness. Therefore, it is necessary to know the roughness function itself or roughness length scale for each roughness. Demirel et al. (2017) and Song et al. (2019, 2020, 2021) have shown the effect that biofouling has on ship resistance using CFD with wall function method considering the roughness function. They have used the roughness functions shown in eq. (4) with the roughness length scale for each roughness conditions shown in Table 1 and 2. Demirel et al. (2014) also calculated the added frictional resistance due to antifouling coatings over flat plate using the wall function method. The roughness function proposed by Grigson was used and the roughness length scale (sand-grain equivalent roughness height) was defined as $k_s = 0.17R_a$, based on measured average roughness height R_a for each coating. Table 3 shows the comparison of calculated and measured C_F at model scale Reynolds number by Demirel et al. Calculated skin friction coefficients agree with measured ones.

$$\frac{U}{u_\tau} = \frac{1}{\kappa}\ln\frac{u_\tau y}{\nu} + B - \Delta U^+ \tag{1}$$

$$k = \frac{{u_\tau}^2}{\sqrt{\beta^*}} \tag{2}$$

$$\omega = \frac{k^{\frac{1}{2}}}{\beta^{*\frac{1}{4}}\kappa y} \tag{3}$$

$$\Delta U^+ = \begin{cases} 0 & \text{for } k^+ < 3 \\ \frac{1}{\kappa}\ln(0.26k^+)^{\sin\left[\frac{\pi\log\left(\frac{k^+}{3}\right)}{2\ \log(5)}\right]} & \text{for } 3 < k^+ < 15 \\ \frac{1}{\kappa}\ln(0.26k^+) & \text{for } \to 15 < k^+ \end{cases} \tag{4}$$

Table 16 - Roughness length scale k_s for coating and fouling shown by Demirel et al. (2017)

A range of representative coating and fouling conditions [6].

Description of condition	NSTM rating[a]	k_s (μm)	Rt_{50} (μm)
Hydraulically smooth surface	0	0	0
Typical as applied AF coating	0	30	150
Deteriorated coating or light slime	10–20	100	300
Heavy slime	30	300	600
Small calcareous fouling or weed	40–60	1000	1000
Medium calcareous fouling	70–80	3000	3000
Heavy calcareous fouling	90–100	10000	10000

[a] NSTM [44].

Table 17 - Roughness length scale k_s for fouling conditions shown by Song et al. (2019)

Roughness length scales of test surfaces, adapted from Demirel et al. (2017a).

Test surface	Barnacle type	Surface coverage (%)	Barnacle height$h$ (mm)	Representative sand-grain roughness height k_G (μm)
B10%	Big	10%	5	174
B20%	Big	20%	5	489
M10%	Medium	10%	2.5	84
M20%	Medium	20%	2.5	165
M40%	Medium	40%	2.5	388
M50%	Medium	50%	2.5	460
S10%	Small	10%	1.25	24
S20%	Small	20%	1.25	63
S40%	Small	40%	1.25	149
S50%	Small	50%	1.25	194

The advantage of using the wall-function method is that the roughness function can be directly applied to the wall boundary condition. After the roughness function is obtained, it is easy to apply it to the wall boundary condition. The roughness functions of hull coatings are investigated by many researchers so far (Yeginbayeva et. al. 2018, Atencio et. al. 2019). However, the relation between the roughness function and surface profile of coatings unclear, especially for ship scale roughness Reynolds number, because the characteristics of roughness profile have many variations and roughness length scale changes depending on it. Therefore, further investigations on roughness functions for coating rough surfaces are needed.

Table 18 - Comparison of CF at model scale Reynolds number by Demirel et al. (2014)

Table 8
The comparison of C_F values at $Re = 5.5 \times 10^6$.

Surface	C_F (CFD)	C_F (experiment)	Difference (%)
Smooth	0.003185	0.003226	−1.26
Silicone 1	0.003460	0.003374	2.54
Silicone 2	0.003481	0.003426	1.60
Ablative Copper	0.003470	0.003401	2.04
SPC Copper	0.003491	0.003438	1.55
SPC TBT	0.003551	0.003500	1.45

12.2 CFD methods for roughness effects using wall resolved method

In the wall resolved CFD using k-omega SST turbulence model, which is widely used in ship flow CFD, the modified wall boundary conditions of omega or k and omega are applied to simulate the effects of the surface roughness. Wilcox (2006) showed a modified wall boundary condition of omega for rough surface which is shown in eq. (5) and (6). Hellsten (1998) introduced a lower limit of k^+which depends on y^+ as an extension of Wilcox's method. Hellsten's wall boundary conditions are shown in eq. (5), (7) and (8). In the method proposed by Knopp et. al. (2009), the modified wall boundary condition not only for omega, but also for k are introduced for the rough surface shown in eq. (9) - (11). Aupoix also has shown the wall boundary conditions of k and omega for rough surface based on Grigson's representation of Colebrook's results.

- Wall boundary condition of omega for rough surface proposed by Wilcox (2006)

$$\omega = \frac{{u_\tau}^2}{\nu} S_R \tag{5}$$

$$S_R = \begin{cases} \left(\frac{200}{k^+}\right)^2 & \text{for } k^+ \le 5 \\ \frac{100}{k^+} + \left[\left(\frac{200}{k^+}\right)^2 - \frac{100}{k^+}\right] e^{5-k^+} & \text{for } 5 < k^+ \end{cases} \tag{6}$$

- Hellsten's modification of Wilcox's wall boundary condition of omega for rough surface (1998)

$$k^+ = \max\left(k^+, 4.3{y^+}^{0.85} \right) \tag{7}$$

$$S_R = \begin{cases} \left(\frac{50}{k^+}\right)^2 & k^+ \le 25 \\ \frac{100}{k^+} & 25 < k^+ \end{cases} \tag{8}$$

- Wall boundary condition of omega and k for rough surface proposed by Knopp (2009)

$$\omega = \min\left(\frac{u_\tau}{\sqrt{\beta}\kappa d_0}, \frac{60\nu}{\beta y^2}\right) \tag{9}$$

$$k = \min\left(1, \frac{k^+}{90}\right)\frac{{u_\tau}^2}{\sqrt{\beta}} \tag{10}$$

$$d_0 = 0.03 k_s \min\left(1, \left(\frac{k^+}{30}\right)^{\frac{2}{3}}\right) \times \min\left(1, \left(\frac{k^+}{45}\right)^{\frac{1}{4}}\right) \times \min\left(1, \left(\frac{k^+}{60}\right)^{\frac{1}{4}}\right) \tag{11}$$

- Wall boundary condition of omega and k for rough surface proposed by Aupoix (2014)

$$\omega = \min\left(\left(\left(\frac{300}{{k^+}^2}\left(\tanh\left(\frac{15}{4k^+}\right)\right)^{-1} + \frac{191}{k^+}\left(1 - \exp\left(-\frac{k^+}{250}\right)\right)\right)\frac{{u_\tau}^2}{\nu}, \frac{60\nu}{\beta y^2}\right)\right) \tag{12}$$

$$k = \max\left(0, \frac{1}{\sqrt{\beta}}\left(\left(\frac{\log\left(\frac{k^+}{30}\right)}{\log(10)} + \left(1 - \tanh\left(\frac{k^+}{125}\right)\right)\right) \times \tan\left(\frac{k^+}{125}\right)\right) \times {u_\tau}^2, 0\right) \tag{13}$$

Orych et al. (2022) showed a comparison of calculated frictional resistance of flat plate and ship with wall boundary conditions proposed by Hellsten, Knopp and Aupoix. The flat plate results are shown in Figure 106. They pointed out that "The performance of the selected roughness models shows that Aupoix-Colebrook yields the most reasonable results when compared to extrapolated model scale experiments and another CFD method."

The wall resolved method itself predicts turbulent boundary layer flow with higher accuracy than wall function method. On the other hand, in case of the calculation with rough wall surface, the wall resolved method requires the complicated wall boundary conditions for turbulent parameter omega and k compared with wall function method. Also, the relation between the roughness function and roughness Reynolds number k^+ is not clear. As well as the wall function method, wall resolved method also needs appropriate roughness length scale k_s for various kind of rough surface in ship scale roughness Reynolds number.

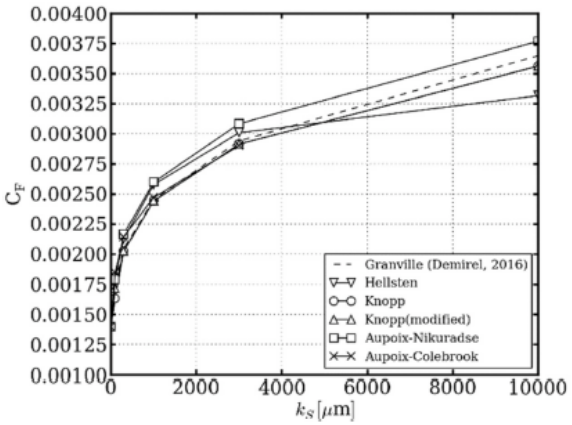

Fig. 18. Roughness model comparison for a flat plate at Re = 2.89 × 10⁹, k-ω SST, k_s range 0–10 000 μm.

Figure 106 - Comparison of calculated CF with various wall boundary conditions for rough surface (Wall resolved calculations) by Orych et al. (2022)

13. IDENTIFY THE NECESSITY OF GUIDELINES FOR CFD METHODS, MODEL TESTS AND SCALING FOR ENERGY SAVING DEVICES

Many different kinds of Energy Saving Devices (ESD) have already been developed,

which makes the creation of generic guidelines for CFD and/or model tests extremely difficult. A classification system for the different ESDs is proposed below, which is a first step towards the creation of guidelines for testing and scaling processes.

Depending on the working principle, existing and emerging energy saving devices can be categorised into five areas:

- Hull resistance reduction measures,
- Propeller flow conditioning devices,
- Propeller/hub modifications,
- Manoeuvring energy saving devices
- Renewable energy assisted propulsion

These categories are broken down further in Figure 107.

They vary in general location with respect to the vessel as shown in Figure 108.

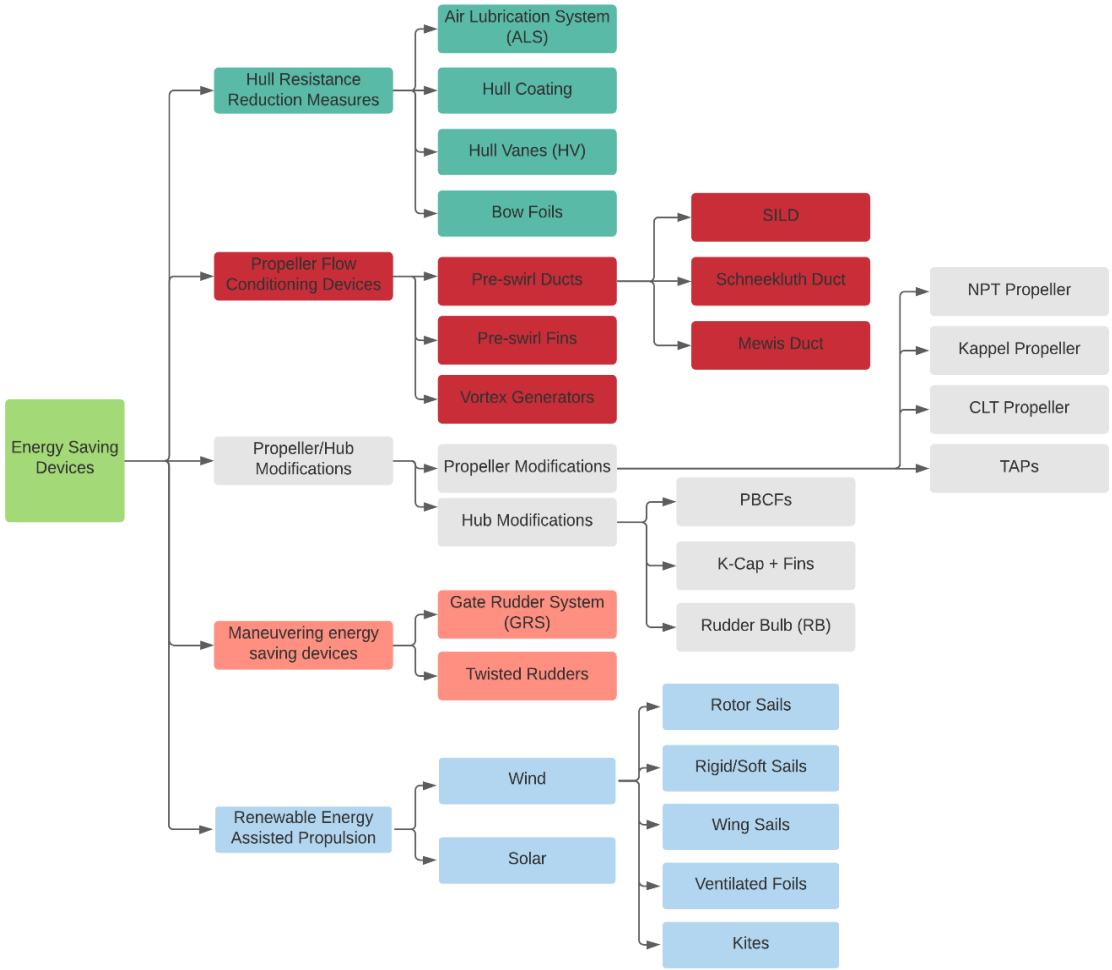

Figure 107 - Categorisation of existing and emerging energy saving devices (ESDs)

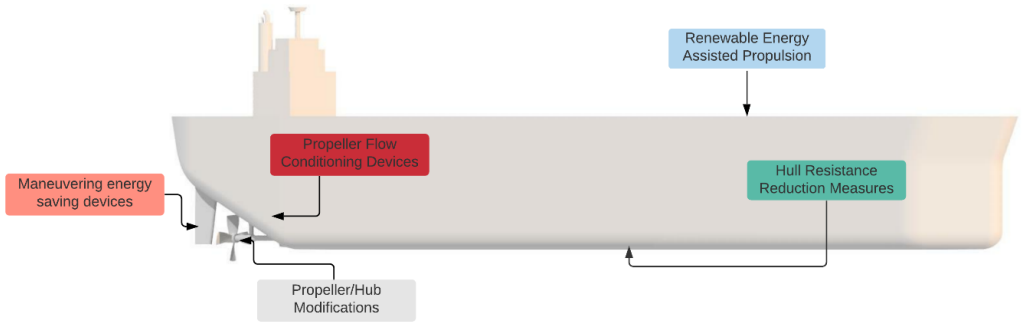

Figure 108 - General application of energy saving devices (ESDs) for a location point of view

Due to the different working principles, it is not considered feasible to develop a uniform approach to test their performance and predict the performance for full-scale conditions. Therefore, the following sessions discuss the scaling methods according to the categories.

13.1.1 Hull Resistance Reduction Measures

In shipping, a large part of the fuel is used to overcome hydrodynamic forces, up to 85% (Ahmadzadehtalatapeh and Mousavi, 2015), hence reducing hull resistance is the most direct way to save energy. To date, three major approaches have been released into the commercial sector which include air lubrication, hull coatings and hull appendages (e.g. hull vane or bow foil). Depending on their working principles, they affect the skin frictional coefficients, wave making resistance, form factor, or wetted surface area. It has been summarised as below:

- Skin frictional coefficients: coating applications, air lubrications.
- Wave making resistance: hull vane, bow foil.
- Form factor: hull vane, bow foil.
- Wetted surface area: air lubrication.

Detailed quantification of the effect of the individual technologies is needed for the scaling of the energy saving devices.

13.1.2 Propeller Flow Conditioning Devices

Propeller flow conditioning devices refer to devices installed upstream of the propeller which improve the flow into the propeller. The devices include pre-swirl duct, pre-swirl fins, wake equalizing duct and vortex generators. The scaling of these devices needs to consider the impact on wake fraction, thrust deduction and form factor. In the situation that the device provides additional thrust (by recovering ‘wasted’ energy), it should be considered as part of the propulsion system.

At ITTC 2021, the guideline was adopted for the scaling of the pre-swirl fin devices. Two methods have been proposed. However, due to the complexity of the devices, the application of such methods depends on the specific device type with limited application until now.

13.1.3 Propeller/Hub Modification

Propeller/hub modifications include development in novel propeller design to improve the performance of the propellers and the new propeller hub design to recover energy behind the propeller (e.g. Propeller Boss Cap Fins). The effect of these devices must be included in the propeller open water tests and the scaling should be combined with the propeller open scaling. However, full scale trials of propeller boss cap fins have not always shown the performance im-

provements predicted by model tests and detailed analysis is required, Kimura & Ando (2019).

13.1.4 Manoeuvring Energy Saving Devices

Manoeuvring Energy Saving Devices are those innovations on rudders to integrate the manoeuvring devices with the propulsion system. The typical devices include Gate rudder, twisted rudder, rudder bulb and rudder with fins. So far, the devices is developed to provide additional thrust for ships, which also affects the rudder resistance. When additional thrust is generated by these devices, they shall be considered to be an integral part of the propulsion unit when considering scaling approaches, i.e. considering rudder resistance to be a component of the hull resistance shall be avoided.

13.1.5 Renewable Energy Assisted Propulsion

Renewable Energy Assisted Propulsion refers to devices using wind or solar energy to either propel the vessel or to provide additional energy that can be used to power the ship's energy saving. Devices using wind energy to produce additional propulsion force include wind sails, Flettner rotors and other wind assisted propulsion devices. The scaling of the performance of such devices shall consider the reduced propeller thrust requirement, leading to different thrust deduction factor, propeller operation and efficiency. It should also consider the effect on the resistance of the ship, such as the effect of an additional yaw angle. For devices like wind turbines or solar panels, which only provide additional energy to the ship's power system, the devices have minor hydrodynamic impact.

13.1.6 CFD application on scaling of the energy saving devices.

As discussed previously, depending on the principle of the energy saving devices, different parameters can be affected by the application of the energy saving devices. Until now, there is no unified approach for the scaling of energy saving devices. It has to discussed retrospectively regarding to individual devices. At the moment, most research has been conducted by using CFD for the full-scale performance prediction. However, the results are not well benchmarked and validated to provide a guideline for CFD modelling for energy saving devices. General guidelines for hull and propeller modelling have been followed, as summarised in Table 19 below. Further research is required conducted in this area to develop the best practice and to assist in the formulation of ITTC guidelines for appropriate modelling of energy saving devices.

Table 19 - Typical CFD modelling approaches and parameters for model and full scale modelling

	Model Scale	Full Scale
Size: Ship length	3-8 m	50-300m
Size: Propeller Dia	150mm-250mm	2-6m
Size: ESD typical reference length	150mm-250mm	2-6m
Turbulence model	SST k-w Realisable K-e	SST k-w Realisable K-e
Wall modelling	Wall function: low Y+	Wall function: high Y+
Y+	1-5 or above 30	above 30
Mesh: near wall	Follow the Y+ guide regarding individual components: propeller, hull, ESD.	
Mesh: Free-surface	Monitor Kelvin wave development Resolve the wave length in 50-80 cells and the wave height in 20 cells	
Time step	Dominated by propeller: propeller advances between 0.5 and 2 degrees per time step (Recommended by ITTC 7.5-03-03-01) Special attention is needed if the propeller is interacting with ESDs.	

14. CONCLUSIONS AND RECOMMENDATIONS

14.1 State of the Art

The work of the JoRes project should be reviewed when it is published in December 24, to determine how the data contained within it can be used by the ITTC to improve its recommended guidelines and procedures.

The work of the GATERS project should also be reviewed, to determine how its data could be used for the assessment of the gate rudders. The large efficiency improvements claimed by the project make this type of Energy Saving Device of particular relevance to the IMO's goals for greenhouse gas reduction, and the availability of both geometric data and full-scale trials data may allow a robust scaling process to be developed.

14.2 Procedures

The following three updated procedures should be adopted by the 30th ITTC:

- 7.5-01-01-01 Ship Models
- 7.5-02-03-01.8 Energy Saving Devices
- 7.5-02-05-01 High Speed Marine Vehicles

The procedures which were only able to be partially completed by the 30th ITTC R&P committee should be completed and reviewed by the 31st ITTC. In particular, the background work done on updating the ITTC's 1978 Performance Prediction Method should be considered a priority, together with the uncertainty analysis worked example which goes with it.

The Waterjet propulsion test uncertainty analysis should also be completed and released. A new dataset, which includes data collected from pressure tappings, is required in order for this to be undertaken.

The review of the *Scaling methods for ships fitted with pre-swirl devices* procedure highlighted that further work and investigation into this type of ESD is required. Since many of these devices are considered to be proprietary, a benchmark using non-commercial ESD designs should be generated and used. However, the use of a non-commercial design may limit the potential for conducting full scale validation, which would be of great value when considering the relatively small improvements in efficiency that these ESDs can create.

14.3 Benchmark study on the effect of Re at model scale and scaling methods for full-scale prediction

The results of CFD simulations conducted by a number of participants showed significant variability between their results, which was potentially of a similar order of magnitude to the scale effects the study was attempting to characterise.

The variability raises the question of whether an accurate full-scale prediction can be made from model-scale data (Schuiling/Kerkvliet *et al* 2024), without knowing the results *a priori* to enable correct calibration of turbulence intensity parameters.

The production of best practice guidelines for conducting CFD simulations of Propeller Open Water Test (POT) should be considered by the ITTC.

Benchmark experimental data for CFD validation of POT would benefit greatly by the inclusion of turbulence intensity measurements and flow visualisation techniques such as paint flow tests.

Fully turbulent model-scale measurements using non-intrusive tripping (Schuiling/ Kirkvliet 2024) may provide better characterization of the full-scale open water performance due to the improved similarity with full-scale flow regimes. The work of the 'Tripping' Joint Industry Project (www.marin.nl/jips/tripping) should be monitored carefully. Further work on this topic should be well integrated with the investigation of laminar flow effects in self-propulsion test.

14.4 Investigation of the issue of laminar effects in self-propulsion test of propeller with low blade area

A significant number of participants in the study reported having issues with low Re during self-propulsion tests. Recent work by Hasuike (2017) and Lucke (2017) showed mixed laminar and transitional flow at model scale, which is different to the fully turbulent flow expected at full scale. The superiority of the 2-POT method was confirmed by highlighting the similarities in the flow regime between open water and behind conditions at low Reynolds number.

It is recommended to conduct the propeller open-water test at multiple Reynolds numbers, particularly for propellers with low blade area ratios. This should provide better understanding of the asymptotic convergence of the propulsive coefficients.

The work of the Tripping Joint Industry Project should be monitored carefully. The novel turbulent stimulator design of Schuiling & Kerkvliet may help alleviate the issue of laminar flow at model scale, both for propeller open water testing and also in the self-propulsion testing.

14.5 Investigation of the issue of extrapolation of model tests with ducted propellers to full-scale according to different Reynolds numbers

Very limited published data are available on the extrapolation to full scale of ducted propeller performance. A small CFD study conducted by a member of the committee showed similar, if not greater, sensitivity to inflow turbulence intensity level to that of an open water propeller.

It is recommended that the problem of Reynolds number sensitivity for a ducted propeller is

deferred until the effects of Reynolds number and laminar-turbulent transitional flow on open propellers is better understood.

14.6 Update of the load variation test method in 1978 ITTC Performance Prediction method

A review of procedure 7.5-02-03-01.4 – *1978 ITTC Performance Prediction Method* found that the formula for relative rotative efficiency (η_R) was incorrect when using a torque identity approach.

The correct formula for η_R, using a torque identity, is:

$$\eta_R = \frac{K_{TM}}{K_{TQM}}$$

Where K_{TM} is the thrust coefficient from the self-propulsion test. K_{TQM} is read from the propeller open water diagram, by using the torque identity to find the advance ratio where K_{QM} intersects the torque curve and reading off the thrust coefficient at the same advance ratio.

The IMO's minimum propulsion power requirements for safe passage have resulted in a change to recommended range of added resistance allowances. A small study of the added resistance in waves for a number of different vessel types indicate that the historically used load variation test allowance of -10% to +20% is insufficient.

It is recommended that, particularly at low speed, testing organisations should increase the range of the load variation test to -10% to +40%.

Added resistance in waves can have non-linear effects, particularly above 30%. Care should be taken to ensure that appropriate data is collected, and also that data are interpolated correctly. Additionally, care should be taken to ensure that air draw into the propellers does not occur when testing at highly overloaded conditions.

To bring the ITTC's 1978 Performance Prediction Method procedure in line with other procedures was found to require more work than originally anticipated. Significant work was done on this update, but it was not completed in time for release in the 30th ITTC. It is recommended that this work is continued by the 31st ITTC.

14.7 Investigation of the requirements for the testing and numerical evaluation of high-speed marine vessels

The flow around the lower edge of a transom stern was noted to affect the running sinkage and trim during testing. This characteristic will affect both physical model experiments and CFD studies.

It was recommended that the sharpness of the transom edge of a physical model is measured using edge gauges and recorded in the model's documentation.

14.8 Investigation of measurement and prediction methods for breaking waves

A range of different techniques were documented for experimental characterisation and measurement of breaking waves, focussing on the behaviour around the bow of a vessel.

Experimental techniques ranged from the use of transparent and semi-transparent models, with cameras viewing from inside the model, to Particle Image Velocimetry (sometimes stereoscopic PIV) based techniques. It was noted, however, that experimental measurements are highly dependent upon experimental conditions and are extremely time consuming, so observations are usually limited to benchmark ships or simplified test cases.

Numerical techniques continue to advance, due to ever increasing computational power. CFD techniques include Unsteady RANS (URANS), Delayed Detached Eddy Simulation

(DDES). In addition to changes in the underlying computational solvers, academic effort has also made progress on higher-order interface capturing schemes. The DDES method, combined with higher order two-phase schemes have been prevalent in recent academic work. However, the computational cost of this approach limits its widespread use and these techniques are generally considered to still be in development.

14.9 Developments in hull and propeller manufacturing

Significant advances have been made in Additive Manufacturing (AM) over recent years, and it is commonly used for the manufacture of appendages by the ITTC community.

Recent work conducted around the world has been investigating the feasibility of printing entire ship models up to 10 m in length. Some organisations have expressed concern about model rigidity and have needed to add aluminium beam reinforcement.

A study conducted by NSWCCD, to be reported by Mosqueda et al (2024), showed that Large Scale Additive Manufacturing (LSAM) of a ship model can achieve standard ITTC model build tolerances. The LSAM manufacturing technique pioneered by Thermwood Inc. appears extremely promising for future model building, which could reduce lead time for model manufacture and also reduce costs.

AM techniques for metals have also made huge advances over recent years, but trial studies indicate that the technology may not yet be sufficiently mature that it can be used for propeller manufacture at this time. The Powder Bed Fusion class of techniques hold the most promise, but are difficult to get right first time. The cavitation testing and open water testing of AM propellers conducted at two Italian universities is exciting, but showed differences in hydrodynamic and cavitation performance when compared to benchmark data. Developments in this field should continue to be monitored, as it must only be a matter of time before processes suitable for model scale propeller manufacture become available.

14.10 Guidelines for model testing of coatings

It was not possible to develop robust guidelines for the model testing of coatings, because insufficient published literature exists at this time. However, a review of the current state-of-the-art was conducted in this field.

Techniques documented included velocity profile method, rotating disk method, towed plate method. The frictional characteristics have been investigated in detail at model scale. However, the behaviour of the roughness functions for coating surfaces at ship scale roughness Reynolds numbers is still not sufficiently clear. As pointed out by Schultz (2004) the rotating disc and rotating drum techniques have potential to investigate the frictional characteristics of coating surfaces at higher roughness Reynolds number regions. Further work is required before guidelines can be issued by the ITTC.

Frictional drag reduction by air lubrication techniques were also reviewed. Air lubrication techniques have already been implemented on ships and shown to provide net energy savings (Mizoguchi *et al* 2010), however a clear understanding of all the flow phenomena is not yet possible. Monitoring of the work in this field should be continued, because this type of technology could be fundamental if the IMO is to achieve its stated goals of achieving net zero greenhouse gas emissions by 2050.

14.11 Review CFD methods for roughness effects

A review of wall-function methods was conducted, including a literature review of recent published work in this field. The roughness functions of hull coatings have been investigated by a number of researchers, however the

relationship between the roughness function and the surface profile of coatings is still unclear, especially for ship scale roughness Reynolds numbers. Further investigations on roughness functions for coating rough surfaces are needed.

For wall-resolved CFD techniques, the review focussed on the k-omega SST turbulence model, because this is widely used in CFD simulations of ship resistance and propulsion. Typically, modified k and omega boundary conditions are applied to simulate the effects of surface roughness. Orych et al (2022) showed a comparison of calculated frictional resistance of flat plate and ship with a variety of wall boundary conditions. Orych's work showed that the Aupoix-Colebrook method yields the most reasonable results when compared to extrapolated model scale experiments and more detailed CFD methods.

While wall-resolved techniques predict turbulent boundary layer flow with higher accuracy than wall function methods, the relationship between the roughness function and the roughness Reynolds number k+ is still not clear. The wall-resolved method also needs appropriate roughness length scale for various types of rough surfaces at ship scales. Further work is still required in this field, in order to determine best practice.

14.12 Identify the necessity of guidelines for CFD methods, model tests and scaling processes for Energy Saving Devices

A huge variety of Energy Saving Devices are currently being developed which makes the creation of generic guidelines difficult. Individual guidelines are likely to be required for specific techniques, such as: frictional resistance reduction; energy recovery devices such as hull vanes; propulsion efficiency improvements via inflow conditioning devices or gate rudders; renewable energy assisted propulsion systems such as Flettner rotors, sails or kites. It should be noted, however, that some of these ESDs interact with other parts of the ship system, so a holistic approach may be required. Additionally, many of the systems exhibit considerable scale effects and savings predicted by model tests cannot always be realised at full scale. Full scale testing of ESDs is therefore required and some work is being undertaken in this field. Determining a robust and reliable scaling process is essential, because many of these techniques would be expected to only give small improvements in efficiency.

Two new guidelines have been prepared by the ITTC Specialist Committee on Wind Powered Ships:

- Guideline for predicting the power saving of wind powered ships
- Conduct and analysis of sea trial for wind-assisted ships.

The 31st Resistance and Propulsion committee should review these documents and incorporate any additional requirements into the self-propulsion test guideline and into the 1978 ITTC Performance Prediction Method, if appropriate.

15. REFERENCES

Ahmadzadehtalatapeh, M., Mousavi, M., "A review on the Drag Reduction Methods of she Ship Hulls for Improving the Hydrodynamic Performance", International Journal of Maritime Technology, Vol 4 (2015) : 51-64

Airtech International, 2021, "Material Properties Specifications Data Sheet. Dahltram_S-150CF-EN".

Atencio, B. N., Chernoray, V., 2019, "A resolved RANS CFD approach for drag characterization of antifouling paints", Ocean Engineering 171, 519–532.

Aupoix, B., 2014. Wall roughness modelling with k-w STT model. In: 10th International ERCOFTAC Symposium on Engineering Turbulence Modelling and Measurements, Sep 2014. MARBELLA, Spain.

Bart, S., Maarten, K., Douwe R., 2024, "An Experimental Study on Visualisation and Passive Control of Model Propeller Boundary Layers", Eighth International Symposium on Marine Propulsors smp'24, Berlin, Germany.

Bhattacharyya, A., Krasilnikov, V., and Steen, S., 2015, "Scale effects on a 4-bladed propeller operating in ducts of different design in open water" In Proceedings of the Forth International Symposium on Marine Propulsors SMP2015, Austin, Texas, USA.

Bhattacharyya, A., Krasilnikov, V., and Steen, S., 2016a, "Scale effects on open water characteristics of a controllable pitch propeller working within different duct designs" Ocean Engineering, 112, 226-242.

Bhattacharyya, A., Krasilnikov, V., and Steen, S., 2016b, "A CFD-based scaling approach for ducted propellers" Ocean engineering, 123, 116-130.

Boorsma, A., 2000, "Improving full scale ship powering performance predictions by application of propeller leading edge roughness", Master of Science Thesis, University of Technology, Delft.

Borda, G. G., et al., 1984, "Resistance, Powering Optimum Rudder Angle Experiments on a 465.9 Foot (142 m) Guided Missile Destroyer (DDG-51) Represented by Model 5415-1 and Fixed Pitch Propellers 4876 and 4877 (U)," DTNSRDC/SPD-0200-08.

Cilia, T., Beretta, D., Gualeni, P., Tani, G., Vivani, M., "Additive Manufacturing Application to a Ship Propeller Model for Experimental Activity in the Cavitation Tunnel", Journal of Ship Production and Design, Bol. 35, No.4, November 2019, pp 364-373.

Dang J., Dong G., Chen H., 2012, "An exploratory study on the working principle of energy saving devices (ESDs): PIV, CFD investigations ad ESD design guidelines", Proceedings of the ASME 31st International Conference on Offshore Mechanics and Arctic Engineering (OMAE), Rio the Janeiro, Brasil.

Demirel, Y. K., Khorasanchi, M., Turan, O., Incecik, A., Schultz, M. P., 2014, "A CFD model for the frictional resistance prediction of antifouling coatings", Ocean Engineering 89, 21–31.

Demirel, Y. K., Turan,O., Incecik, A., 2017, "Predicting the effect of biofouling on ship resistance using CFD", Applied Ocean Research 62, 100–118.

Eça, L., Hoekstra, M., 2011, "Numerical aspects of including wall roughness effects in the SST k-ω eddy-viscosity turbulence model", Comp Fluids 40:299–314.

Fontes, J.V.H., Martínez-Flores, A., Hernandez, I.D., Mendoza, E., Silva, R., 2022, "Flow Kinematics in the Generation of Different Types of Green Water Events with Incident

Wave Trains", Ocean Engineering, 258: 111519.

Furcas, F., Gaggero, S., 2021 "Pre-Swirl Stators design using a coupled BEM-RANSE approach" Ocean Engineering, vol. 222, Article Number 108579.

Gaggero, S. 2020 "Influence of laminar-to-turbulent transition on model scale propeller performances. Part I: fully wetted conditions", Ship and Offshore Structures, 17(4), pp. 772–791.

Gaggero, S. and Martinelli, M., 2022, "Pre-Swirl fins design for improved propulsive performances: application to fast twin-screw passenger ships" Journal of Ocean Engineering and Marine Energy, vol. 9.

Gaggero, S., Rizzo, C. M., Tani, G., and Viviani, M., 2013 "Design, analysis and experimental characterization of a propeller in decelerating duct", In Third International Symposium on Marine Propulsors (SMP2013), Launceston, Tasmania, Australia.

Govindrak, R.B., Junghans, E., Andersen, I., ki Lim, Y., Lindstrom, P., "Additive manufactured marine component – Ni Al bronze propeller", Procedia Structural Integrity, 34:20-25.

Hengelmolen, V. and Wellens, P. R., 2022, "An Experimental Study on Added Resistance Focused on the Effects of Bow Wave Breaking and Relative Wave Measurements", International Shipbuilding Progress, 69: 61-89.

Hellsten, A., 1998, "Some Improvements in Menter's K-Omega SST Turbulence model", 29th AIAA, Fluid Dynamics Conference. Fluid Dynamics and Co-located Conferences, https://doi.org/10.2514/6.1998-2554.

Hasuike N., Okazaki M., Okazaki A., Fujiyama K., 2017, "Scale effects of marine propellers in POT and self propulsion test conditions", Fifth International Symposium on Marine Propulsors smp'17, Espoo, Finland.

Ishii, N., Yagi, H., Yuasa, H., 1983, "Model Testing of Propeller Cavitation Roughening the Leading Edge of Blades", Journal of the Society of Naval Architects of Japan, 153.

ITTC, 1975, "Report of Propeller Committee", 14th ITTC Full Conference Proceedings, Ottawa, Canada.

ITTC, 2021, "Report of Propeller and Resistance Committee", 29th ITTC Full Conference Proceedings.

Jacobi, G., Thill, C.H., Huijsmans, R.H.M., 2022, "Pressure Reconstruction from PIV Measurements in the Bow Region of a Fast Ship", Ocean Engineering, 252: 110318.

Jin, Q., 2022, "A Combined Volume of Fluid and Immersed Boundary Method for Simulations of Ship Bow Breaking Waves", PhD Thesis, University of Southampton.

Kerkvliet, M., Baltazar, J., Schuiling, B. and Eça, L., 2024 "A Numerical Study on Model Propeller Performance Prediction Including Transitional and Passively Controlled Boundary Layer Considerations", Proceedings of the 8th International Symposium on Marine Propulsors, Berlin, Germany.

Kim, J.H., Choi, J.E., Choi, B.J., Chung, S.H., and Seo, H.W., 2015, "Development of energy-saving devices for a full slow-speed ship through improving propulsion performance" International Journal of Naval Architecture and Ocean Engineering, vol.7, no. 2, pp 390-398.

Kim, M.C., Shin, Y.J., Lee, W.J., Lee, J.H., 2017, "Study on extrapolation method for self-propulsion test with pre-swirl device" Proceedings of the International Symposium on Marine Propulsion, Espoo, Finland.

Kimura, K., Ando, S., "A Method to predict Full Scale Performance of the Propeller Boss Cap

Fins", Sixth International Symposium on Marine Propulsors, SMP 19, Rome, Italy.

Knopp, T., Eisfeld, B., Calvo, J. B., 2009, "A new extension for k-ω turbulence model to account for wall roughness", Int. J. Heat Fluid Flow 30 (1), 54-65, 101016/jiheatfluidflow200809009.

Koushan, K., Krasilnikov, V., Nataletti, M., Sileo, L., and Spence, S., 2020 "Experimental and Numerical Study of Pre-Swirl Stators PSS" Journal of Marine Science and Engineering, vol. 8.

Larsson, L. Stern, F. Bertram, V., "Benchmarking of Computational Fluid Dynamics for Ship Flows: The Gothenburg 2000 Workshop", Journal of Ship Research 47 (01): 63-81, 2003

Lee, E.J., Mousaviraad, M., Weil, C.R., Jiang, M.J., Fullerton, A.M. and Stern, F., 2021, Assessment of experiments and CFD for the semi-planing R/V Athena Model in calm water, *Ocean Engineering*, Vol. 236, p.109254.

Lee J.T., Kim M.C., Suh J.C., Kim S.H., Choi J.K., 1992 "Development of preswirl stator-propeller system for Improvement of Propulsion Efficiency: a Symmetric Stator Propulsion System", Journal of the Society of Naval Architects of Korea, vol. 41, no. 3, pp. 13-21

Lee, W.J., 2015 "Study on Full-Scale Performance Prediction for Pre-Swirl Device Model Test Results", Ph.D. Thesis, Pusan National University

Li, C., Duan, W-Y., Zhao, B-B., 2022a, "Breaking Wave Simulations for a High-Speed Surface Vessel with Hybrid THINC and HRIC Schemes", Applied Ocean Research, 25: 103257.

Li, D-Q, Lindell, P, Werner, Sücke T., 2019, "Transitional flow on model scale propellers and their likely influence on performance prediction", Sixth International Symposium on Marine Propulsors smp'19, Rome, Italy.

Li, Z., Zhang, X-S., Wan, D-C., 2022b, "Research Progress on the Hydrodynamic Performance of Water-Air-Bubble Mixed Flows Around a Ship", Journal of Hydrodynamics, 34(2): 171-188.

Longo, J., & Stern, F., 1998, "Resistance, Sinkage and Trim, Wave Profile, and Nominal Wake Tests and Uncertainty Assessment for DTMB Model 5512." Paper presented at the SNAME 25th American Towing Tank Conference, Iowa City, Iowa, USA.

Lücke T., Streckwall H., 2017, "Experience with Small Blade Area Propeller Performance", Fifth International Symposium on Marine Propulsors smp'17, Espoo, Finland.

Mallat, B., Germain,G., Billard, J-Y., Gabillet, C. 2022, "Breaking Wave Bubble Measurements Around Ship Model by Optical Probe", Ocean Engineering, 246: 110438.

MARIN, 2024, "Tripping JIP", Retrieved April 8,2024 from https://www.marin.nl/en/jips/tripping, .

Mewis F. and Guiard T., 2011, "Mewis duct – New development, solutions and conclusions", Proceedings of the 2nd International Symposium on Marine Propulsors, Hamburg, Germany.

Mosqueda, K., (2024), "Large Scale Additively Manufactured Model Feasibility Study and Resistance Experiments", NSWCCD-80-TR-2024-001.

Nicorelli, G., Villa, D. and Gaggero, S., 2023, "Pre-Swirl Ducts, Pre-Swirl Fins and Wake-Equalizing Ducts for the DTC Hull: Design and Scale Effects", Journal of Marine Science and Engineering, vol. 11 no.5

Olivieri, A., Pistani, F., Wilson, R., Campana, E.F., Stern, F., A., 2007, "Scars and Vortices

Induced by Ship Bow and Shoulder Wave Breaking", Journal of Fulid Engineering ASME, 129: 1445-1459.

Orych, M, Werner, S., Larsson, L., 2022, "Roughness effect modelling for wall resolved RANS – Comparison of methods for marine hydrodynamics", Ocean Engineering 266, 112778.

Rubino, G. and Abdel-Maksoud, M., 2024, "Model- and Full-Scale Tip-Rake Marine Propellers: Analysis of the Scale Effects in Open Water", Proceedings of the 8th International Symposium on Marine Propulsors, Berlin, Germany.

Shin H.J., Lee J.S., Lee K.H., Han M.R., Hur E.B., Shin S.C., 2013, "Numerical and experimental investigation of conventional and unconventional preswirl duct for VLCC", International Journal of Naval Architecture and Ocean Engineering, vol. 5, no. 2, pp 413-430.

Song, S., Demirel, Y. K., Atlar, M., 2019, "An investigation into the effect of biofouling on the ship hydrodynamic characteristics using CFD", Ocean Engineering 175, 122–137.

Song, S., Demirel, Y. K., Atlar, M., Dai, S., Day, S., Turan, O., 2000, "Validation of the CFD approach for modelling roughness effect on ship resistance", Ocean Engineering 200.

Song, S., Ravenna, R., Dai, S., Muscat-Fenech, C. D., Tani, G., Demirel, Y. K., Atlar, M., Day, S., Incecik, A., 2021, "Experimental investigation on the effect of heterogeneous hull roughness on ship resistance", Ocean Engineering 223.

Staiano, G., Gloria, A., Ausanio, G., Lanzotti, A., Pensa, C., Martorelli, M., "Experimental study on hydrodynamic performances of naval propellers to adopt new additive manufacturing process", International Journal on Interactive Design and Manufacturing (2018) 12:1-14

Suzuki, T., 1974, "Effect of Turbulence Stimulating Device on the Results of Propeller Open Water and Self-propulsion Tests",

Tasdemir, A., Nohut, S., "An overview of wire arc additive manufacturing (WAAM) in shipbuilding industry", Ships and Offshore Structures, 16:7, 797-814.

Wang, J., Ren, Z., Wan, D-C., 2020, "Study of a Container Ship with Breaking Waves at High Froude Number Using URANS and DDES Methods", Journal of Ship Research, 1-11.

Wang, X., Zhu, R., Jiang,Y., 2023, "Numerical investigation on nonlinear ship waves by LCM and WSAM", Ocean Engineering, 284: 115076.

Wilcox, D. C., 2006, "Turbulence modeling for CFD Third Edition", DCW Industries, Inc.

Wilson, R., Carrica, P., and Stern, F., 2007, "Simulation of Ship Breaking Bow Waves and Induced Vorticies and Scars", International Journal for Numerical Methods in Fluids, 54-4: 419-451.

Wu, D., Wang, J., Wan, D-C., 2021, "Delayed detached eddy simulation method for breaking bow waves of a surface combatant model with different trim angle", Ocean Engineering, 242: 110177.

Yeginbayeva, I. A., Atlar, M., 2018, "An experimental investigation into the surface and hydrodynamic characteristics of marine coatings with mimicked hull roughness ranges", Biofouling, 34:9, 1001-1019.